# Fate of Silver Nanoparticles in Lake Mesocosms

A Thesis Submitted to the Committee on Graduate Studies in Partial Fulfillment of the Requirements for the Degree of Master of Science in the Faculty of Arts and Sciences

TRENT UNIVERSITY

Peterborough, Ontario, Canada



Environmental and Life Sciences M. Sc. Graduate Program

May 2014

## ABSTRACT

### Fate of Silver Nanoparticles in Lake Mesocosms

Lindsay Furtado

The fate of silver nanoparticles (AgNPs) in surface waters determines the ecological risk of this emerging contaminant. In this research, the fate of AgNPs in lake mesocosms was studied using both a continuous (i.e. drip) and one-time (i.e. plug) dosing regime. AgNPs were persistent in the tested lake environment as there was accumulation in the water column over time in drip mesocosms and slow dissipation from the water column (half life of 20 days) in plug mesocosms. In drip mesocosms, AgNPs were found to accumulate in the water column, periphtyon, and sediment according to loading rate; and, AgNP coating (PVP vs. CT) had no effect on agglomeration and dissolution based on filtration analysis. In plug mesocosms, cloud point extraction (CPE), single-particle-inductively coupled mass spectroscopy (spICP-MS), and asymmetrical flow field-flow fractionation (AF4-ICP-MS) confirmed the temporal dissolution of AgNPs into $Ag^{+}$ over time; however, complexation is expected to reduce the toxicity of Ag+ in natural waters.



**Key Words:** silver nanoparticles, fate, mesocosms, cloud-point extraction, asymmetrical flow field flow fractionation, single-particle-inductively coupled plasma mass spectroscopy

## AWKNOWLEDGEMENTS

Completing a Masters of Science degree has been a challenging and rewarding experience and I would like to thank all of the people who helped me throughout this process. I have immense gratitude for my supervisors, Dr. Chris Metcalfe and Dr. Holger Hintelmann, for providing me the opportunity to conduct this research and guiding me through the process. Their support, scientific insight, and suggestions were invaluable to this research. I'd also like to thank all of my research colleagues for helping me with the techniques used in this research and for their company in the lab. In particular, Brian Dimock for helping me prepare for field sampling, as well as assisting with the Ag analysis in periphyton and sediment. Dr. Ehsan Hoque and Dr. Lena Telgmann for providing assistance with the AF4 and ICP-MS analysis. Also, Brenda McIlwain for guiding me around the lab. I want to thank Dr. Jim Ranville and Dr. Denise Mitrano from the Colorado School of Mines for performing the spICP-MS analysis and providing invaluable insight and suggestions for the AF4 analysis. I also want to thank all of the lake ecosystem nanosilver (LENS) project members who helped out in the mesocosm study, in particular Jennifer Vincent and Graham Blakelock. Special thanks to Beth Cheever for leading the mesocosm study and mentoring me in my research and analysis. I also want to express my gratitude to my committee member, Dr. Jane Kirk, for both her scientific and life mentoring. Finally, I'd like to thank my fellow class/lab mate Jillian Fischer for being my confidant during this whole process and for helping me to de-stress over our yoga nights and dinner parties after long days in the lab. Financial support was gratefully provided by the Ontario Graduate Scholarship (OGS) and the National Science and Engineering Research Council (NSERC). Field work was conducted at the Experimental Lakes Area (ELA). Analyses were conducted in the Water Quality Centre at Trent University and in Dr. Jim Ranville's lab at the Colorado School of Mines. Finally, I want to thank all my loved ones for always supporting my ambitions. In particular, I want to thank my parents, Jose and Louisa Furtado, who have instilled in me the importance of education and have always provided me words of encouragement when I had doubt in my abilities. And I am so thankful for my partner, Derek Snider, for always supporting and believing in me.

## LIST OF FIGURES

## LIST OF TABLES

## LIST OF APPENDICES

### Chapter 2 Supplementary Information

**Chapter 3 Supplementary Information**

## TABLE OF CONTENTS

# Chapter 1: Introduction and Literature Review

## 1.1. Introduction

Silver nanoparticles (AgNPs) are used in a variety of commercial products as an antibacterial agent (1). As the production and use of AgNPs continues to increase (2), it is inevitable that they will be released into the environment. Although AgNP toxicity to a variety of organisms has been demonstrated (3), evaluating the ecological risk requires sufficient information on exposure to link with toxicological effects (4). The release of AgNPs into surface waters is expected (5, 6), and subsequent transformations and distribution will dictate toxicity (7, 8). Therefore, an understanding of the fate of AgNP in natural aquatic environments is imperative to risk assessment. Robust and sensitive analytical methods will be needed to quantify and characterize AgNPs and their associated transformation products in natural waters.

This chapter will provide: i) an overview of the literature with respect to: defining AgNPs and its' current uses, its' predicted environmental concentrations (PEC), AgNP toxicity, and the environmental fate related to aquatic matrices, and ii) a review of promising analytical methods available for AgNP quantification and characterization. Finally, the objectives for this research will be outlined, which aim to address the research gaps regarding the fate and analysis of AgNP in natural aquatic systems.

## 1.2. Literature Review

### 1.2.1 AgNP definition and current uses

Nanoparticles are defined as particles with one or more dimensions less than 100 nm in size. Nanomaterials are manufactured products that contain nanoparticles. Silver nanoparticles (AgNPs) are the nanoparticle most widely used in nanomaterials, with 388

products in 2013 (2). AgNPs popularity is related to its high reactivity and antibacterial properties, and AgNP nanomaterials are now used in medical equipment, bandages, antibacterial creams and ointments, clothing, shoe liners, food wrappers and containers, and household appliances (1). The global production and use of nanomaterials is rapidly increasing, estimated to be in the thousands of tons in 2004 and projected to grow to over half a million tons by 2020 (3).

### 1.2.2. AgNP release and environmental concentrations

The release of AgNPs into the environment is inevitable due to the widespread and increasing use of these particles in nanomaterials. AgNP release into municipal and industrial wastewater is expected as a result of product use, disposal, and weathering (6). For example, studies have shown that AgNPs are released from textiles during washing (9-11) and from the weathering of paints used in outdoor applications (12). AgNPs can either directly enter the aquatic environment through discharges of untreated wastewater, or can be transported via sewage systems into wastewater treatment plants (WWTPs) (6). Depending upon the degree of removal of AgNPs in the WWTP, there is potential for AgNPs to be released into rivers and lakes through effluent discharges (5, 6), as illustrated in Figure 1.1. A large proportion of AgNPs entering WWTPs are expected to accumulate in biosolids as a result of sorption and sulfidation (13-15). Regardless, the potential for the release of AgNPs into surface waters is of concern, especially in cases where wastewater remains untreated.

It is uncertain what concentrations of AgNP are predicted in WWTP effluent and in surface waters. Modelling studies have generated PEC that range from 16.4-18 000 ng $L^{-1}$ in WWTP effluent (6, 16) and 0.088-619 ng $L^{-1}$ in surface waters (6, 16-19). An

issue with these modelling studies is that there is a lack of knowledge about important parameters that could affect PEC estimates, such as: production rates, application and environmental release volumes, physiochemical properties, and environmental fate and behaviour of the AgNPs (4). Furthermore, it is difficult to validate these modelling studies because there is a lack of appropriate methods that can be used to analyze AgNPs in complex matrices and at environmentally relevant concentrations (3, 4). Few studies have investigated the measured effect concentrations (MEC) of AgNPs in the environment. Hoque et al. (20) measured a AgNP concentration of 1.9 µg $L^{-1}$ in WWTP influent in Peterborough, ON, CAN. Li et al. (15) measured a similar concentration of AgNPs in the WWTP influent in Germany (<1.5 µg $L^{-1}$), which was reduced by 95% after treatment resulting in concentrations <12 ng $L^{-1}$ in the effluent. The PEC and MEC values reported in the literature indicate that AgNP release into surface waters are expected to occur in the ng $L^{-1}$ to µg $L^{-1}$ range, and these concentrations will likely rise with increased production and use of nanomaterials.

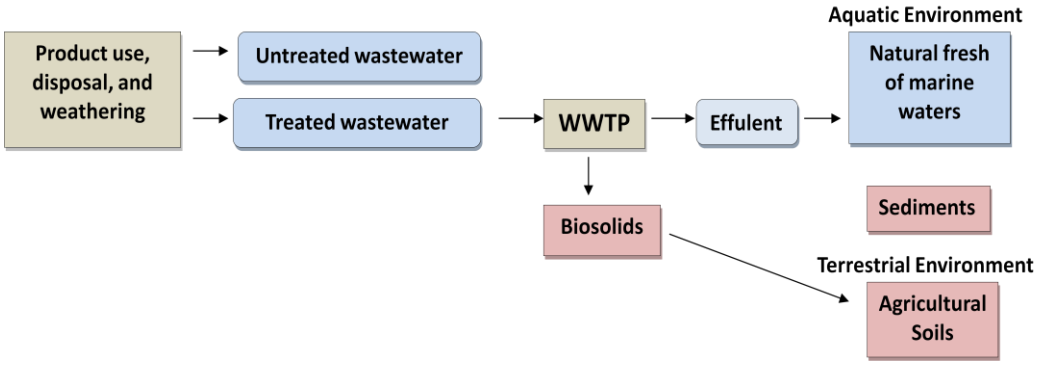


**Figure 1.1.** Pathways for the release of AgNP into the environment as a result of their transport with municipal or industrial wastewater. Arrows represent the flow of AgNPs. Figure adapted from Blaser et al. (6).

### 1.2.3. AgNP toxicity

AgNPs have been shown to be toxic to a variety of aquatic organisms. Organisms from lower trophic levels are particularly sensitive to AgNP toxicity, including bacteria (21-23), zooplankton (24-26) and algae (27, 28). Toxicity to lower trophic organisms is of concern due to the important ecological roles that these organisms provide. For example, AgNPs could impact important microbial ecosystem services such as nitrification (29-31) and decomposition (31). Studies preformed on natural bacterioplankton have shown that AgNP exposure reduces bacterial production (32) and changes community composition (33), which could also impact ecosystem functions. AgNP toxicity to fish has also been demonstrated, although toxic effects usually occur at high ppb or ppm concentrations (34-36).

The mechanisms of AgNP toxicity are not entirely understood. AgNP exposure has been shown to: i) lead to formation of reactive oxygen species (ROS), leading to oxidative stress and potentially apoptosis (37-40), ii) inhibit ionoregulation (i.e. $Na^+/K^+$ channels) (41), and iii) dissipate membrane potential, leading to a reduction in ATP levels (42). However, it is currently under debate whether toxicity is due to the effects of the nanoparticles themselves, the effects of $Ag^+$ released by oxidation of the AgNPs (i.e. dissolution), or both (43). There is some evidence that the majority of AgNP toxicity results from exposure to released $Ag^+$. Some studies have shown $AgNO_3$ (which dissociates to $Ag^+$) is more toxic than AgNPs, based on total Ag mass, and that the toxicity of AgNPs increases as a function of the release of $Ag^+$ (44-47). Toxicity due to released $Ag^+$ has also been demonstrated in experiments in which the addition of cysteine to AgNP suspensions mitigates toxicity; presumably by complexing with the free $Ag^+$

(26, 27, 29, 30, 45, 48). Furthermore, AgNP toxicity has been eliminated in anaerobic environments that reduce the oxidative dissolution of $Ag^+$ (49). Toxicity related to the nanoparticles themselves may be the result of their adhesion to cells, leading to membrane damage (21-23), as only particles <10 nm have been shown to pass through trans-membrane pores (50). The effects of size and speciation of AgNPs on toxicity illustrates the importance of understanding transformations of these materials in the environment.

### 1.2.4. AgNP transformations and their effects of fate and toxicity

AgNP dissolution and agglomeration are the most important transformation processes altering fate and toxicity (Figure 1.2) The extent of these transformations will depend on physiochemical conditions, such as dissolved organic carbon (DOC), pH, ionic strength, redox, particle specific properties (i.e. size and surface coating), and concentration. The next section will discuss these concepts in detail.

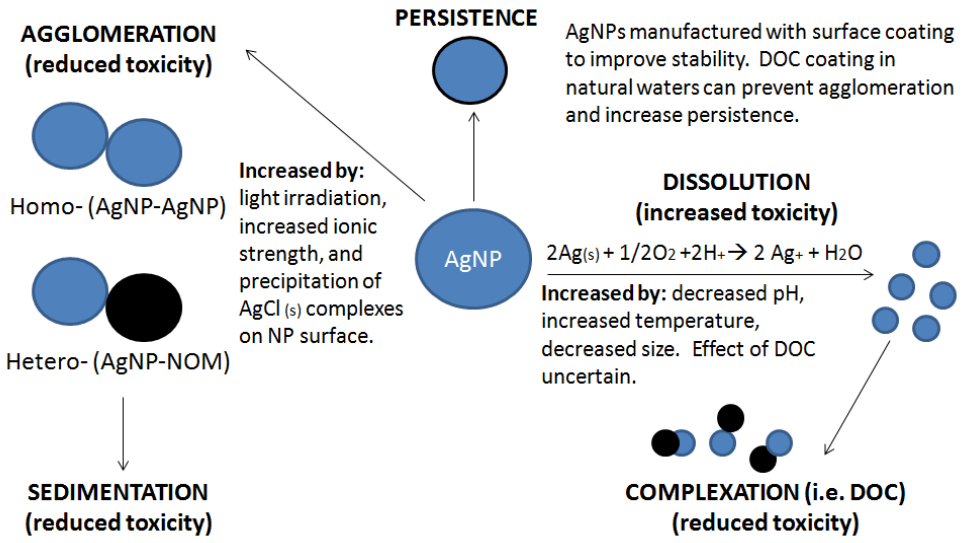


**Figure 1.2.** Major AgNP transformations expected to occur in natural waters and their effect on fate and toxicity.

#### *1.2.4.1 AgNP agglomeration*

Agglomeration is the physical process by which particles attach to each other (51). It can be described as homoagglomeration (i.e. AgNP with AgNP) or heteroagglomeration (e.g. AgNP-with natural organic material, NOM). Agglomeration is often governed by the Derjaguin and Landau, Verwey and Overbeek (DLVO) theory of colloidal stability, in which the tendency of AgNPs to agglomerate depends on van der Waals attractive forces overcoming the energy barrier caused by the repulsive forces between two charged particles (51, 52). In DLVO theory, the repulsive forces result from the electrical double layer that forms around particles in suspension (51). However, there are also non-DLVO forces that prevent agglomeration as a result of adsorption by a polymer or NOM (51).

AgNP agglomeration depends on chemical, physical, and biological factors. An increase in ionic strength causes AgNPs to aggregate because excess electrolytes screen the surface charge and reduce the electrical double layer that surrounds particles (53-56). Once ion concentrations exceed the critical coagulation concentration (CCC), the energy barrier is completely eliminated, resulting in a change in kinetic regimes from slow, reaction limited cluster agglomeration (RLCA) to rapid, diffusion limited cluster agglomeration (DLCA) (57). Agglomeration can also be induced by precipitation of $AgCl_{(s)}$ (53, 54) or $AgS_{(s)}$ (58) on AgNP surfaces that form "bridges" between particles. Sunlight can also cause agglomeration by photodegrading the coating on AgNP, leading to destabilization (59). Conversely, DOC improves stability by adsorbing to AgNP surfaces and inducing steric and electrostatic repulsion (55, 60-62). It is important to note that low concentrations of AgNPs in the environment relative to the high amounts of

other particles (e.g. bacteria, algae), will likely result in heteroagglomeration rather than homoagglomeration (7). For example, AgNPs have been shown to physically attach to cell walls of bacteria (21-23) and algae (63). However, more experimentation is needed to understand nanoparticle heteroagglomeration (51).

Agglomeration alters the fate and toxicity of AgNPs. In surface waters, AgNPs that remain unagglomerated will likely be suspended in the water column and persistent in the environment (61). Conversely, agglomeration will lead to denser particles and sedimentation (52, 61), reducing exposure to pelagic organisms. Kennedy et al. (62) demonstrated that as the aggregate size of AgNPs increases, the Ag concentration in the water decreases due to sedimentation. Also, Velzeborer et al.(64) attributed an absence of toxicity in bioassays with aquatic organisms to agglomeration and sedimentation of the nanoparticles, resulting in reduced exposure. Agglomerated AgNPs are also less toxic due to their larger size and reduced ability to interact with cell membranes (65, 66). This concept is consistent with a study by McLaughlin and Bonzongo (67) where bioassays using natural waters with high ionic strength/ DOC ratios lead to larger particle sizes in suspension and lower toxicity to algae and zooplankton relative to natural waters with low ionic strength/ DOC. These studies demonstrate that in order to understand fate and toxicity, it is essential to evaluate the extent of agglomeration.

#### *1.2.4.2. AgNP dissolution*

AgNP dissolution describes the release of ionic Ag ($Ag^{+}$) from the particle's metallic core. Dissolution occurs when $Ag^{0}$ at the AgNP surface is oxidized to $Ag_2O$ and "dissolves" to release $Ag^{+}$ in the presence of dissolved oxygen (68). Thermodynamic calculations suggest that AgNPs should completely dissolve over time in aerobic

environments (68). However, studies looking at long-term dissolution have observed that a limiting value is reached, where there is no longer a significant increase in Ag+ concentration (68). This may be due to other environmental conditions that control the rate of dissolution.

AgNP dissolution is controlled by the surrounding physiochemical environment. Dissolution rates increase with decreasing pH, increasing temperatures, and only occur in the presence of dissolved oxygen (68-70). The presence of electrolytes can also affect dissolution. Dissolution of the $Ag_2O$ surface layer can be prevented by the adsorption and accumulation of $Ag^+$ at the particle surface (53). Electrolytes (i.e. $Cl^-$) can promote dissolution by increasing $Ag_2O$ solubility and/or replacing adsorbed $Ag^+$ (53-55, 71). The effect of $Cl^-$ on dissolution may depend on the relative concentrations of Cl and Ag. Levard et al. (72) observed that the rate of AgNP dissolution was slower at low $Cl^-$ concentrations due to the formation of insoluble $AgCl_{(s)}$ species, whereas at high $Cl^-$ concentrations, soluble $AgCl_x^{(x-1)}$ species dominated and increased dissolution rates.

The effect of DOC on AgNP dissolution is not known (62, 73). Liu et al. (68) found that humic acids (HA) prevented dissolution, suggesting that HAs were adsorbed to the surface and blocking AgNP oxidation sites and/or act as reductants, converting $Ag^+$ to $Ag^{(0)}$. However, Gao et al. (74) reported that the dissolved Ag (dAg) concentration remain constant regardless of HA concentration. Gondikas et al. (73) showed that cysteine, a low molecular weight thiol amino acid, increases dissolution. The mechanism by which thiols increase dissolution may be similar to that of $Cl^-$ or may be the result of the reduced agglomeration imparted by coating with thiol groups (73). For example,

agglomeration has been shown to decrease AgNP dissolution due to reduced surface area and availability of reactive sites (57, 73).

Natural waters will affect the fate and toxicity of $Ag^+$. Although AgNP dissolution has been shown to increase toxicity (70), the toxicity of the released $Ag^+$ also depends on it remaining biologically available (75) . Free $Ag^+$ is unlikely to be present in natural waters due to its cationic nature and strong affinity for ligands (76). Speciation of $Ag^+$ depends on the relative concentration of ligands and the Eh-pH conditions. For example, Levard et al. (8) predicted $Ag^+$ speciation in freshwater and seawater based on thermodynamic constraints, and predicted that in freshwater, $Ag^+$ would be expected to preferentially complex with thiol-containing ligands present in DOC, rather than $Cl^-$. Little complexation to $AgCl_{(x)}$ is expected to occur in freshwaters due to the low Ag/Cl ratios, and also because of the much higher stability constant associated with thiols in DOC compared to $Cl^-$. Conversely, soluble $AgCl_{(x)}$ species will form at the higher Cl/Ag ratios typical of seawater. In anaerobic environments where inorganic sulphur is present (i.e. $HS^-$ and $S_2^-$), silver sulfide complexes will dominate because of its high formation constant (logK= ~13). This may also be true in surface waters with very low $Ag^+$ concentrations (<nM) as inorganic sulphur has been found in oxic waters in submicromolar concentrations (77). The presence of reduced sulphur in oxygenated water has been attributed to its complexation with iron, copper, or zinc that stabilize $HS^-$ and $S^{2-}$ species and prevent it from becoming oxidized (i.e. $SO_4^{2-}$ ) (78). $Ag^+$ is then able to displace iron, copper, or zinc, and bind to the reduced sulphur species because it is more thiophilic (78). Finally, both ionic Ag and complexed Ag also readily adsorb to particulate matter (76).

The speciation of $Ag^+$ will impact the toxicological effects of AgNPs. DOC will significantly reduce toxicity due to $Ag^+$ complexation and reduced bioavailability (60, 62, 71). For inorganic ligands, the solubility of dAg complexes will control toxicity. For example, the formation of soluble $AgCl_{(x)}$ complexes was found not to alter AgNP toxicity to bacteria (72), whereas the formation of insoluble $AgCl_{(s)}$ (72) and $Ag_2S_{(s)}$ (79) greatly reduced bacterial toxicity. Understanding the extent of AgNP dissolution and resulting $Ag^+$ complexation in natural waters is essential to risk assessment.

#### *1.2.4.3. Particle Specific Properties*

Particle specific properties have been shown in laboratory experiments to influence AgNP dissolution and agglomeration. Dissolution is accelerated for AgNPs with smaller particle sizes, due to an increased surface area to volume ratio (80, 81). Another important particle property to consider is the surface coating added to synthesised AgNPs to improve stability in consumer products and in turn, maximize anti-bacterial properties (65). The surface coating can either cause electrostatic or steric repulsive forces that prevent agglomeration. Polyvinylpyrrolidone (PVP), a sterically stabilized coating, and citrate (CT), an electrostatic stabilized coating, are the coatings most commonly used for AgNPs (82). PVP-AgNPs have been found to have reduced agglomeration (55, 71, 83) and greater dissolution (45, 70, 84) compared to CT-AgNPs. However, these properties have yet to be studied in natural waters at environmentally relevant concentrations.

#### *1.2.4.4. Concentration*

AgNP concentration may influence the extent of agglomeration and dissolution. Agglomeration has been shown to increase with AgNP concentration as a result of the

increased frequency of particle-particle interactions (62). Higher AgNP concentrations result in greater dAg concentrations. However, lower concentrations lead to proportionally higher dissolution, possibly because sample dilution drives the equilibrium towards releasing more Ag+ (85). The aforementioned results were generated from laboratory experiments, and the effect of concentration on the rate of AgNP dissolution and aggregation has yet to be investigated in natural waters.

### 1.2.5. Methodologies for AgNP analysis

Currently there are a limited number of analytical techniques appropriate for quantifying and characterizing AgNP transformations in the environment (86, 87). Some of the problems for analysis under environmentally relevant conditions are the low concentrations of AgNPs, high complexity of the sample matrix, difficulties in sample preparation, artefacts and sample stability, polydispersivity, and the lack of reference and standard materials for calibration (88). Commonly used techniques for characterizing the size of AgNPs include dynamic light scattering (DLS) and transmission electron microscopy (TEM). However, these techniques lack sensitivity, and so detection limits (i.e. mg $L^{-1}$) are much higher than expected environmental concentrations (89). In addition, it is not possible to quantify concentrations of AgNPs using these techniques (89). Size fractionation by filtration, cloud-point extraction (CPE), asymmetric flow field flow fractionation with online ICP-MS (AF4-ICP-MS), and single-particle-inductively coupled mass spectroscopy (spICP-MS) are techniques with potential for quantifying the size and/or form (i.e. dissolved versus particulate) of AgNPs at environmentally relevant concentrations. The following section will describe these methods in detail.

#### *1.2.5.1 Size Fractionation by Filtration*

Filtration can be used to separate AgNPs into different size fractions (90). Using this method, the Ag form is operationally defined based on the size of the membrane pores. For example, Farmen et al. (34) defined particulate Ag as that removed by a 0.2 µm membrane and colloidal Ag as that removed by a 10 kDa membrane (3 nm>Ag<220 nm). For natural waters, the particulate fraction would also include Ag associated with bacteria (0.2-1 µm) and algae (>1 um), and other forms of particulate organic matter (POM) (91). Ag passing through a 3-10 kDa ultrafiltration (UF) membrane has been operationally defined as dissolved Ag (dAg) in the majority of the literature. The dAg includes Ag+ and Ag+ complexes that are less than the nominal pore size of the ultra-filters (1-2 nm)(59, 68).

The separation of different size fractions is a major challenge for filtration. It has been reported that filters can retain particles with sizes that are less than the nominal pore size of membrane filters, including AgNPs (92) and POM (91). Poor recovery of dAg using centrifugal ultrafiltration has also been observed (93, 94). Interactions of AgNP/$Ag^{+}$ with the filter, pore blockage as a result of filter cake formation, and membrane polarization are common artefacts that reduce recovery in the filtrate (86, 92). AgNP recovery using filtration may be improved by avoiding polar membranes, such as nylon (92). In terms of ultrafiltration, the efficiency of the separation may be improved by re-circulating or stirring the sample on top of the membrane during filtration (86). Although recovery is a challenge, the advantages of filtration include simplicity and the ability to use sensitive analytical techniques (e.g. ICP-MS) to quantify the Ag concentration in each fraction.

#### *1.2.5.2. Cloud Point Extraction*

CPE was originally developed by Liu et al. (95) to pre-concentrate and quantify trace AgNPs in environmental waters. In the CPE method, a surfactant is added to a sample at a concentration that exceeds the critical micelle concentration (CMC) and then heated to its "cloud point" temperature (96). Above the cloud point, micelles form and an additional surfactant rich phase is created. The surfactant rich phase contains non-polar substances (i.e. AgNPs) inside the micelles, while polar substances (i.e. dAg) remain in the aqueous phase (96). Centrifugation is applied to separate the two phases, in which the AgNPs concentrated in the surfactant rich phase can be measured directly using Electrothermal Atomic Adsorption Spectroscopy (ET-AAS) (96) or can be microwave digested for subsequent ICP-MS analysis (95). To improve AgNP extraction efficiency, the pH of the solution is adjusted to the zero point charge (zpc) of AgNP, and thiosulfate ($S_2O_3^{2-}$) is added to complex with any $Ag^+$ adsorbed on the AgNP surface (95).

Advantages to the CPE method include its low-cost and ability to pre-concentrate samples, which improves AgNP detection limits to $\mu g\ L^{-1}$ or $ng\ L^{-1}$ (95). Furthermore, it has been shown that the size and shape of AgNPs are preserved during extraction and storage in the surfactant-rich phase, offering the potential for characterization with TEM and energy dispersive x-ray spectroscopy (EDS) (95). Chao et al. (97) also suggested the dAg concentration, including that adsorbed to AgNPs and associated with the matrix, could be determined from the difference between the total Ag in the sample and the AgNP content measured by CPE (97). Although a small number of CPE method development studies have been published (95-97), this method has yet to be applied to a study of AgNP transformations.

### *1.2.5.3. Asymmetric Flow Field Flow Fractionation (AF4)*

AF4 is a chromatography-like technique that separates particles based on their diffusion coefficient to provide a continuous size distribution eluting in the mobile phase. The AF4 theory has been described in detail elsewhere (98), but a brief description is provided here. In AF4, analyte separation takes place along a thin channel comprising of one permeable wall covered by an ultrafiltration (UF) membrane (Figure 1. 3). A longitudinal flow moves the particles through the channel; while a cross flow is applied perpendicular to the channel and pushes the particles towards the UF membrane. In a normal (Brownian) mode of fractionation, particle diffusion opposes the cross flow force, causing smaller particles with higher diffusion coefficients to move further away from the UF membrane than larger particles. Due to the parabolic flow profile of the longitudinal flow, velocity decreases towards the walls. The smaller particles that move closer to the center of the flow channel travel faster and have shorter retention times as compared to larger particles. An ICP-MS detector can then be coupled to the AF4 to monitor the size distribution. The hydrodynamic diameter of particles can be calculated by either AF4 theory or by an external calibration curve using different sized NP standards (98). The mass concentration of particles can be determined by external calibration with NP standards, standard addition analysis, or by flow injection with dAg standards (20).

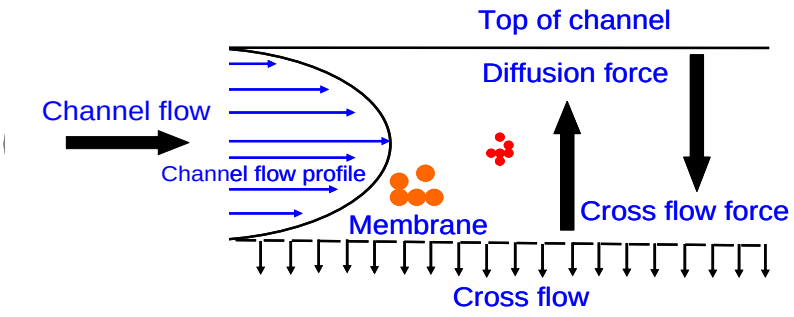


**Figure 1. 3.** Schematic illustrating AF4 principals. Diagram courtesy of Ehsaun Hoque.

AF4-ICP-MS has become one of the most common and promising methods for AgNP analysis (20, 99-105). Major advantages to AF4 are that it can provide a wide size range of separation (1 nm to 50 µm) (106), while hyphenation with ICP-MS offers elemental specificity and sensitivity to µg $L^{-1}$ detection limits (89). The method also has proven utility for studying dAg complexes, aggregation, and NP surface coatings (104). For example, AF4-ICP-MS has provided evidence of AgNP dissolution, in which the formation of dAg-complexes was inferred by detecting Ag at early retention times in the AF4 fractogram in the presence of proteins (104) and DOC (107). Analysis by AF4-ICP-MS also showed an increase in the size of AgNPs after a 28 day biological exposure, which was attributed to coating of the AgNPs with proteins and/or aggregation (105). AgNP coating with NOM (100) and sulfide (89) has also been observed using AF4-ICP-MS, and these coating were determined to decrease particle-membrane interactions, resulting in increased signal intensity.

Particle-membrane interactions remain the biggest challenge for AF4 analysis. It can result in poor recoveries due to analyte adsorption and also incorrect particle sizing due to delayed particle elution (98, 104). Recent studies have observed different retention times among similarly sized NPs as a result of different surface properties and thus, different attractive Van-Der-Waals forces between the NP and membrane (108, 109). AF4 methods thus require optimization, particularly for the cross-flow and mobile phase, to minimize particle-membrane interactions, while at the same time providing sufficient separation (110, 111). Furthermore, appropriate standards that adequately represent the studied particles are required (98, 108, 111, 112).

#### *1.2.5.4. single particle Inductively Coupled-Mass Spectroscopy (spICP-MS)*

Analysis of AgNPs using spICP-MS is an emerging analytical method that has demonstrated great utility for environmental monitoring. As described by Pace et al. (113) spICP-MS utilizes conventional ICP-MS instrumentation that can be used in single particle mode by changing analytical conditions. In traditional ICP-MS, the concentration of total Ag in a sample is calculated from the intensity of Ag ions that reach the detector over a long dwell time of 0.3-1 seconds. Conversely, spICP-MS can distinguish between AgNPs and dAg by operating with a short dwell time (i.e. <10 ms) and measuring each individual intensity reading over time. The dAg is distinguished as a continuous background signal because it is homogenously distributed within the sample. AgNPs (or its aggregates) are identified as a pulse in intensity above the background dAg as a cluster of $Ag^{+}$ ions that are generated in the nebulizer and reach the detector simultaneously. This analytical technique works on the fundamental assumption that each pulse represents a single AgNP and/or aggregate. The particle number concentration can be determined by the frequency of pulses and the particle size can be calculated from the signal intensity using an algorithm that relates intensity to particle size. The pulse intensity is related to particle size using dAg standards and the transport efficiency (Figure 1.4).

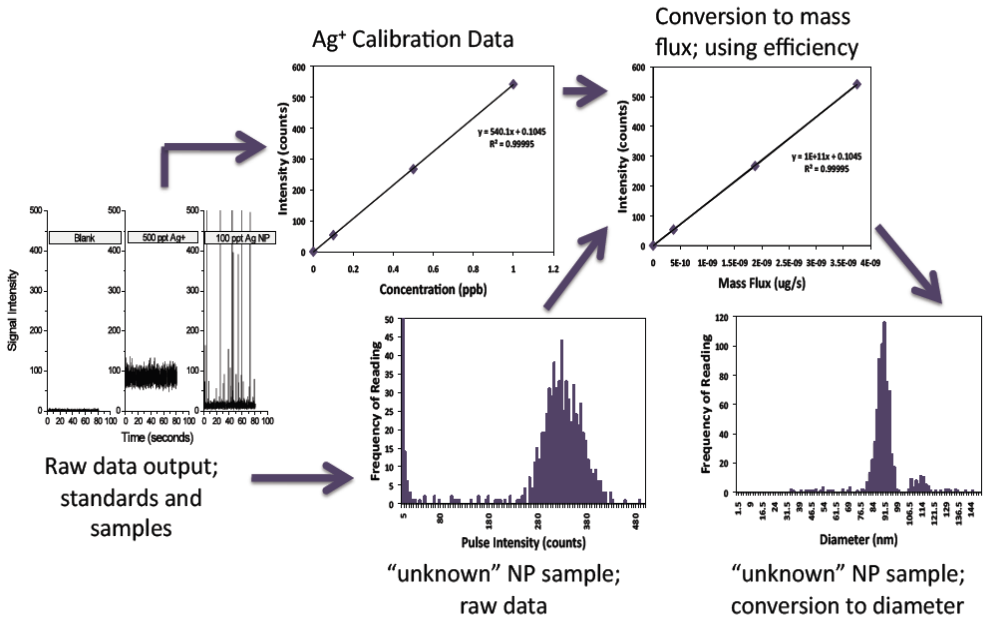


**Figure 1.4.** Data processing scheme for relating pulse height to nanoparticle (NP) diameter. Figure from Mitrano et al. (92).

As illustrated in Figure 1.4, the dAg standards result in a continuous signal and the relationship between intensity and concentration is used to produce a calibration curve. The dAg concentrations are converted to mass flux using the transport efficiency (accounts for differences in mass delivery of dAg verses AgNP). The "unknown" AgNP sample produces pulses of intensity about the background dAg and the frequency of readings is plotted against intensity. The pulse intensity in the histogram is converted to diameter using the mass flux calibration curve and the assumption that each AgNP has a spherical geometry.

The greatest advantage of spICP-MS is that is can provide detailed qualitative and quantitative information about different Ag forms, including the particle size distribution, mass concentration of dAg and AgNPs, and particle number concentration (114). Furthermore, it has detection limits for AgNP characterization (ng $L^{-}$) that are relevant for expected environmental concentrations (104). Compared to CPE, the method requires

little sample preparation beyond dilution of the sample so that particles in suspension pass individually through the ICP-MS nebulizer. Compared to AF4-ICP-MS, sp-ICP-MS offers rapid sample throughput, and little additional method development is needed for a given matrix or AgNP type because there is no potential for artefacts resulting from particle-membrane interactions (104). The largest limitation to the method is the size detection limit (115), in which the lowest AgNP size detected by spICP-MS has been ~20 nm (104, 114, 116). Overall, the method is not well established and there has been little application to AgNP analysis in complex matrices. (115). Some studies have used spICP-MS to analyze Ag in WWTP effluent (92, 116), but its efficacy for environmental fate studies and understanding AgNP transformations has yet to be demonstrated.

### 1.3 Conclusion

Understanding the environmental fate of AgNPs is an essential component for risk assessment, as its transformation products and movements within surface waters will greatly alter toxicity. AgNP transformations have mostly been evaluated under controlled laboratory conditions, where the effects of only one or two environmental factor(s) are studied at one time in attempt to predict environmental fate. There are two challenges with such studies for risk assessment. First, in natural environments, the presence of numerous physio-chemical conditions and organisms complicate an understanding of AgNP transformations. Second, laboratory studies are often only preformed in water and thus, cannot demonstrate the effect of these transformations on the distribution of AgNPs in the environment among biotic and abiotic compartments, such as suspended particles, periphyton, and sediment. A comprehensive study is needed that illustrates the environmental fate of AgNPs in a natural lake environment, with all of

the important environmental factors and compartments. Furthermore, the effect of AgNP surface coating (i.e. PVP vs. CT) and concentration on environmental fate has yet to be investigated in a natural aquatic environment.

Mesocosms, which are enclosures placed in natural environments, allow studies to be preformed under more realistic conditions than laboratory studies (117). Recent reviews have highlighted the need for research on AgNPs using mesocosms experiments to better simulate environmental conditions (3, 8). Although a few mesocosm studies have been preformed with AgNPs (118, 119), these studies were conducted using unrealistically high AgNP concentrations (mg $L^{-1}$). One reason for this is that the majority of the developed analytical methods available to quantify AgNPs and their associated transformations have very high detection limits. Over recent years, there have been significant advances to develop more sensitive techniques (i.e. spICP-MS, CPE, AF4-ICP-MS) that show promise for AgNP analysis. However, they have had limited application in environmental fate studies. Finally, given the uncertainties of different analytical methods a variety of different analytical techniques should be preformed when evaluating AgNP transformations to validate results and to compensate for the limitations associated with each method (120).

### 1.4. Research Objectives and Predictions

The primary objective of this research was to evaluate the fate of AgNPs in natural waters using studies with lake mesocosms. The specific aims were to:

1) Determine the persistence, transformations (i.e. agglomeration, dissolution), and distribution of AgNPs in mesocosms dosed using continuous additions over time, designated as “drip” mesocosms (Chapter 2). A secondary objective was to evaluate

the effect of loading (i.e. amount) and type of surface coating (i.e. PVP, citrate) on the fate of AgNPs. The predictions for this chapter were:

a) AgNPs will not accumulate in water column over time due to quick dissipation from the water column to other environmental compartments (i.e. sediment and periphyton).

b) PVP-AgNPs have reduced agglomeration and increased particle persistence as compared to CT-AgNPs

c) PVP-AgNPs have greater dissolution than CT-AgNPs

d) Increased AgNP loading results in higher rates of agglomeration

e) Decreased AgNP loading results in higher proportion of dissolution

f) AgNPs accumulate in the environment in a dose-dependent manner

2) Determine the persistence, transformations (i.e. agglomeration, dissolution), and distribution of AgNPs in mesocosms dosed using a single addition, designated as "plug" mesocosms (Chapter 3). In order to conduct these studies, various analytical techniques were applied to characterize transformations of AgNPs. The predictions for this chapter were:

a) AgNPs will quickly dissipate from the water column to other environmental compartments over time (i.e. sediment and periphyton).

b) AgNP agglomeration in natural waters includes both hetero- and homoagglomeration and leads to larger particle sizes

c) AgNPs will dissolve over time and release Ag+, which leads to smaller particle sizes

d) Released Ag+ will complex with other ligands (i.e. DOC) found in natural waters

# Chapter 2: Effect of Loading Rate and Surface Coating on the Fate of Silver Nanoparticles in Lake Mesocosms

## 2.1 Introduction

Silver nanoparticles (AgNPs) are increasingly being used in consumer products due to their antibacterial properties, raising concerns about the potential impacts of these materials when released into the environment. Life cycle analysis and modelling studies indicate that AgNPs can enter surface waters through discharges of municipal or industrial wastewater (5, 6). AgNP toxicity has been reported for a variety of aquatic organisms, including bacteria (32), zooplankton (25), algae (27), and fish (34). However, insufficient knowledge of AgNP fate in aquatic systems has made it challenging to assess the impacts of this emerging contaminant in natural waters.

Physical and chemical transformations will influence the distribution and toxicity of AgNPs in aquatic environments. AgNPs can persist as stable particles in nanoform or agglomerate with other particles, leading to sedimentation (61, 74). Homoagglomeration with other AgNPs or heteroagglomeration with natural organic material are important fate processes (51). In oxic environments, dissolution may also occur through the release of $Ag^{+}$ from the AgNP surface (54), increasing the potential for toxicity from exposure to the free ion (45, 70). The extent of these transformations depends on a variety of factors. Site-specific physiochemical conditions such ionic strength (54), DOC (62, 74), pH (68), dissolved oxygen (DO) (68, 121), temperature (68, 70) and light (59) may affect agglomeration and dissolution. Particle-specific properties, such as surface coating, can also affect AgNP stability (55, 70, 71, 84). Furthermore, AgNP concentration may also affect agglomeration (62) and dissolution rates (71).

AgNP transformations have been evaluated primarily under controlled laboratory conditions that manipulate only one or two environmental factors. These results may not predict the fate and behaviour of AgNP in natural environments, where numerous physiochemical and biological factors interact and vary temporally. Mesocosm studies provide more realistic experimental conditions and address the need for research that better simulates natural conditions (8, 117). Mesocosms have been used previously to evaluate the fate of AgNPs in estuarine (119) and wetland (118) environments. However, these studies used a single application of AgNP at concentrations several orders of magnitude higher than estimated exposure levels in the low $\mu g\ L^{-1}$ or $ng\ L^{-1}$ range (4).

The objective of this study was to evaluate AgNPs environmental fate in lake mesocosms, including the effect of loading rate and surface coating, on the persistence, transformations, and distribution of the nanoparticles. Littoral mesocosms were dosed continuously with 1) polyvinylpyrrolidone AgNPs (PVP-AgNPs) at high (92.6 $\mu g\ L^{-1}$), medium (23.1 $\mu g\ L^{-1}$), and low (5.8 $\mu g\ L^{-1}$) concentrations and 2) citrate AgNPs (CT-AgNPs) at high concentrations. The persistence, agglomeration, and dissolution of AgNPs were monitored by size fractionation using filtration. The distribution of AgNPs within the lake environment was determined using an end of study mass balance of total Ag in the primary environmental compartments of water, particles, periphyton, and sediments.

## 2.2. Materials and Methods

### *2.2.1. Field Site*

The study was conducted at the Experimental Lakes Area (ELA) in northwestern Ontario, Canada (49°40'N, 93°44'W). The ELA is a research facility comprising a set of protected lakes and a field station which has been widely used to evaluate the effects of anthropogenic inputs to lakes though whole ecosystem manipulation and monitoring (122). The remote location allows for experimental manipulation without concern of background anthropogenic impacts. The mesocosm study was conducted in Lake 239 (L239), which is a small, oligotrophic, headwater lake on the Canadian Shield, surrounded by boreal forest. It has an area of 56 ha, maximum depth of 30 m and a mean depth of just over 10 m. This lake has been monitored for limnological parameters for over 50 years.

### *2.2.2. Mesocosms*

Ten littoral mesocosms were installed in a sheltered bay at the south end of the L239. The dimensions of the two mesocosms were 2 m in diameter and 1.5 to 1.7 m in depth, giving theoretical volumes of >5,000 L. However, because of evaporation and collapsing of the mesocosm walls, the actual volumes of water in the mesocosms were lower and declined over time. For the purposes of calculating a nominal dosing concentration, it was assumed that the mesocosms contained 4,000 L of water. Open-bottom mesocosms were suspended from a floating ring and sealed to the sediments with sandbags (Figure 2.1). The walls of the mesocosms were composed of impermeable polyethelyene (Curry Industries, Winnipeg, Manitoba, CAN). Thus, the only losses of water from the system were from evaporation, sample withdrawal, and exchange with sediment pore water. The mesocosms were installed one week before dosing to allow for

settling of any particulate material that was re-suspended during installation. The exact volume of each mesocosm was determined at the end of the study by adding 12.31 g of NaCl and measuring the resulting concentration of $Cl^-$ using a chloride ion selective electrode.

**Figure 2.1.** Aerial view of 12 mesocosms installed in L239 (left) and the design of the littoral mesocosm (right).

### *2.2.3. Silver Nanoparticle Material*

The AgNPs used in this study were described by the supplier (NanoComposix, San Diego, CA) as 50 nm CT capped and 50 nm PVP capped material. The stock solutions of PVP-AgNPs and CT-AgNPs were in aqueous suspensions of milliQ water and 2 mM citrate buffer, respectively, with nominal concentrations of 1.0 mg Ag $mL^{-1}$. Acid digestion and inductively coupled plasma-mass spectroscopy (ICP-MS) analysis verified that the concentration of the stock solutions was 0.96 mg Ag $mL^{-1}$ for PVP-AgNPs and 1.02 mg Ag $mL^{-1}$ for CT-AgNPs. Ultrafiltration using 3 kDa Amicon Ultra-4 centrifugal filtration (Millipore Inc.) indicated that 2.5% and 2.4% of the total Ag mass was comprised of dissolved Ag (dAg) for PVP-AgNPs and CT-AgNPs, respectively, which was assumed to be $Ag^{+}$. Accompanying size information provided by the supplier indicated that the AgNPs were monodispersed (Table 2.1).

**Table 2.1.** Size and surface charge (i.e. Zeta Potential) information determined by transmission electron microscopy (TEM) and Dynamic Light Scattering (DLS) provided by the supplier for the two AgNP material used in the mesocosms.

| AgNP | Diameter (TEM) | Hydrodynamic Diameter (DLS) | Zeta Potential (DLS) |
|---|---|---|---|
| **50 nm PVP** | 48.3 nm | 56.3 nm | -36.9 mV |
| **50 nm CT** | 49.1 nm | 54.9 nm | -55.9 mV |

### *2.2.4. Treatments*

The loading type used in this study was designated as "drip" in which CT- and PVP-AgNPs were added to mesocosms every other day. Treatments were designed to investigate: 1) the effect of surface coating (high PVP drip vs. high CT drip), and 2) the effect of loading rate (low, medium, high drip PVP). Each treatment was replicated twice, along with two controls to which no AgNPs were added. Dosing occurred over a time period of 51 days to obtain a cumulative, nominal concentration at the end of the study of 5.8, 23.1, 92.6 μg $L^{-1}$ for low, medium, and high drip treatments, based on a nominal volume of 4000 L.

Dosing began on June 23$^{rd}$, 2012 and ended on August 12$^{th}$, 2012. For each dosing, 14.24 mL (high drip), 3.56 mL (medium drip), or 0.89 mL (low drip) of AgNP stock solution were added to each mesocosm approximately 10 cm below the surface of the water. The AgNPs were mixed throughout the water column using a vertical haul of a plastic disk ~45 cm in diameter. Care was taken not to disturb the sediments during mixing.

### *2.2.5. Water Chemistry*

The temperature, conductivity, and DO were measured at three different depths of the water column in each mesocosm (surface, 1 m, and just above sediments) prior to

each sampling using a multiparameter probe (YSI30-25FT, YSI Inc., Yellow Springs Ohio, USA). Surface water samples were taken weekly and analyzed for pH using a ROSS Ultra® Electrode (Thermo Scientific) and DOC concentration using an O.I. Analytical 1030D carbon analyzer (Xylem Scientific, Graden Instruments, Oakville, ON, CAN). Near the beginning of the study (July 2nd, 2012) mesocosm water was analyzed for major inorganic anions by ion chromatography (Dionex ICS-1100, Thermo Scientific, Bannockburn, IL, USA; EPA Method 9056A) and for major inorganic cations by flame atomic adsorption spectrophotometry (Varian FS240, Varian Inc., Walnut Creek, CA, USA; EPA Method 7000B).

### *2.2.6. Sample Collection*

Water, suspended particles, periphyton on the mesocosm walls, and sediments were sampled from each mesocosm. Water and sediment (0-3 cm depth) were sampled before the study to determine background concentrations of Ag. Following the initial AgNP addition, water and particles were sampled on a weekly basis, whereas sediment and periphyton were only sampled at the end of the study.

*2.2.6.1. Water and Particles:* At the center of each mesocosm, the water column was well mixed with a disk before sample collection. A volume of 8 L of water was collected from ~10 cm below the surface and pre-filtered through a 35 µm mesh to remove macroplankton and detritus (referred to from here on as unfiltered water). The collected water was then sequentially filtered into different fractions. Each fraction was operationally defined to represent different forms and species of AgNP and ionic silver (Table 2.2).

**Table 2.2.** Operationally defined forms of Ag in various fractions of filtration. The associated Ag components in each fraction are indicated.

| Fraction | Form of Ag | Hetero-agglomerated AgNPs/Ag+ (i.e. algae and bacteria) | Homo-agglomerated AgNP (>200 nm) | Free AgNP (200-50 nm) | Complexed Ag+ (i.e. Ag-DOC, AgCl) | Free Ag+ |
|---|---|---|---|---|---|---|
| Unfiltered water | Total Ag | ✓ | ✓ | ✓ | ✓ | ✓ |
| 0. 2 µm retentate | Particulate Ag | ✓ | ✓ | | | |
| 0.2 µm filtrate | Colloidal/ Dissolved Ag | | | ✓ | ✓ | ✓ |
| 3 kDa filtrate | Dissolved Ag | | | | ✓* | ✓ |

* Only small molecular weight complexes less than 1-2 nm in size. i.e. AgCl or Ag associated with small organic molecules that are part of the fulvic acid fraction.

A 40 mL sub-sample of unfiltered water was collected into 50 mL falcon tubes (BD Biosciences, Mississauga, ON, CAN) for total silver (TAg) analysis. A 300-500 mL sub-sample of unfiltered water was filtered through a 1.2 µm pre-filter (47 mm, Millipore, Billerica, MA, USA), and then through a 0.2 µm polycarbonate membrane. Then, a 40 mL subsample of the 0.2 µm filtrate was transferred into a 50 mL falcon tubes for colloidal/dissolved Ag analysis. Subsequently, a 40 mL aliquot of the 0.2 µm filtrate was processed through a 3 kDa ultrafiltration (regenerated cellulose) membrane using a 200 mL Amicon® stirred cell ultrafiltration unit (Millipore, Billerica, MA, USA) to isolate dissolved Ag (dAg). A 40 mL sub-sample of the 3 kDa ultrafiltrate was transferred into 50 mL falcon tubes to analyze the amount of dAg in the water phase fraction. Unfiltered water, 0.2 µm filtrate, and 3 kDa filtrate samples were immediately acidified with trace-metal grade nitric acid ($HNO_3$) supplied by SCP Science (Baie-Durfe, QC, Canada) to a final concentration of 4 % (v/v). The 1.2 and 0.2 µm membranes were placed in 20 mL polypropylene scintillation vials with 20 mL of 4 % (v/v) $HNO_3$ (trace metal grade) for

particulate Ag analysis. All samples were stored at 4$^{o}$C until analysis. The average recovery of PVP- and CT-AgNPs (20 µg $L^{-}$) through the 0.2 µm membranes were 92% and 98%. The average recovery of $Ag^{+}$ (10 µg $L^{-}$) through the 3 kDa ultrafiltration membranes was 64%.

*2.2.6.2. Periphyton*: At the start of the experiment, two strips of polypropylene wall material (100 cm x 5 cm) were hung vertically in each mesocosm from a pipe that lay across the top of the flotation rings. Over time, strips were naturally colonized with periphyton that was assumed to represent periphyton on the mesocosm walls. At the end of the experiment, periphyton films were scraped from each strip and diluted with lake water. The resulting slurry was homogenized, and two sub samples from each strip were filtered through pre-weighed glass microfiber filters (Whatman GF/F, nominal 0.7 µm pore size). The GF/F filters were dried at 60$^{o}$C and weighed to determine the biomass of periphyton. Filters were stored frozen until Ag analysis. Any residual Ag that may have been adsorbed to mesocosm wall material was sampled by placing a 6 x 5 cm piece of cleaned strip into 40 mL of 4% $HNO_3$.

*2.2.6.3. Sediments:* Sediments were sampled from two locations in each mesocosm at the end of the experiment. An in-house built corer made of polycarbonate tubes (8 cm diameter) were used to collect intact sediment cores. Each core was sectioned into three layers (0-2 cm, 2-4 cm, 4-6 cm), which were stored frozen until analysis. Sediment cores were analyzed for bulk density, loss on ignition, and particle size. Bulk density was determined by drying each core to a constant mass at 60$^{o}$C, pulverizing the sample, and weighing the dried mass. For loss on ignition, one sub-sample of each dried core was heated at 400$^{o}$C for 10 hours. Particle sizing was preformed on two subsamples per core using a Horiba LA-950.

### *2.2.7. Silver determination*

All samples were analyzed for Ag using an X Series 2, Thermo Scientific ICP-MS (Nepean, ON, Canada). The methods used for samples from different environmental compartments are described below.

*2.2.7.1. Water and particulate samples*: Pre-acidified unfiltered water and 0.2 µm retentate samples were heated for six hours at 70$^{o}$C prior to ICP-MS analysis to ensure all Ag was released from suspended material. The Ag in unfiltered water, 0.2 µm filtrate, 0.2 µm retentate, and 3 kDa ultrafiltrate samples were measured against an external calibration curve using standard solutions of Ag (SCP Science, Baie-Durfe, Quebec, Canada). The calibration curve was prepared by serial dilution using 4 % (v/v) $HNO_3$ in milli-Q water and ranged from 0.78 -200 µg $L^{-}$. An aliquot of indium standard solution (SCP Science, Baie-Durfe, Quebec, Canada) was added to each sample (5 µg L-1) as an internal standard to correct for changes in sensitivity and non-spectral inferences during analysis. Data on $^{107}$Ag and $^{115}$In were acquired in steady state mode. Detection limits were determined from each set of water samples analyzed from blank samples. Blank samples consisted of milliQ water acidified to 4% $HNO_3$ with 5 µg $L^{-}$ of indium. The average limit of detection (LOD) (3*SD) was 0.02 ± 0.01 and the average limit of quantification (LOQ) (10* SD) was 0.07 ± 0.05 µg $L^{-}$.

*2.2.7.2. Sediment and periphyton sample*s: Total Ag in sediment and periphyton samples were analyzed by strong-acid digestion with isotope dilution (123). Prior to digestion, each sample was enriched with an aliquot of a stable Ag isotope ($^{109}$Ag) as an internal standard. For sediment samples, 1 g of dry material (3 sub-samples per core) was digested according to procedure modified from EPA Method 3050B. The digestion was preformed in 40 mL glass vials by adding 10 mL of concentrated $HNO_3$ ($cHNO_3$) with

reflux at 120ºC for 2 hours, an additional 5 mL of conc. $HNO_3$ with reflux at 120 ºC for 2 hours, and 3 mL of conc. $H_2O_2$ with reflux for 2 hours. After digestion, the volume of the sediment digestate was reduced to <4 mL and re-constituted to 40 mL using milliQ water so that the final acid concentration was less than 10%. Sample were thoroughly mixed and left overnight to allow residual particulates to settle to the bottom. For periphyton samples, filters (2 sub-samples per strip) were digested with 20 mL of c$HNO_3$ in 40 mL glass vials and heated at 120$^{o}$C until the samples lost their color (~6 hours). After digestion, the periphyton samples were re-constituted to 40 mL using milliQ water. The undigested GF/F filters were subsequently removed and the vial was left overnight to allow any remaining filter particulates to settle to the bottom. An aliquot of each periphyton sample was additionally diluted 10x before ICP-MS analysis.

Mass traces for $^{107}$Ag and $^{109}$Ag were acquired in steady state mode and the recovery of $^{109}$Ag in each sample was used for total Ag quantification. Blanks and reference material were analyzed with each batch of samples. The average recovery of Ag from a standard reference material of sediment (NIST SRM 1994 New York/ New Jersey Waterway sediment) was 6.5 ± 0.2 mg/kg, which was similar to the certified concentration values (6.4 ± 1.7 mg/kg) (SI Table 2.1). There are no available standard reference materials of periphyton, so instead a standard reference material of oyster tissue (NIST #1566b) was used. The average Ag recovered was 0.522 ± 0.005 mg/kg and was lower than the certified concentration values (0.666 ± 0.009 mg/kg). The reliability of the methods was further verified with analysis of spiked Ag onto L239 sediment and GF/F filters, in which recovery was 100% for GF/F filters and ranged from 100-123% for

sediment (SI Table 2.2). The LOD for sediment and periphtyon analysis were 7 ng and 51 ng, respectively (3*SD of blanks).

### *2.2.8. Statistical Analysis*

Linear regression of silver concentrations over time in the mesocosms were performed for each Ag fraction (unfiltered water, 0.2 µm filtrate, and 0.2 µm retentate) to test for changes in Ag concentration over time. All variables were $\log_{10}$ transformed to optimize linearity and normality of the relationship. No regression analysis was performed on the 3 kDa ultrafiltrate fraction due to the large percentage of values below quantification limits. For each fraction, an analysis of covariance (ANCOVA) was performed to test for differences in slopes (temporal patterns) and intercept (concentration) among mesocosms with: 1) different loading rates (i.e. low, medium, vs. high drip) and 2) different surface coatings (i.e. CT high drip vs. PVP high drip). The Shapiro-Wilk Test was used to test the normality of residuals ($\alpha$=0.05) and the Levene's Test for Variance ($\alpha$=0.05) was used to test for constant variance amongst groups. Tukey's multiple comparisons procedure was preformed to determine if there were differences in the least square means ($\alpha$=0.05) of regression lines. ANCOVA was preformed using JMP10 statistical software.

Statistical differences between the two sediment cores from each mesocosm were assessed using a Student's t-test ($\alpha$=0.05). The sub-samples from the two sediment cores from each mesocosm were then combined (n=6). For periphyton, statistical differences between two mesocosm strips were assessed using a Mann-Whitney Rank Sum Test ($\alpha$=0.05). The sub-samples from each mesocosm were then combined (n=4). Statistical differences in sediment and periphyton concentraions among mesocosms with different

loading rates and different surface coatings were tested using ANOVAs. All concentration data was log transformed to improve normality and equal variance. Tukey's multiple comparisons procedure was preformed to determine if there were differences between mesocosms ($\alpha$=0.05). Student t-test and ANOVA analysis were preformed in SigmaStat statistical software.

A mass balance for Ag at the end of the study was calculated for each of the mesocosms. The mass balance had four components: 1) Ag in water (colloidal Ag) 2) Ag on particles (particulate Ag) 3) Ag in periphyton 4) Ag in sediment. The % Ag recovered in each mesocosm was determined by the following equation (refer to SI p.111 for detailed calculations):

$$\%\ Ag\ recovered = \frac{Ag\ in\ water\ + Ag\ in\ particles + Ag\ in\ sediment + Ag\ in\ periphyton}{Cumulative\ Ag\ added}$$

## 2.3. Results

### *2.3.1. Water Chemistry*

DO levels did not vary with depth and the entire water column was oxic throughout the study, with DO levels of 7-8 mg $L^{-1}$ (SI Table 2.3). Temperature increased over the duration of the study from 21°C to 24°C, with the surface 2-3°C warmer than the bottom (SI Table 2.4). Conductivity was similar in all mesocosms (~~31-37 µS $cm^{-1}$), with a gradual increase over time (SI Table 2.5). The pH in the mesocosms varied from 6.8-7.4 (SI Table 2.6). Ionic strength was low in all mesocosms (SI Table 2.7). DOC ranged from 7-10 mg $L^{-1}$ (SI Table 2.8).

### *2.3.2. Total Silver*

TAg concentrations in unfiltered water from each mesocosm were monitored over time to evaluate the persistence of Ag in each treatment. TAg increased incrementally over time in mesocosms which received multiple additions of AgNPs (Figure 2.2). Loading rate had a significant effect on the persistence of Ag in the water column (ANCOVA, $p<0.01$), with final TAg concentrations of 1.7-2.4 μg $L^{-1}$ for the low drip PVP, 8.2-8.7 μg $L^{-1}$ for the medium drip PVP, and 35.4-40.2 μg $L^{-1}$ for the high drip PVP treatments. Concentrations were similar among replicates of the same treatment (Tukey's analysis of LS means, $p>0.05$ between treatments). The final TAg concentration increased approximately 4x among increasing loading rate treatments, which matched the increase in the total mass of AgNP added to each treatment. However, TAg accumulated at the same relative rate over time in each mesocosm, regardless of loading (ANCOVA, $p = 0.676$). The results from the regression and ANCOVA analysis are summarized in SI Table 2.9 and SI Table 2.10.

The effect of surface coating on the accumulation of TAg was unclear due to variation among replicate mesocosms of the same treatment (Figure 2.2). TAg accumulated at the same rate in each mesocosm regardless of surface coating (ANCOVA, $p = 0.098$). However, the final TAg concentration accumulated differed between the two CT-AgNP replicates, with one CT-AgNP mesocosm having significantly lower TAg concentration compared to the other CT-AgNP replicate and one PVP-AgNP high drip mesocosm (ANCOVA, $p < 0.02$).

Despite net accumulation over time in all drip treatments, Ag was continually being removed from the water column throughout the duration of the study. TAg measured in the mesocosms was always less than the cumulative amount of Ag added

(Figure 2.3). The concentrations measured at the end of the study were 30-40% of the nominal target concentrations.

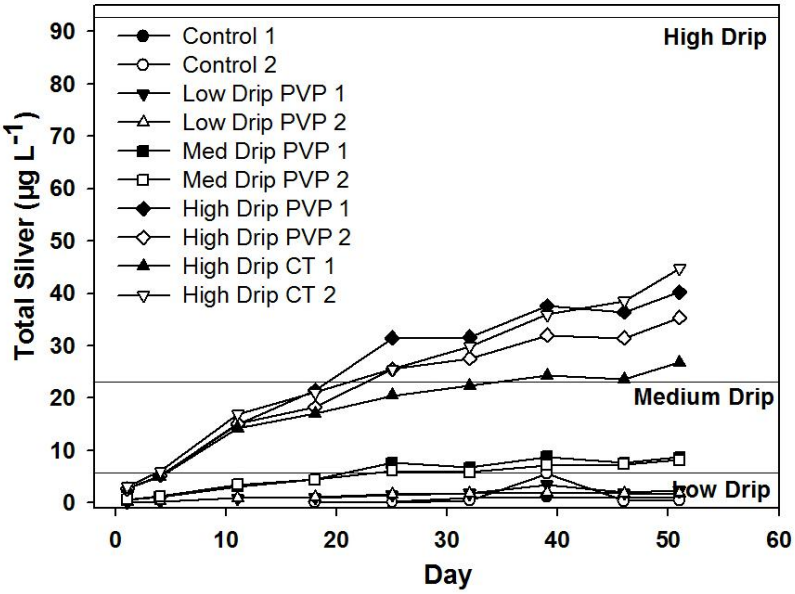


**Figure 2.2.** TAg concentration (µg $L^{-1}$) in drip mesocosms over time. Reference lines show target concentration based on theoretical mesocosm water (4,000 L).

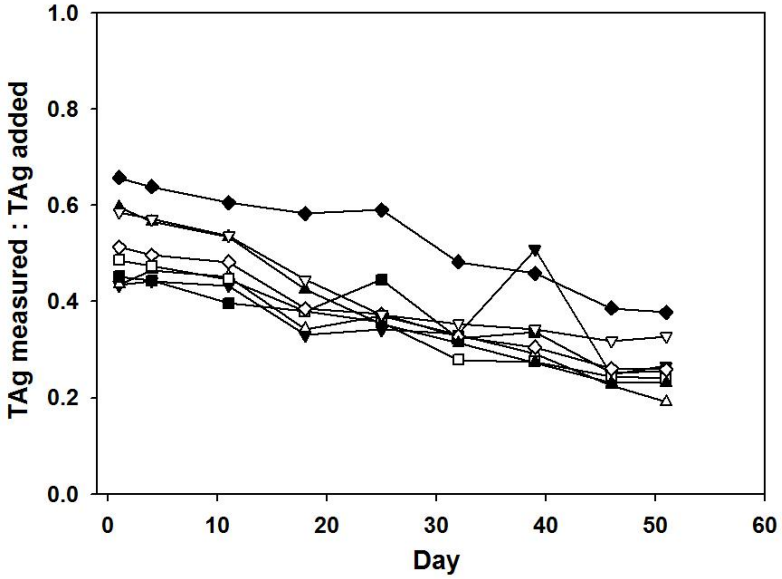


**Figure 2.3.** Proportion of TAg measured (µg) to the cumulative TAg added (µg) over time. The mass of TAg was determined using the measured mesocosm volumes determined at the end of the study (SI Table 2.13).

### *2.3.3. Colloidal and Particulate Silver*

Mesocosm water was filtered through a 0.2 µm membrane and the Ag concentration in the filtrate and retentate was measured in attempt to distinguish between Ag present in the colloidal and the particulate phase, respectively. Ag concentraions in the particulate phase are indicative of agglomeration; while the colloidal fraction may include $Ag^{+}$ complexed to DOC or inorganic ligands, as well as AgNPs. Colloidal Ag generally increased over time; whereas, particulate Ag increased for the first 18 days of the experiment and then fluctuated for the remainder (Figure 2.4). Loading rate had a significant effect on Ag accumulation in both the colloidal and particulate fractions (ANCOVA, $p<0.01$). Concentraions of colloidal Ag at the end of the study were: 0.7-0.9, 3.5-6.2, and 23.9-24.8 µg $L^{-1}$ for low, medium, and high drip PVP, respectively. Concentraions of particulate Ag at the end of the study were 1.0-1.4, 2.6-4.9, 18.2-30.9 µg $L^{-1}$ for low, medium, and high drip PVP, respectively. Concentrations were similar among replicates of the same treatment (Tukey's analysis of LS means, $p>0.05$ between treatments).

Although loading rate affected the amount of Ag accumulated, the accumulation rate was similar in both particulate (ANCOVA, $p=0.643$) and colloidal (ANCOVA, $p=0.655$) fractions among loading rates. Ag also accumulated at the same rate among PVP and CT high drip mesocosms in the colloidal (ANCOVA, $p=0.968$) and particulate (ANCOVA, $p=0.404$) fractions. Furthermore, concentrations were similar among all high drip PVP and CT mesocosms for both colloidal Ag (ANCOVA, $p=0.919$) and particulate Ag (ANCOVA, $p=0.175$). Some of regression lines used in the ANCOVA for the 0.2 µm filtrate analysis had residuals that did not pass normality (i.e. Low Drip PVP 2 ($p=0.03$),

Med Drip PVP 2 (p=0.02), CT 1 (p=0.04). However, the ANCOVA is robust to violations of normality (124).

Colloidal Ag concentration decreased sharply from days 11 to 18 in all drip mesocosms (Figure 2.4). This decline was accompanied by a sharp increase in the particulate Ag concentration during the same time period. The percentage of TAg found in both the filtrate and the retentate also this trend across all mesocosms, regardless of treatment (Figure 2.4). Combined, the TAg found in the retentate and filtrate added up to 99 ± 7 % of the TAg measured in the unfiltered water.

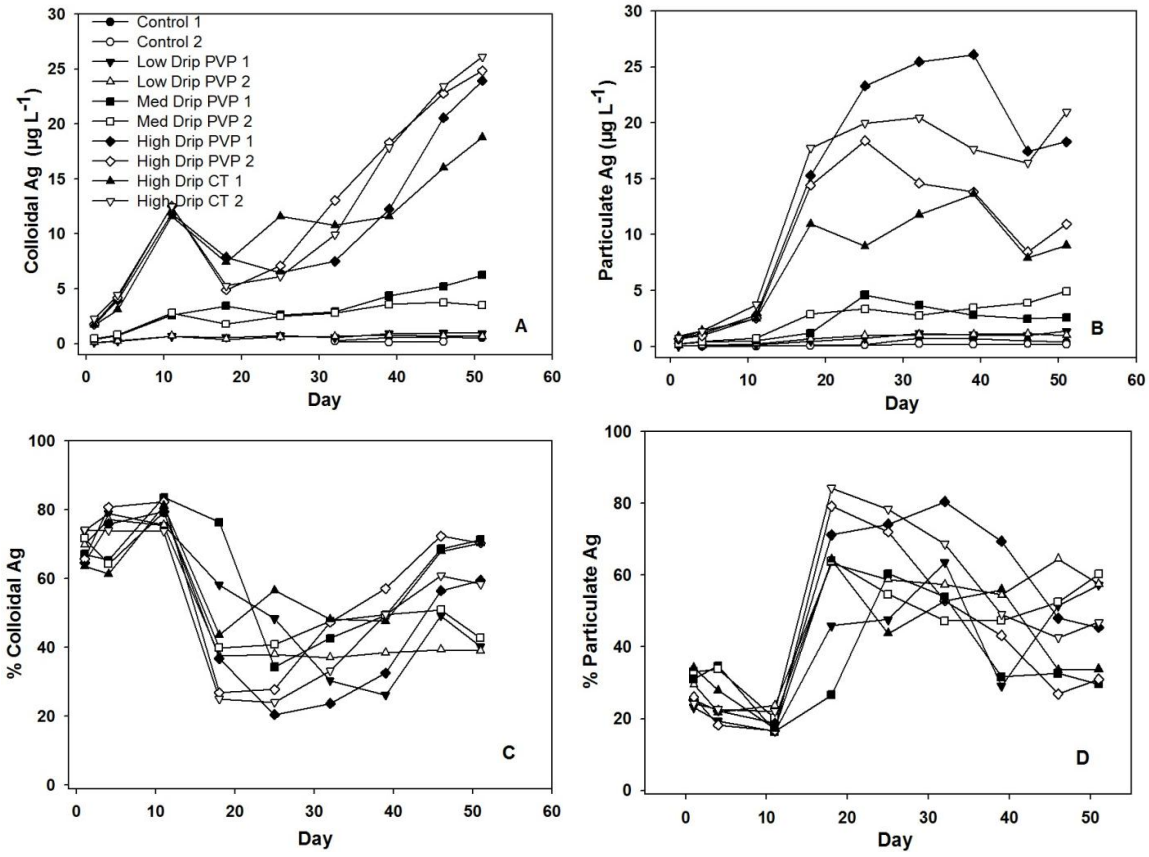


**Figure 2.4.** Concentration of (a) colloidal Ag and (b) particulate Ag in drip mesocoms over time. Percentage of measured TAg found in the (c) colloidal and (d) particulate fractions over time.

### *2.3.4. Dissolved Silver*

The 0.2 µm filtrate from each mesocosm was filtered through a 3 kDa membrane to quantify the dAg fraction, including $Ag^+$ that was present in the mesocosms. Overall, very little dAg was detected in the 3kDa ultrafiltrate (Table 2. 3). In the low drip and medium drip PVP treatments, dAg concentrations were below the limit of detection (<LOD) or limit of quantification (<LOQ) throughout the entire study, except for a few instances. In the high drip PVP and CT mesocosms, dAg was consistently detected after 39 days, with concentrations generally less then 1 µg $L^{-1}$. The dAg concentrations in the high drip mesocosms were variable through time and between replicates, and as a result, there were no differences between the dissolution rates for CT- and PVP-AgNPs. The results for the control samples were not reliable due to operational errors in setting up the ultrafiltration equipment for each time point and/or contamination of the filtration unit (i.e. control samples were always prepared first); therefore these data are not shown.

**Table 2. 3.** Dissolved Ag concentrations (µg $L^{-1}$) in drip mesocosms over time

| **Treatment** | **Low Drip PVP** | | **Med Drip PVP** | | **High Drip PVP** | | **High Drip CT** | |
|---|---|---|---|---|---|---|---|---|
| **Day** | **1** | **2** | **1** | **2** | **1** | **2** | **1** | **2** |
| **1** | <LOD | <LOD | <LOD | <LOD | <LOD | <LOD | <LOD | <LOD |
| **4** | <LOD | <LOD | <LOD | <LOD | <LOD | <LOD | <LOD | <LOD |
| **11** | <LOD | <LOD | <LOD | <LOD | 0.04 | <LOD | 0.12 | <LOD |
| **18** | <LOD | <LOD | <LOD | <LOD | 0.14 | <LOD | 0.08 | <LOD |
| **25** | <LOD | <LOD | <LOD | <LOD | 0.04 | <LOD | 0.05 | <LOD |
| **32** | <LOD | 0.04 | <LOQ | <LOQ | <LOD | <LOQ | 0.06 | 0.05 |
| **39** | 0.05 | <LOQ | <LOQ | <LOQ | 0.12 | 0.05 | 0.37 | 0.11 |
| **46** | <LOQ | <LOD | <LOD | 0.07 | 0.09 | 0.09 | 0.18 | 0.24 |
| **51** | <LOQ | <LOD | 0.06 | <LOQ | 3.41 | 0.76 | 0.15 | 0.24 |

### *2.3.5. Ag in Sediment*

The mesocosms contained sandy loam, organic poor sediment (loss on ignition <4 %) with bulk densities varying from 0.18-0.62 g $cm^{-3}$ (SI Table 2.11). The varying bulk density could have also been an artefact of the sampling, as the top layers were sandy and difficult to section. Ag concentrations (ng $g^{-1}$) in the 0-2 cm sediment horizon were not statistically different between cores taken from the same mesocosm, except for the low drip PVP mesocoms and high drip CT mesocosm replicate 2 (t-test, $p<0.05$). However, these differences may have been the result of varying bulk densities as there were no statistical differences in these cores when comparing concentrations as ng $cm^3$. Ag concentrations were highest in first 2 cm of sediment, and then decreased with depth (Figure 2.5).

Loading rate had a significant effect on the Ag concentration accumulated in the 0-2 cm sediment horizon (ANOVA, Tukey's, $p<0.05$), with values of 0.419 ± 0.045 and 0.250 ± 0.012 µg $g^{-1}$ for control mesocosms, 0.526 ± 0.173 and 0.595 ± 0.185 µg $g^{-1}$ for low drip PVP mesocosms, 1.101 ± 0.238 for medium drip mesocosm 1, 2.803 ± 1.002 and 3.140 ± 0.856 µg $g^{-1}$ for high drip PVP mesocosms (Figure 2.5). However, Ag concentrations were similar between the control 1 mesocosm and both low drip PVP 1 ($p=0.374$) and low drip PVP 2 ($p=0.878$) mesocosms. This may be a result of Ag contamination found in the control 1 mesocosm. When comparing surface coating, high drip CT treatments had concentrations of 5.304 ± 0.158 and 5.214 ± 0.796 µg $g^{-1}$, which were signifigantly higher than both high drip PVP replicates (ANOVA, Tukey's, $p<0.05$). Concentrations were similar among replicates of the same treatment (ANOVA, Tukey's test, $p>0.05$), except for the control mesocosms ($p=0.025$). The ANOVA comparing

loading rates did not pass equal variance, but but was close (Levene medium test, p=0.41) and had equal sample sizes so the test was accepted

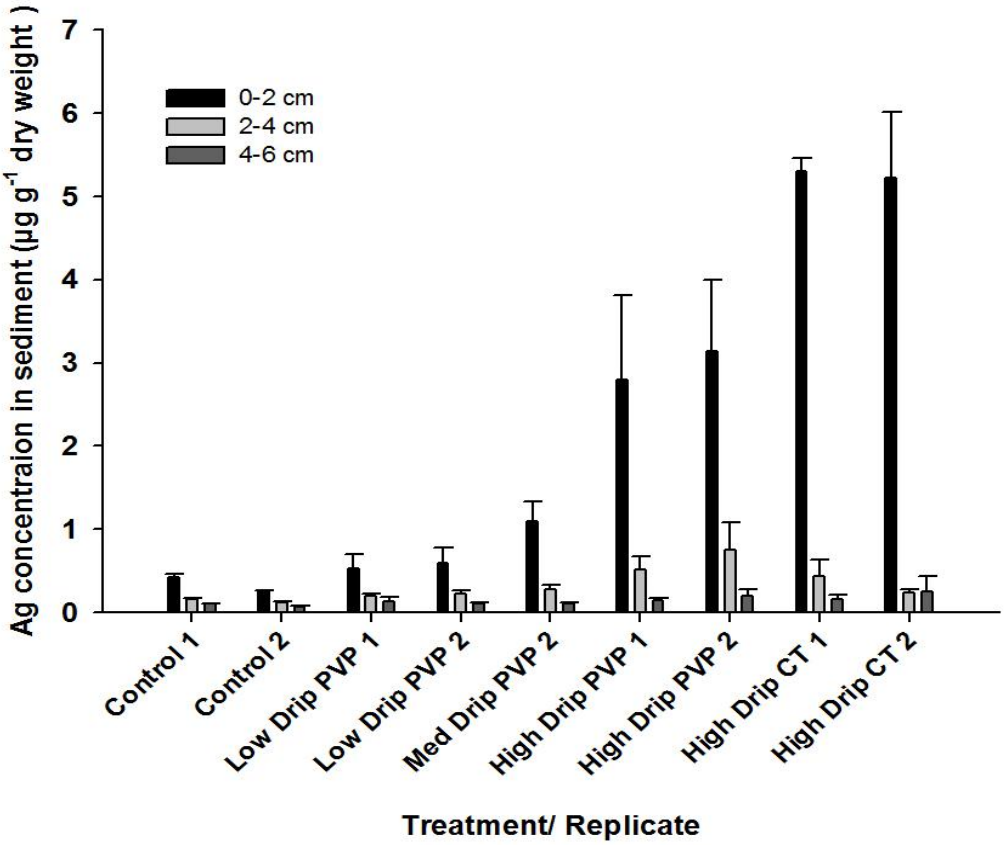


**Figure 2.5.** Total Ag concentrations at various depths in cores of mesocosm sediments (µg per $cm^3$ of dry sediment). Mean concentrations from two cores per mesocosm are presented, in which each core was sub-sampled 3 times for replicate Ag analysis (n=6). Both cores from Medium Drip PVP 2 and one core from High Drip CT 1 were removed from the data set due to inconsistent results SI Table 2.12.

### *2.3.6. Ag in Periphyton*

Ag concentrations in periphyton harvested from the mesocosm walls were measured at the end of the study from two strips suspended in each mesocosm (Figure 2.6). Ag concentrations were not statistically different between strips taken from the same mesocosm (Mann-Whitney Rank Sum Test, p>0.33). Ag loading rate had a significant effect on the Ag concentrations in periphyton (ANOVA, Tukey's test,

$p<0.05$), with values of 136 ± 16 and 37 ± 9 µg Ag $g^{-1}$ for control replicates, 177 ± 9 and 283 ± 28 µg Ag $g^{-1}$ for low drip PVP replicates, 628 ± 58 and 829 ± 94 µg Ag $g^{-1}$ for medium drip PVP replicates, and 3536 ± 371 and 3412 ± 209 µg Ag $g^{-1}$ for high drip PVP replicates. However, Ag concentration were similar in the low drip 1 and control 1 mesocosms ($p=0.082$). When comparing surface coating, high drip CT treatments had concentrations of 2282 ± 129 and 2593 ± 371 µg Ag $g^{-1}$, which were significantly lower than high drip PVP treatments ($p<0.05$). Concentrations were similar among replicates of the same treatment (ANOVA, Tukey's test, $p>0.05$), except for the control and low drip PVP treatments.

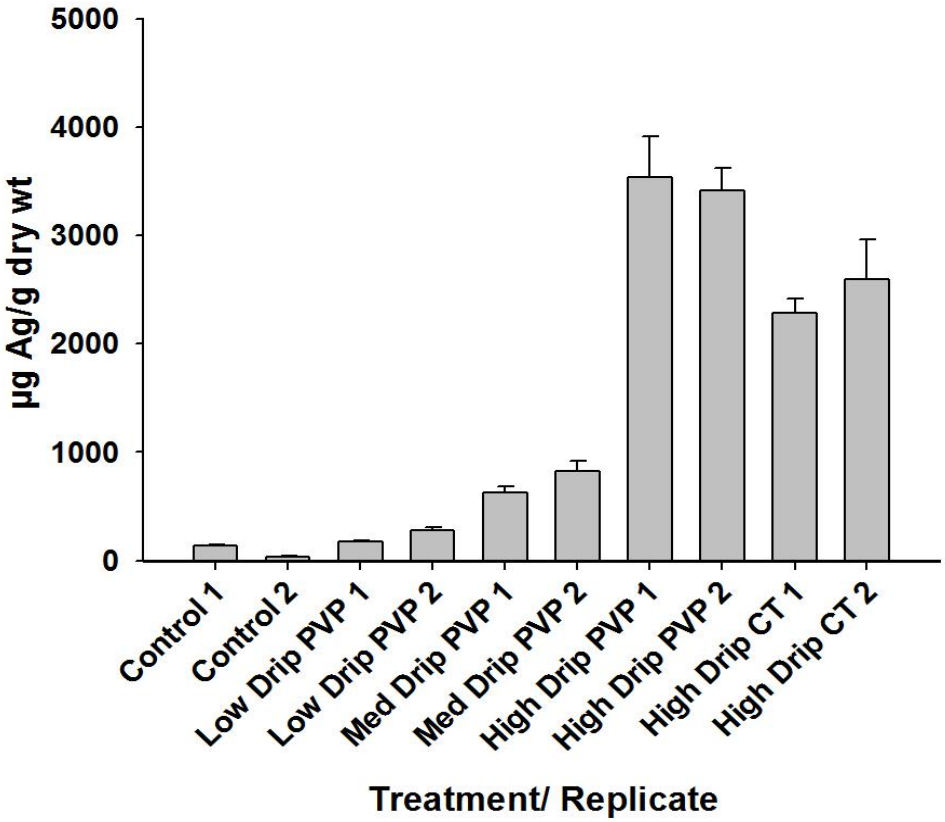


**Figure 2.6.** Total Ag concentration in periphyton harvested from mesocosm wall material (µg $g^{-1}$ dry weight). Mean values of two strips sub-sampled twice for Ag analysis are presented (n=4). The high drip PVP replicate 2 mesocosm only represents the results from one strip, as the other one was lost during sampling (n=2).

### *2.3.7. Ag Mass Balance*

The mass balance of Ag (%) in the main environmental compartments was calculated at the end of the study to evaluate the distribution of Ag within the lake environment. The environmental compartments analyzed were water (colloidal Ag), particles (particulate Ag), sediment, and periphyton on mesocosm walls. The Ag recovered amonst these environmental compartments ranged from 42-73% (Table 2.4). The mass balance is based on the measured water volumes in each mesocosm determined at the end of the study (SI Table 2.13). Generally, the proportion of total Ag sequestered in each compartment, in decreasing order, was the water column (water and particles) > sediment > periphyton. Almost no Ag (0.2 ± 1%) remained adsorbed to mesocosm wall material after periphyton was removed. The relative mass of Ag found in each environmental compartment showed no consistent trend with loading rate or between PVP- and CT-AgNPs.

**Table 2.4.** Ag mass balance determined at the end of the study. The range of recovery values for the periphtyon include low and high estimates of slurry volume as explained in SI p.111 Data for each sediment core (average ± sd of replicate Ag analysis; n=3) and each periphyton strip (average ± sd of replicate Ag analysis; n=2) is presented. n.a. = not analyzed.

| **treatment** | **Low Drip PVP** | | **Medium Drip PVP** | | **High Drip PVP** | | **High Drip CT** | |
|---|---|---|---|---|---|---|---|---|
| **replicate** | 1 | 2 | 1 | 2 | 1 | 2 | 1 | 2 |
| **Ag mass added (µg)** | 20 470 | | 81 880 | | 327 520 | | 327 520 | |
| | | | | **% Ag Added** | | | | |
| **water column** | | | | | | | | |
| **colloidal** | 11 | 8 | 19 | 11 | 24 | 19 | 17 | 20 |
| **particulate** | 15 | 11 | 8 | 14 | 17 | 8 | 8 | 15 |
| **periphyton** | | | | | | | | |
| **strip 1** | 4±0 - 10±0 | 7±1 - 15 ±2 | 7±0 - 15 ±0 | 8±0 - 18 ±0 | 4±0 - 10 ±0 | 4±2 - 10±1 | 3±0 - 8±0 | 3±0 - 7±1 |
| **strip 1** | 4±1 - 8±2 | 6 ±1- 14±1 | 5±0 - 10 ±1 | 5±0 - 10 ±1 | 8±0 - 18 ±0 | n.a | 4±0- 10±0 | 3±1 - 6±2 |
| **sediments** | | | | | | | | |
| **core 1** | 11±6 | 19±8 | n.a | 12±3 | 16±1 | 13±1 | n.a. | 21±2 |
| **core 2** | 24±3 | 37±6 | n.a | 18±3 | 18±6 | 19±4 | 27±1 | 20±3 |
| **total** | 41-60 | 45-71 | - | 42-61 | 61-77 | 44-56 | 55-62 | 58-63 |

## 2.4. Discussion

### 2.4.1. Persistence of Ag in the Water Column

The significant accumulation of total Ag over time (~30-40% of targeted levels) suggests that AgNPs were relatively stable and persisted in the tested lake environment. The AgNP persistence in our study is a result of both the high DOC levels and low ionic strength of L239 water, which stabilizes AgNPs (61). For example, Gao et al. (74) determined that TOC concentrations <10 mg $L^{-1}$ contributed to the increase in total Ag suspended in a water column, likely due to improved stability of AgNPs. In our study we found that TAg accumulated in the water column according to loading rate, however

loading rate did not affect the rate of TAg accumulation. The effect of surface coating on AgNP persistence was difficult to determine due to the variability between the two CT-AgNP replicates. We hypothesize differences in TAg concentrations among the high drip mesocosms may have been a result of varying mesocosm volumes as colloidal and particulate Ag analysis did not suggest differences in AgNP agglomeration and thus, particle stability.

**2.4.2. Differences in Agglomeration between Loading Rates and Surface Coatings**.

Neither loading rate nor surface coating influenced collidal and particulate Ag accumulation rate or percentage of Ag in these fractions, suggesting no treatment effects on agglomeration in our study. These results are not conistent with laboratory studies that have shown the rate of AgNP agglomeration increased with increased AgNP concentration due to greater particle-particle interactions (62). The results also contradict studies that have indicated PVP-AgNPs to have reduced agglomeration compared to CT-AgNPs as a result of the greater stability of steric interactions among PVP-AgNPs compared to electrostatic interactions among CT-AgNPs (55, 71, 83). We suggest that these discrepancies are explained by the low AgNP concentrations and the natural water matrix of the mesocosms.

The concentrations of AgNPs used in the present study were orders of magnitude lower than those used in many laboratory studies which have reported significant effects of concentration and surface coating. For example, Kennedy et al. (62) added 4 orders of magnitude more Ag to their treatments, even at the lowest concentration (500 mg $L^{-1}$ - 4,000 mg $L^{-1}$), which may explain why agglomeration increased with AgNP concentration due to more particle-particle interactions. Huynh and Chen (55) reported greater stability of PVP-AgNPs as compared to CT-AgNPs , but this study was

conducted with very high concentrations of AgNPs (>1,000 mg $L^{-1}$). In the present study in lake mesocosms, no difference in stability and agglomeration was observed across treatments, perhaps because interactions between particles were infrequent at low concentrations, preventing homoagglomeration. Furthermore, each individual AgNP addition was at extremely low concentrations. These mesocosm results, which are at concentrations approaching those expected in natural waters (4), indicate that homoagglomeration will be minimal and not a major factor affecting AgNP behaviour.

The high DOC in the water matrix might also explain why differences in agglomeration between treatments were not observed. DOC prevents homoagglomeration and improves stability by adsorbing to AgNP surfaces and inducing both steric and electrostatic repulsion (55, 62, 74). In lab experiments, DOC concentrations in water as low as 4 mg $L^{-1}$ (62) and as high as 10 mg $L^{-1}$ (61), which are within the concentrations found in our mesocosms, have been shown to completely inhibit agglomeration. Furthermore, the rapid agglomeration of CT-AgNPs in synthetic freshwater has been shown to be prevented in the presence of humic acids (4 mg $L^{-}$), whereas PVP-AgNPs had no significant agglomeration regardless of humic acid addition (71).

The low ionic strength in the mesocosm water may have also prevented agglomeration. A high ionic strength causes AgNPs to agglomerate because excess electrolytes screen the surface charge and reduce the electrical double layer that surrounds particles, which then increases the extent of particle-particle interactions (54, 83). Once ion concentrations exceed the critical coagulation concentration (CCC), the energy barrier is completely eliminated, resulting in rapid agglomeration (54). By comparison, the ionic strength of L239 water was well below the CCC that induces rapid agglomeration of

PVP-AgNPs (111 mM NaCl; 4.9 mM $CaCl_2$) and CT-AgNPs (48 mM NaCl; 2.1 Mm $CaCl_2$) (55). Biotic factors in natural environments are another important consideration when assessing AgNP agglomeration and stability. In the present study, Ag retained in the particulate fraction would not only include homoagglomerates of AgNPs, but also Ag associated with particulate organic material (POM), including bacteria (0.2-1 μm) and algae (>1 μm) (91). Heteroagglomeration with POM is probable in natural environments, as AgNPs can associate with the cell walls of algae (63) and bacteria (21). Given the low AgNP concentrations and high DOC levels, we hypothesize that the majority of particulate Ag in our study is comprised of heteroagglomerates or bioaccumulated forms of AgNP/ $Ag^+$. Unrine et al. (107) found no AgNP agglomeration in the presence of plant-derived dissolved organic material (DOM) in their microcosm study as a result of the influence of DOM on AgNP stability. In the present mesocosm study, the variations observed in the percentage of TAg found in the particulate fraction over time may reflect temporal variations in POM. For example, the sharp increase in the amount of Ag found in the seston and bacterioplankton Ag fractions between day 11 and 25 could be a result of an algal bloom observed around this time.

### 2.4.3. Low Concentrations of Dissolved Ag in Natural Waters

Very little dAg was detected in our study, making it difficult to assess differences among treatments. Previous laboratory studies have demonstrated increased particle dissolution at lower particle concentrations (71, 85) and higher dissolution rates of PVP-AgNPs as compared to CT-AgNPs (70, 84). However, estimating dissolution by measuring dAg pools is problematic in natural waters as $Ag^+$ complexes with natural ligands. For example, $Ag^+$ strongly associates (logK=9) with DOC (125) and has also been shown to readily accumulate in algae as a result of adsorption on the cell membrane

and/or intracellular uptake (126). These complexes on DOC and algae would have been retained on the 3 kDa filter and 0.2 µm filter, respectively. Therefore, more dissolution of $Ag^+$ may have been occurring than was reflected in the dAg concentrations in the 3 kDa ultrafiltrate. Dissolution of $Ag^+$ is considered to be a mechanism causing AgNP toxicity (45, 70). The low amounts of free $Ag^+$ observed in our study suggest that natural matrices, particularly those with sufficient concentrations of DOC, may reduce the negative impacts of AgNPs in freshwaters as a result of $Ag^+$ complexation (62, 71).

### 2.4.4. Distribution of Ag in Lake Mesocosms

Despite the presence of Ag in the colloidal and particulate fractions of the drip mesocosms, Ag was continuously being removed from the water column, as less than 40% of the target concentrations were reached. The accumulation of Ag in sediments and periphyton indicate that these compartments may be important sinks for Ag in lakes. Ag likely enters the sediments via agglomeration or adsorption to POM and subsequent sedimentation. This process is dependent on aggregate size (62) and can reduce exposure of planktonic biota to AgNP (64). The adsorption and/or absorption of AgNPs and/or $Ag^+$ to periphyton was another important sink for AgNPs and/or dAg. Fabreaga (127) observed accumulation of Ag in biofilms in a dose-dependent manner in experiments with AgNPs. Cleveland et al. (119) also reported rapid accumulation of Ag in biofilms after 12 hrs of AgNPs being dosed to estuarine mesocosms.

We found differences in Ag found in sediment and periphtyon between CT and PVP AgNP treatments. CT-AgNP treatments accumulated greater concentrations of Ag in the sediment, whereas PVP-AgNP treatments accumulated greater concentrations of Ag in the periphtyon. Greater sediment Ag concentrations in CT treatments may have resulted from increased agglomeration and subsequent sedimentation; however the total

Ag, particulate Ag, and colloidal Ag results in the water column did not conclude differences in AgNP stability. Alternatively, we hypothesize that lower sediment Ag concentration in PVP-AgNP treatments are the result of a greater amount of Ag being adsorbed to periphtyon as compared to the CT-AgNP treatments. For example, El Badawy (128) suggested that the surface coating of AgNPs may effect interactions with biological surface membranes. The effect of surface coating on sedimentation and adsorption to biological surfaces are interesting questions that require further investigation in more controlled settings and with greater replication.

The results of our mass balance calculations indicate that the sediments and periphyton are not the only compartments to which Ag partitions. The colloidal, particulate, sediment, and periphyton fractions accounted for 41-77% of the Ag added. Two other likely pools unaccounted for in this study include zooplankton and macrophytes. Zooplankton species were abundant in mesocosms as they were seeded with ~1,300 zooplankton at the beginning of the experiment. However, many of the zooplankton species would have been removed from water samples by screening with the 35 µm mesh. Zooplankton can accumulate Ag when exposed to both ionic and particulate forms (25, 129). Sediments in the mesocosms also contained a relatively uniform cover of submerged macrophytes, which grew during the course of the experiment. Vascular plants have been shown to sequester Ag when exposed to AgNPs (130). Macrophytes take up many trace nutrients, including metals from sediments (131). Epiphytic biofilms may have also sequestered Ag from their macrophyte hosts, as has been shown for other trace elements (132), but this pool was not accounted for in the present study.

### 2.4.5. Study Limitations

Mesocosm studies can be subject to major outliers and variability caused by initial differences in *in situ* conditions that become enhanced over time, largely because the mesocosm walls prevent horizontal advection and mixing (133). The large variability between replicates limits the sensitivity of using limnocorrals to detect differences caused by treatment manipulations. Similarly, the ability to detect differences among treatments in the present study may have been limited by both the small number of replicates and the wide variation of some variables among replicates of the same treatment.

Some of the variation in Ag concentrations among the same treatments, for example TAg concentration in high drip treatments, may have been a result of varying volumes among mesocosms. We only measured mesocosm volumes once at the end of the study. However, the volume of L239 changed over the course of the summer and mesocosm volumes likely followed suit. Mesocosms were observed every other day, and fluctuations in volume were obvious over time. Differences in location of the 12 mesocosms in relation to the mouth of the bay likely resulted in different volume losses and gains among mesocosms.

The AgNP persistence in the water column and accumulation in the sediments are likely over and underestimated, respectively, due to the frequent disturbance caused by mixing the water column before each sampling and every other day following AgNP dosing. The mixing before sampling was done to ensure that biotic samples for a parallel study were representative of the entire water column. While comparisons among drip treatments within this study are appropriate as all of the treatments were similarly mixed, caution is required in making comparisons to other studies.

We quantified pools of Ag present in different fractions. While these pools can be used to infer the degree of agglomeration and persistence, we did not measure the rates of specific transformations. In addition, the size-fractionating method used to measure particulate Ag is largely inferential and cannot distinguish among AgNP homoagglomerates, AgNP heteroagglomerates, or $Ag^+$ adsorbed to POM. As previously discussed, assessing the dissolution of AgNPs using filtration techniques is challenging, as any released $Ag^+$ is likely to complex with DOC or accumulate in POM. Furthermore, we recognize that the method of filtration to examine particulate Ag may also not be sensitive enough to detect differences in AgNP size among homoagglomerates (for example, if they were less than the 200 nm pore size).

Accuracy in the mass balance calculations is limited by the estimation of the total volumes of environmental compartments. For example, there was great variability in the bulk density of sediments collected in the cores, which may reflect the heterogeneity of the sediments and the difficulty in sectioning the sandy sediments. The amount of periphyton biomass in the mesocosms is also uncertain due to 1) uncertainty in the volumes of periphyton slurry in collected samples, and 2) uncertainty in the surface area of the mesocosm walls. The surface area was based on the initial measured height of the water column and the assumption that the walls were cylindrical, which changed over time due to water loss.

## 2.5. Conclusion

This is the first study to investigate the fate of AgNPs using large, *in situ* enclosures at environmentally relevant AgNP concentrations. Furthermore, the use of a continuous doing regime may better simulate the continuous low level release of AgNPs from WWTPs. This mesocosm study indicates that AgNPs are moderately persistent in the water column, but also partition into the benthic compartment of soft water lakes. We also suggest that site specific characteristics, such as DOC content, ionic strength, and biotic interactions, may be more important determinants of AgNP transformations in natural environments than loading rate or surface coatings (i.e. PVP and CT).

The relative stability of AgNPs may increase the exposure of pelagic organisms to this contaminant in surface waters with low ionic strength and relatively high DOC. However, the extent of agglomeration (65), dissolution (70), and $Ag^{+}$ complexation to natural ligands are also important determinants of toxicity (62). Therefore, the results of this study are an important element in determining whether AgNPs are toxic to aquatic organisms in natural waters. In a companion study, we applied more sensitive and selective particle sizing techniques to the plug mesocosms including single particle-ICP-MS and asymmetrical flow field flow fractionation-ICP-MS in order to improve our understanding of the transformations of AgNPs in natural waters.

## Chapter 3: Applications of Various Analytical Techniques to Characterize the Fate of Silver Nanoparticles in Lake Mesocosms

### 3.1. Introduction

Silver nanoparticles (AgNPs) are used in various commercial products because of their antimicrobial properties (1), and because of the growing use of these products there is potential for AgNPs to be released into the environment (5). For example, AgNPs can be released from clothing during washing, and subsequently enter freshwater ecosystems via discharges of municipal wastewater (5, 9). AgNP concentrations in surface waters are predicted to be in the ng $L^{-1}$ to low µg $L^{-1}$ range (4). Toxicity of AgNPs to aquatic organisms has been demonstrated at µg $L^{-1}$ levels (24, 32, 34), which raises concerns about the ecological risks of exposure to AgNPs.

Agglomeration, dissolution, changes in chemical speciation, and surface modifications are important transformations that control the toxicity and fate of AgNPs in the aquatic environment. Homoagglomeration between AgNPs has been shown to reduce the bioavailability and toxicity of AgNPs (65) and promote sedimentation from the water column (62,74). Heteroagglomeration, including adsorption or absorption with biotic particles may also affect AgNP stability in natural waters (51). Dissolution of the surface layer of AgNPs releases $Ag^{+}$ (54), which is significant because the toxicity of AgNPs has been related to the release of dissolved Ag (dAg), which includes $Ag^{+}$ (45, 47). However, the chemical speciation of the released $Ag^{+}$ may reduce its' bioavailability and toxicity (62, 74, 121). Furthermore, surface modifications of AgNPs from adsorption of natural ligands may alter toxicity by impacting agglomeration and dissolution rates (58, 73). Bench-scale experiments have shown that ionic strength (54, 57), dissolved organic

carbon (DOC) (62, 74), pH (68), dissolved oxygen (DO) (68, 121), temperature (68, 70), and light (59) are factors that affect agglomeration and dissolution of AgNPs in natural waters. However, to better understand AgNP transformations, research is required under realistic environmental conditions. Thus far, the few studies on transformations of AgNPs in experimental mesocosms/microcosms have used high concentrations (i.e., mg $L^{-1}$) (107, 118, 119), perhaps due to the limited methods available for analyzing AgNPs at environmentally relevant concentrations in complex matrices (87).

In recent years, several sensitive analytical techniques have been developed that show promise for analysis of AgNPs at environmentally relevant concentrations. Cloud point extraction (CPE) was developed by Liu et al.(95) to pre-concentrate AgNPs using surfactants and complexing agents. Asymmetric flow field-flow fractionation (AF4) has been applied to the analysis of particle size distributions of nanoparticles, and when coupled with inductively coupled plasma mass spectroscopy (AF4-ICP-MS), offers elemental specificity and sensitivity (20, 105). Finally, single particle ICP-MS (spICP-MS) is an emerging analytical method that has great potential for monitoring the size and concentration of AgNPs (92, 113, 114). However, few studies have applied these techniques simultaneously for the analysis of AgNPs at environmentally relevant concentrations in natural waters. Furthermore, it may be advantageous to combine multiple techniques when analyzing AgNP transformations to validate results and compensate for the limitations associated with different analytical methods.

The objective of this study was to determine the fate of AgNPs in natural lake water in terms of its persistence, transformations, and distribution within the environment. To conduct these studies, it was necessary to assess and apply various techniques for determining the concentrations and sizes of AgNPs and the concentrations of other Ag

species in aquatic matrices. Studies were conducted in mesocosms deployed in a lake in the Experimental Lakes Area (ELA), ON, Canada. The mesocosms were spiked with a one-time addition of AgNPs at a nominal concentration of 60 µg $L^{-}$. Samples were subsequently collected for analysis by size fractionation by filtration, CPE, spICP-MS, and AF4-ICP-MS to monitor changes in AgNP size and form over time. Modelling techniques were used to predict the speciation of $Ag^{+}$ released by dissolution of AgNPs. Finally, the mass balance was calculated for the distribution of total Ag among various compartments in the mesocosms.

## 3.2. Materials and Methods

### *3.2.1. Field Site and Mesocosms*

Two littoral mesocosms were deployed in lake 239 (L239) at the ELA in northwestern Ontario, Canada ($49^{o}40'$N, $93^{o}44'$W). The mesocosms were 2 m in diameter 1.7 m deep resulting in a theoretical mesocosm volume >5,000 L. However, due to evaopartation and collapsing of mesocosm walls a nominal volume of 4,000 L was assumed. The volumes measured in the two mesocosms at the end of the experiment using $Cl^{-}$ as a tracer were 2,824 L and 3,068 L, respectively. Mesocosms were open to bottom sediments and were suspended from a floating ring and sealed to the sediments with sandbags. The sediment was characterized as a sandy loam with an average content of 55 ± 4% silt and 45 ± 4% sand. The average loss on ignition was 4% (SI Table 3.1).

### *3.2.2. Silver Nanoparticle Material*

The AgNPs used were purchased from NanoComposix (San Diego, CA) as polyvinylpyrrolidone (PVP) capped material with an average particle size of 50 nm. The stock suspension of PVP-AgNPs was supplied in milliQ water at a nominal concentration

of 1.0 mg Ag $mL^{-1}$. Acid digestion and ICP-MS analysis verified that the concentration was 0.96 mg Ag $mL^{-1}$ and amicon ultracentrifugation (3 kDa) showed that 2.5% of the total Ag mass was comprised of dAg, which was assumed to be $Ag^{+}$. Size information provided by the supplier indicated that the AgNPs were monodispersed, with a TEM diameter of 48.3 nm and a hydrodynamic diameter of 56.3 nm.

### *3.2.3. Silver Nanoparticle Dosing*

A volume of 240 mL of AgNP stock suspension was added to each mesocosm on July 11$^{th}$, 2012 to achieve a nominal concentration of 60 µg $L^{-1}$, based on the theoretical volume of 4,000 L. After dosing, the water column was mixed using a vertical pass of a ~45 cm plastic disk. The study ended after 33 days on August 13$^{th}$, 2012.

### *3.2.4. Water Chemistry Monitoring*

Temperature, conductivity, and dissolved oxygen (DO) were measured at three different depths of the water column (surface, 1 m, and just above sediments) prior to sampling using a model YSI30-25FT multiple parameter probe purchased from YSI Inc. (Yellow Springs Ohio, USA). The pH of each sample was measured in the laboratory at ELA using a ROSS Ultra® Electrode (Thermo Scientific). DOC was measured weekly throughout the study with an O.I. Analytical 1030D carbon analyzer (Xylem Scientific, Graden Instruments, Oakville, ON, CAN), according to methods described previously (134). Lake water was analyzed for major inorganic anions by ion chromatography (Dionex ICS-1100, Thermo Scientific, Bannockburn, IL, USA) (EPA Method 9056A) and for major inorganic cations by flame atomic adsorption spectrophotometry (Varian FS240, Varian Inc., Walnut Creek, CA, USA) (EPA Method 7000B).

### *3.2.5. Water Sampling and Preparation*

Intensive water sampling was carried out for the first 4 days (0, 1, 3, 6, 12, 24, 48, 96 hr) after AgNP dosing. After the first 4 days, samples were collected weekly. The water column in the mesocosm was mixed with a disk for a few minutes before sample collection so an integrated water sample could be taken. A volume of 8 L of water was collected from ~10 cm below the surface and pre-filtered through a 35 µm mesh coarse filter to remove macroplankton and detritus (referred to from here on as unfiltered water). The collected water was then subsampled for a variety of analyses (Figure 3.1). The various forms of Ag represented by each of the techniques are summarized in Table 3.1.

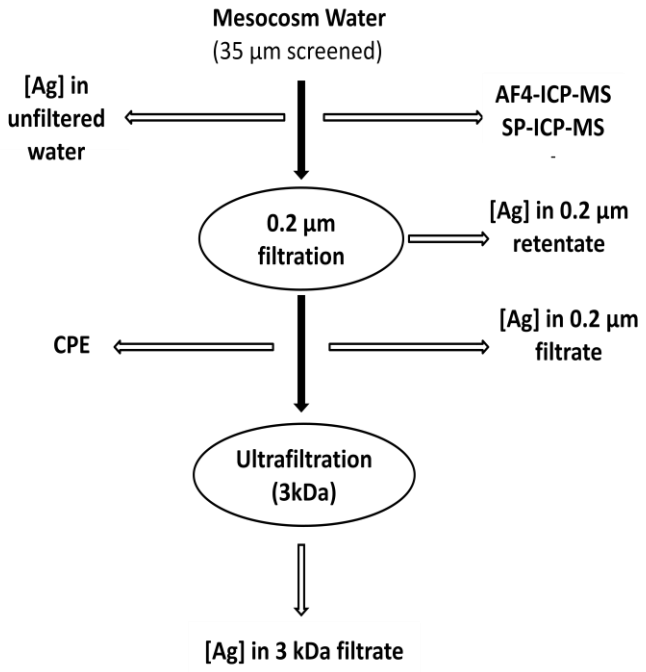


**Figure 3.1** Processing of mesocosm water for Ag analysis by various analytical techniques.

**Table 3.1.** Forms of Ag quantified by various methods employed in the study

| Method | Form of Ag quantified |
|---|---|
| Unfiltered Water | Total Silver (TAg):<br>• unagglomerated AgNPs<br>• agglomerated AgNPs<br>• free Ag+<br>• Ag+ complexed with POM, DOC, and inorganic ligands |
| Filtration | |
| 0.2 µm retentate | Particulate Ag:<br>• agglomerated AgNP (>200 nm)<br>• Ag+ complexed with POM (i.e. bacteria, algae) |
| 0.2 µm filtrate | Colloidal and Dissolved Ag (dAg):<br>• unagglomerated AgNPs (<200 nm)<br>• free Ag+<br>• Ag+ complexed with DOC and inorganic ligands |
| Ultrafiltrate (~1 nm) | dAg:<br>• free Ag+<br>• Ag+ complexed to inorganic or low molecular weight DOC ligands |
| CPE | • AgNP (concentration and size) |
| AF4-ICP-MS | |
| Nanoparticle Peak | • AgNP (concentration and size) |
| Void/ Early Eluting Peak | • Ag+ complexed with DOC |
| spICP-MS | • AgNP (concentration and size)<br>• Ag+ |

*3.2.5.1 Unfiltered water*

After each sampling event, a sub-sample of unfiltered water (40 mL) was collected and placed into 50 mL plastic Falcon tubes (BD Biosciences, Mississauga, ON, CAN) for TAg analysis. The samples were immediately acidified with trace metal grade nitric acid ($HNO_3$) (SCP Science, Baie-Durfe, Quebec, Canada) to a final concentration of 4% (v/v) and stored at 4 °C until analysis. The samples were heated for six hours at 70$^{o}$C before ICP-MS analysis to ensure all Ag was released from suspended material. Samples of unfiltered water were also immediately flash frozen in liquid nitrogen in 5 mL

Cryogenic vials (Corning Inc. Corning, NY, USA) and stored at -80°C. The aim for the flash freezing was to preserve the size and agglomeration state of AgNPs at the time of sampling until spICP-MS and AF4-ICP-MS analysis could be performed.

*3.2.5.2. 0.2 µm Filtration*

Mesocosm water was filtered to obtain size fractions of <200 nm and >200 nm to indicate the extent of agglomeration. A 300-500 mL sub-sample of whole water was sequentially filtered through polycarbonate 47 mm diameter filters with pore sizes of 1.2 µm and then 0.2 µm purchased from Millipore Inc. (Billerica, MA, USA). A 40 mL sub-sample of the 0.2 µm filtrate was then dispensed into 50 mL Falcon tubes and immediately acidified (4% $HNO_3$) for analysis of colloidal and dAg (<200 nm). The 1.2 and 0.2 µm membranes were preserved and digested in 20 mL polypropylene scintillation vial with 20 mL of 4% $HNO_3$ for analysis of particulate Ag (>200 nm). All extracts were stored at 4$^{o}$C and then heated for six hours at 70$^{o}$C before ICP-MS analysis. The recovery of 50 nm PVP-AgNPs through the 0.2 µm membranes was 93 ± 3% (20 µg $L^{-1}$ spike in 400 mL of milliQ, n=3).

*3.2.5.3. Ultrafiltration*

Water samples were analyzed for dAg by ultrafiltration with 3 kDa (~ 1 nm) membranes. Two different ultrafiltration techniques were used and compared: i) stirred ultrafiltration and ii) ultra-centrifugal filtration. Both filtrations were performed on pre-filtered samples to remove particulates that could block membrane pores and decrease the efficiency of the separation. Stirred ultrafiltration was performed using a 200 mL Amicon® stirred cell unit with a 3 kDa regenerated cellulose membrane (Millipore Inc.). Immediately after sample collection, the 0.2 µm filtrate (40 mL) was passed through the 3

kDa filter membrane under vacuum (50 psi), while the sample was stirred in the reservoir above the filter (80 rpm). Centrifugal filtration was performed using Amicon® 4 mL Ultra Centrifugal Filters with a 3 kDa regenerated cellulose membrane (Millipore Inc.). For these samples, flash-frozen unfiltered water samples were thawed and then pre-filtered through 0.45 µm nylon syringe filters (25 mm; Canadian Life Sciences, Peterborough, ON, Canada) before passing through the 3 kDa membranes by centrifuging at 4.4 rpm for 90 min. Each filtrate was acidified to 4% $HNO_3$ and stored at 4$^{o}$C until analysis. Recovery tests were preformed for each method in deionized water (DI) and L239 water at various Ag+ concentraions, refer to the SI for the results (p.127).

*3.2.5.4 CPE*

CPE was previously reported to pre-concentrate and quantify trace concentrations of AgNPs in environmental waters (95, 135). CPE used in this study was modified from previous methods to pre-concentrate larger volumes of water sample. A 40 mL sample of water was placed in a 50 mL falcon tube and the pH adjusted to zero point charge ($pH_{pzc}$) using 2% $HNO_3$. A $pH_{pzc}$ could not be found between pH 2-10, although the zeta potential did become more positive with decreasing pH (SI Figure 3.1). As a result, the pH of samples was adjusted to 3. This value was used for the previous CPE studies using PVP-AgNPs as pH values lower than this could result in significant dissolution (95, 135). Once the pH was adjusted, 0.5 mL of 1 M $Na_2S_2O_3$ (Caledon, Georgetown, ON, CAN) and 2 mL of 5% (w/v) of non-ionic TX-114 surfactant (Sigma Aldrich, Toronto, ON, CAN) were added. The solution was mixed and incubated in a water bath at 40$^{o}$C for 30 min. Samples were then centrifuged at ~828 g for 5 min to facilitate phase separation. The surfactant rich phase was removed and prepared by microwave-assisted digestion (ETHOS, Milestone, Sorisole, Italy) in 9 mL of c$HNO_3$ (70% v/v) and 3 mL of c$H_2O_2$

(30% v/v; Sigma Aldrich). The microwave digestion program consisted of a 5 min ramp-up to 120$^{o}$C, 10 min at 120$^{o}$C, 5 min ramp-up to 180$^{o}$C and 30 min at 180$^{o}$C. After digestion, the volume was reduced to 1 mL on a hot-plate in acid-cleaned 20 mL glass vials and re-diluted to 10 mL using milliQ water (18.3 MΩ; Milli-Q Element System, Millipore). The final solution was concentrated by a factor of 4 and had an acid concentration less than 10% so that it could be analyzed directly by ICP-MS. Transmission electron microscopy (TEM) was performed to characterize the size of extracted AgNPs in mesocosm samples. TEM was performed with a Philips CM-200 instrument at 200kV coupled with a Genesis 4000 Energy Dispersive X-ray Spectroscopy (EDS). The sample was mounted onto a carbon coated grid for analysis. Final operating conditions are listed in SI Table 3.2. To validate the CPE technique, the extraction efficiency of AgNPs was measured both in the presence and absence of $Ag^{+}$ in DI water and L239 water (SI Table 3.3). The effect of particle concentration and particle size on extraction efficiency was also assessed (SI Table 3.4; SI Table 3.5). A detailed discussion of the method validation results is provided in the SI (p.120).

### *3.2.6. Sediment Sampling and Preparation*

Sediments were sampled from two random locations in each mesocosm at the end of the experiment. Polycarbonate tubes (8 cm diameter) were used to collect intact sediment cores. Each core was sectioned into three layers (0-2 cm, 2-4 cm, 4-6 cm), which were stored frozen until analysis. Prior to strong-acid digestion, a known amount of $Ag^{109}$ (Isoflex, San Francisco, CA, USA) was added to each sample as an internal standard. Sub-samples from each core (1 g each, n=3) were digested according to a procedure modified from EPA Method 3050B in 40 mL glass vials by adding 10 mL of conc. $HNO_3$ with reflux at 120ºC for 2 hours, an additional 5 mL of conc. $HNO_3$ with

reflux at 120 ºC for 2 hours, and 3 mL of conc. $H_2O_2$ with reflux for 2 hours. The volume of the sediment digests were reduced on a hot-plate to 4 mL and re-constituted to 40 mL using milliQ water so that the final acid concentration was less than 10%. Sample were thoroughly mixed and left overnight to allow residual particulates to settle to the bottom before ICP-MS analysis.

### *3.2.7. Periphyton Sampling and Preparation*

At the start of the experiment, two strips of polypropylene wall material (1 m x 0.05 m) were hung vertically in each mesocosm from a PVC pipe that lay across the top of the flotation rings. Over time, strips were naturally colonized with periphyton that was assumed to be representative of the periphyton on mesocosm walls. At the end of the experiment, periphyton films were scraped from each strip and diluted with lake water. The resulting slurry was homogenized, and two sub samples from each strip were filtered through pre-weighed glass microfiber filters (Whatman GF/F, nominal 0.7 µm pore size), which were stored frozen until analysis. Prior to strong acid digestion, filters were dried at 60$^{o}$C and weighed to determine the biomass of periphyton and subsequently spiked with a known amount of $^{109}$Ag as an internal standard. Filters were digested with 20 mL of concentrated $HNO_3$ in 40 mL glass vials and heated (120$^{o}$C) until the samples lost their color (~6 hours). The periphyton digests were re-constituted to 40 mL using milliQ water. The undigested filters were subsequently removed and the vial was left overnight to allow any remaining filter particulates to settle to the bottom. An aliquot of each periphyton sample was additionally diluted 10 x before ICP-MS analysis.

### *3.2.8. Silver Analysis*

Water, periphyton, and sediments were analyzed for Ag by ICP-MS using a model X Series 2, instrument purchased from Thermo Scientific (Nepean, ON, Canada). The samples from different environmental compartments required different analytical methods.

#### *3.2.8.1. Water Samples*

The Ag concentrations in unfiltered water, 0.2 µm filtrate, 0.2 µm retentate, CPE, and 3 kDa ultrafiltrate samples were measured against an external calibration curve ranging from 0.78 -200 µg $L^{-}$ using standard solutions of Ag (SCP Science, Baie-Durfe, Quebec, Canada) prepared in milliQ water acidified to 4% $HNO_3$ (trace metal grade). An aliquot of indium (SCP Science, Baie-Durfe, Quebec, Canada) was added to each sample as an internal standard to correct for changes in sensitivity and non-spectral inferences during analysis. Mass traces for $^{107}Ag$ and $^{115}In$ were acquired in steady state mode. The detection limits were determined for each set of water analysis from blank samples analyzed throughout the run. Blank samples consisted of milliQ water acidified to 4% $HNO_3$ with 5 µg $L^{-1}$ of indium. The limit of detection (LOD) (3*SD) was 0.02 µg $L^{-}$ and the limit of quantification (LOQ) (10* σ) was 0.07 µg $L^{-}$.

#### *3.2.8.2. Periphyton and Sediment Samples*

Ag concentrations in periphyton and sediment digests were determined using isotope dilution methods (123). Mass traces for $^{107}Ag$ and $^{109}Ag$ were acquired in steady state mode and the recovery of $^{109}Ag$ in each sample was used for total Ag quantification. Blank and reference material were analyzed for each batch of samples. The average recovery of Ag from a standard reference material of sediment (NIST SRM 1994 New

York/ New Jersey Waterway sediment) was 6.5 ± 0.2 mg/kg, which was similar to the certified concentration values (6.4 ± 1.7 mg/kg). There are no available standard reference materials of periphyton, so instead a standard reference material of oyster tissue (NIST #1566b) was used. The average Ag recovered was 0.522 ± 0.005 mg/kg and was lower than the certified concentration values (0.666 ± 0.009 mg/kg). The LOD determined from the blanks (3*SD) was 7 ng for sediments and 51 ng for periphyton.

### *3.2.9. spICP-MS Analysis*

A Perkin Elmer NexION 300Q (Waltham, Massachusetts, USA) was used for spICP-MS analysis. The optimization and validation of this analytical method has been described in previous studies (92, 104). The instrumentation and operating parameters are summarized in Table 3.2. The instrument parameters were tuned to generate the maximum $^{107}$Ag intensity prior to data acquisition. External calibration of a blank and four dAg solutions ranging from 0 to 1 µg $L^{-1}$ was carried out in single particle mode. The intensity of $^{107}$Ag for each standard solution over the entire length of the analysis was then averaged. The transport efficiency of AgNPs into the plasma was determined by the mass-based approach described by Pace et al. (113) and was found to be 4.0% using a 100 nm Au (Nanocompsosix) NP standard. The particle concentration detection limit for spICP-MS analyzing 40 nm AgNPs was quantified to be 2.5 ng $L^{-1}$ using the data collection method and instrumentation detailed above (104). The particle size detection limit under these given run conditions was approximately 30 nm AgNP.

**Table 3.2. spICP-MS instrumentation and operating parameters**

| | |
|---|---|
| ICP-MS model | NexION 300Q (Perkin Elmer) |
| Nebulizer | Miramist (Meinhardt) |
| Spray Chamber | 25 mL Cyclonic (Perkin Elmer) |
| Sample flow rate | 1.2 mL $min^{-1}$ |
| Dwell time | 10 ms |
| Analyte | $^{107}Ag$ |
| Total analysis time per sample | 4 min |

For analysis of samples collected from the mesocosms, flash-frozen samples were thawed in a water bath at room temperature (~5 min) and sonicated for 5 min. Samples were diluted in DI water (1:5000) immediately before spICP-MS analysis to avoid particle coincidence. To monitor instrumental drift over time, a single $Ag^+$ standard of 100 ng $L^{-1}$ was analyzed in spICP-MS mode after every ten samples. If drift in the standard signal was detected, the particle sizing equation was adjusted accordingly.

The calculations and analysis of spICP-MS data have been described in detail in previous studies (92, 104). Briefly, raw intensity data was exported to Microsoft Excel for data analysis. AgNPs were distinguished from the dAg background by plotting the raw intensity data as pulse intensity versus number of pulses, where any values below the first minimum in the histogram were considered background/dissolved Ag. The intensity of the AgNP pulses was subsequently corrected by subtracting the background intensity. The calibration curve for dAg standards was converted to mass flux using the transport efficiency of silver mass into the plasma. The Ag mass in each AgNP pulse was extrapolated from the mass flux calibration curve and converted to particle diameter assuming spherical geometry. The mean particle diameter was then calculated from this data. The particle concentration was determined from the number of AgNP pulses measured in a sample adjusted by the dilution factor. Based on the mean particle

diameter and particle concentration, the Ag concentration was calculated by the following equation:

$$Ag\ concentraion = \frac{particles\ concentraion * particle\ volume * Ag\ density}{transport\ efficieny}$$

### *3.2.10. AF4-ICP-MS Analysis*

AF4-ICP-MS analysis was performed using an AF2000 Focus model instrument purchased from Postnova Analytics (Salt Lake City, UT, USA) that was directly interfaced to a Thermo X Series ICP-MS. A 50 µg $L^{-1}$ solution of In was introduced via a mixing-tee at a flow rate of 77 µL $min^{-1}$ to correct for changes in sensitivity during analysis (SI Figure 3.2). The In solution was used for daily tuning of the instrument prior to data acquisition. A full description of the ICP-MS instrumentation and data acquisition parameters when used as an AF4 detector is provided in SI Table 3.6. NanoXact standards supplied by Nanocomposix of PVP (20 mg Ag $L^{-1}$) stabilized in water were used for size calibration. The manufacturer provided size information by TEM and DLS that verified the particles to be monodispersed (SI Table 3.7).

AF4 separations were conducted as described previously (104). The carrier fluid and cross-flow were optimized to obtain the greatest recovery and peak height of 50 nm PVP-AgNPs (SI Table 3.8). The surfactants sodium doceyl sulphate (SDS) (Sigma-Aldrich) and FL-70 (Fischer Scientific) were tested as carrier fluids. To determine the recovery of 50 nm PVP AgNP standards, the areas of particles injected (100 µg $L^{-1}$) with no cross-flow (n=1) and with cross-flow (n=3) were compared. AgNP recovery and peak height was optimal (109 ± 9 %) using a carrier fluid of 0.05% (w/v) SDS in milliQ water

with 0.7 mL $min^{-1}$ cross-flow. The final AF4 operating parameters chosen for analysis of mesocosm samples are summarized in Table 3.3.

**Table 3.3.** AF4 channel description and operating parameters

| | |
|---|---|
| Spacer Thickness | 350 µm |
| Membrane Type | regenerated cellulose with 10 kDa MWCO |
| Injection Volume | 100 µL |
| Carrier Fluid | 500 mg $L^{-1}$ SDS |
| Channel Flow | 1.0 mL $min^{-1}$ |
| Cross Flow | 0.7 mL $min^{-1}$ |
| Focus Flow | 0.2 mL $min^{-1}$ |
| Rinse Flow | Cross flow off, 1.0 mL $min^{-1}$ |
| Focusing Time | 10 min |
| Elution Time | 35 min |
| Rinse Time | 10 min |
| Total Analysis Time | 55 min |

AgNP concentration was determined using an external calibration curve generated by injecting 50 nm PVP AgNP standards into the system under the same operating conditions as those used for analysis of samples (20). The LOD (3*SD of noise) of the method was 1.0 µg $L^{-1}$ determined by the peak height of a 10 µg $L^{-1}$ 50 nm PVP standard. A complete description of the method optimization and validation experiments is provided SI (p. 123).

For analysis of water samples collected from mesocosms, flash frozen samples were thawed in a water bath at room temperature (~5 min) and then sonicated (5 min). Each sample sat for 30 min before injection to allow any micron sized particulates to settle out. Filtration was avoided as a preparative method for AF4 analysis due to previous studies that indicated that filtration could modify particle size distributions (136). A daily 50 nm PVP AgNP standard (100 µg $L^{-1}$ in milliQ) was injected to compare the hydrodynamic diameter of fresh particles to those collected in the mesocosm samples, as

well as to measure AgNP concentration using a one-point calibration curve. A daily injection of PVP-AgNPs consisting of a mixture of 40 and 80 nm size standards (100 µg $L^{-1}$ in milliQ) was analyzed for size calibration and to account for any drift in retention time. This was followed by a milliQ rinse to ensure that there was no sample carry-over before analysis of mesocosm samples.

AF4-ICP-MS fractures were analyzed using OriginPro 9 (OriginLab, Northampton, MA, USA). The $^{107}Ag$ intensity was normalized using the internal standard. Data was smoothed using the Savitzky-Golay method with polynomial order of 1 and 100 points of window. The elution time was converted to hydrodynamic diameter using the daily size calibration curve. The mean hydrodynamic diameter was determined from the modal peak. The Ag concentration in the nanoparticulate peak was quantified using the daily one-point external calibration curve (concentration vs. area).

### *3.2.11 Speciation Modelling*

The speciation of Ag+ released from AgNPs was predicted using MINEQL+ 4.6 (Environmental Research Software, Hallowell, ME, USA). Input data included the concentration and equilibrium constants of major inorganic anions and DOC in the mesocosms (Table 3.4). The concentration of the other major cations measured in Lake 239, ionic strength corrections, and the DO concentration (8 mg $L^{-}$) were also included in the model, and the system was considered open to the atmosphere ($pCO_2$= -3.5).

**Table 3.4.** Input data for Ag ligands used for MINEQL+ modelling

| Complex | Ligand concentration ($mg\ L^{-1}$) | logK |
|---|---|---|
| AgCl | 0.27 | 3.3 |
| $AgSO_4$ | 2.25 | 1.3 |
| Ag-DOC* | 8.3† | 9 |
| H-DOC* | pH =7 | 4 |
| DOC Binding Sites* | 35 nmol per mg C $L^{-1}$ | |

*Values obtained from previous modelling studies (78, 125)
† average value measured between both replicates and all time points

### *3.2.12 Mass Balance*

Partitioning of Ag among the various compartments in the mesocosms was estimated by calculating the mass balance at the end of the experiment in four compartments: 1) colloidal Ag, 2) particulate Ag, 3) Ag in periphyton, and 4) Ag in sediment. Ag mass in the colloidal and particulate compartments were calculated based on the Ag content in those fractions and the mesocosm volume measured at the end of the study. The Ag mass in the periphyton was calculated by first determining the Ag mass on each strip, based on the periphtyon Ag content in each sub-sample (µg) and the proportion of the volume of whole periphtyon slurry relative to the volume of the sub-sample that was filtered. The volume of the whole slurry was not recorded for each sample, so the Ag/strip area was calculated for each sample using both the smallest and largest known slurry volume and presented over the range. The Ag mass per strip surface area (µg Ag $cm^{-2}$) was then multiplied by the estimated surface area of the mesocosm walls. Ag mass in the sediment was calculated by first subtracting the average background sediment concentration taken from cores collected pre-experiment (0.27 ± 0.05 µg Ag $g^{-1}$; 0-3 cm deep) from the average concentrations of the post-experimental cores. The concentration was multiplied by the corresponding bulk density (µg $cm^{-3}$) to determine the Ag mass (g) within the dry sediment volume ($cm^{-3}$), which was then

multiplied by the total sediment volume for each core section (2 m benthic area x 2 cm sampling depth). The total Ag recovered (%) in each mesocosm was determined as the sum of Ag in each of the four compartments, divided by the total Ag added (240,000 µg).

## 3.3 Results and Discussion

### *3.3.1 Water Chemistry*

Water chemistry parameters were similar between mesocosms. Conductivity ranged from 32-34 µS $cm^{-1}$ over the course of the experiment (SI Table 3.9). The water columns of the mesocosms were oxic throughout the duration of the experiment, with DO levels ranging between 7-8 mg $L^{-1}$ (SI Table 3.9). Water temperatures and pH ranged from 24 to 27°C (SI Table 3.9) and 7.1-7.4 (SI Table 3.10), respectively. Average DOC concentrations were 8.3 ± 0.5 mg $L^{-1}$ (SI Table 3.11). The concentration of major cations and anions found in L239 indicate a low ionic strength, with $Cl^-$ concentrations of 0.27 mg $L^{-1}$ (SI Table 3.12).

### *3.3.2. Unfiltered Water*

There was relatively slow dissipation of TAg from the water column. The TAg concentrations in the two mesocosms were 71 and 70 µg $L^{-1}$, respectively at 1 h after addition and declined to 16 and 18 µg $L^{-1}$, respectively after 33 days (Figure 3.2). The dissipation half-life (DT50) for TAg in the two mesocosms was 18 d and 21 d, respectively, although there is some evidence that concentrations declined more rapidly over the first 24 hrs post-dosing (Figure 3.2). The persistence of AgNPs in these lake mesocosms was much longer than observed previously in estuarine mesocosms, where AgNPs were rapidly removed from the water column within the first 24 hrs, perhaps because of the high ionic strength and high $Cl^-$ concentrations (119). Conversely, AgNPs

dosed to wetland mesocosms had a settling time of 8 days, longer than expected based on previous homoagglomeration studies, which was attributed to the high organic matter concentrations (118). In the present lake mesocosm study, the relatively high DOC concentration and the low ionic strength of Lake 239 water likely reduced homoagglomeration and thus, increased AgNP persistence. DOC improves AgNP stability by adsorbing to the surface and inducing steric and electrostatic repulsion (62, 100), and at low ionic strengths there are fewer electrolytes available to reduce the surface energy barrier necessary to cause agglomeration (54). Therefore, the Ag persistence and water chemistry conditions in the Lake 239 mesocosms may signify that homoagglomeration was minimal, which would slow sedimentation out of the water column. Another potential reason for the slower disappearance from the water column is related to the adsorption to biotic particles, such as bacteria, as discussed in detail in the spICP-MS section.

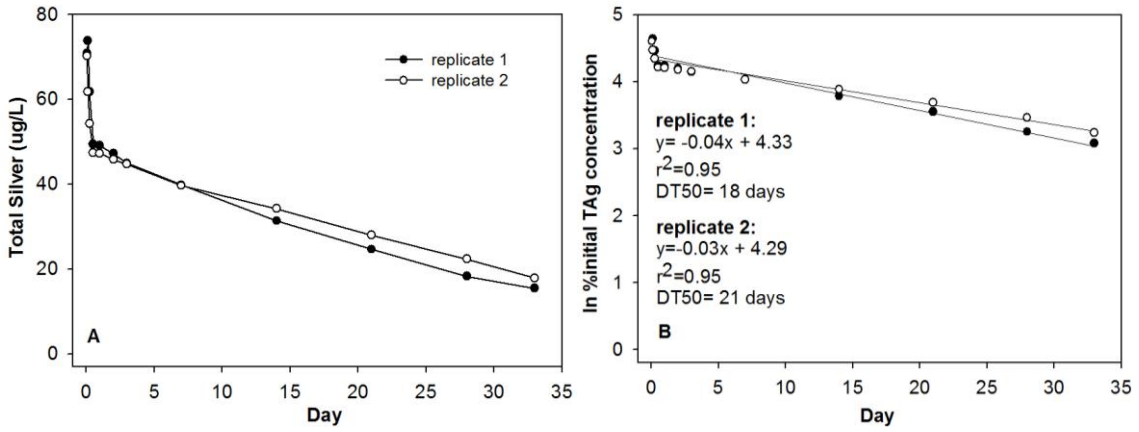


**Figure 3.2**. TAg concentrations (µg $L^{-1}$) over time in the two mesocosms (A) and the first order kinetics of loss determined in plots of in concentration vs. time (B). Note: the 0 hr time point was not included in the analysis of TAg because the Ag concentration measured indicated that the AgNPs were not yet homogenously mixed throughout the water column.

### *3.3.3. 0.2 µm Filtration*

The Ag concentration in the particulate phase (i.e. retentate) and colloidal/dissolved phase (i.e. filtrate) decreased with time Figure 3.3. However, the percentage of TAg found in the particulate and colloidal/dissolved phases varied over time. A greater proportion of Ag was in the colloidal/dissolved then particulate phase (44-74% versus 21-56%, respectively) (Figure 3.3). The presence of particulate Ag indicates that agglomeration occurred, in which the variability in the %TAg found in the particulate phase may be the result of varying concentrations of POM (i.e. algae and bacteria), that could change the extent of heteroagglomeration. AgNPs have been shown to physically attach to cell walls of bacteria (21-23) and algae (63). Conversely, intracellular uptake of AgNPs is unlikely as the particles must be small enough to pass through trans-membrane pores, which are <10 nm in bacteria (137) and 5-20 nm in algae (138).

Agglomeration contributes to the removal of Ag from the water column through AgNP sedimentation (52, 61). However, the significant portion of Ag consistently found in the colloidal/dissolved phase might explain the persistence of Ag observed in this study. The presence of DOC in the mesocosms appears to improve the stability of the AgNPs. In a previous study, a significant portion of PVP-AgNPs were retained on a 0.7 µm filter (i.e. particulate) when placed for 24 h in water, but in the presence of plants, which released DOC, no agglomerates were observed by filtration (107). The presence of particulate Ag (as defined by the 0.2 µm retentate) is consistent with homo- or hetero-agglomeration, although this analysis cannot differentiate between the two forms of agglomeration. More sophisticated analytical techniques are required to confirm the presence of AgNPs and the presence of agglomeration.

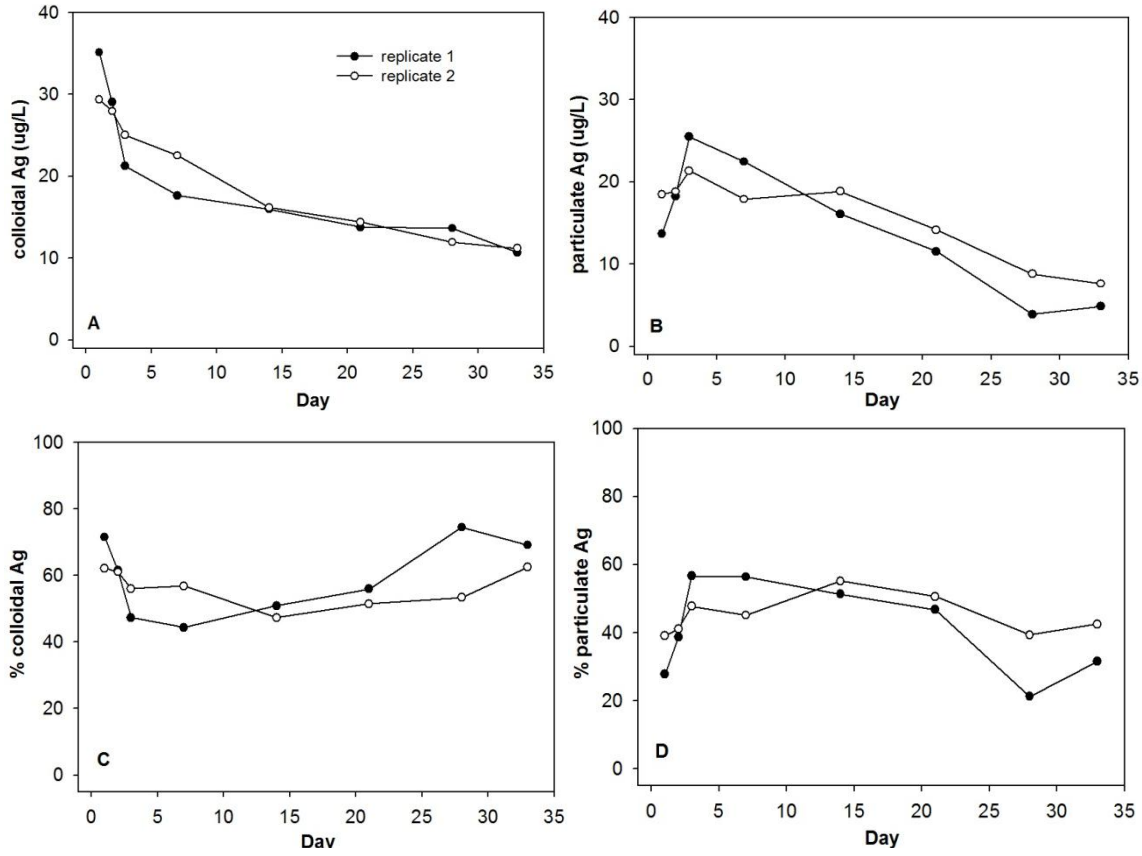


**Figure 3.3.** Ag concentration (µg $L^{-1}$) in the colloidal phase (A) and particulate phase (B) the percentage of TAg found in the colloidal phase (C) and particualte phase (D) of mesocosms over time. The sum of Ag found in the retentate and filtrate accounted for 101 ± 3% of TAg in the unfiltered water.

### *3.3.4. 3 kDa Ultrafiltration*

There were detectable Ag concentrations in the 3 kDa ultrafiltrate prepared by stirred ultrafiltration throughout the entire study, but concentrations were generally less than 1 µg $L^{-1}$ and variable through time and between replicates (Table 3.5). To verify results, flash frozen samples from mesocosms were prepared by centrifugal filtration using the same 3 kDa regenerated cellulose membrane. Similar to stirred ultrafiltration, the samples were pre-filtered (0.45 µm) to remove large particulates that may clog membrane pores and decrease the effective pore size. There were detectable Ag

concentrations in the filtrate samples collected over the first 24 h, after which dAg was generally below the LOD and LOQ. The Ag detected in the first 24 h could be $Ag^+$ ions already present in the stock solution. Based on 2.5% dAg measured in the stock, we could have initially added ~1.6 µg $L^-$ of $Ag^+$. The initial dAg detected in the mesocosm water could also have been due to an initial release of chemisorbed $Ag^+$ from the AgNP surface (84). Subsequently, any $Ag^+$ initially released in the mesocosms and/or generated by dissolution was probably removed from the dissolved phase by complexing with larger molecular weight DOC or adsorption to particulate organic matter (POM). Farmen at al. (34) also found that concentration of Ag in the 3 kDa filtrate significantly decreased between 0 h and 24 hr due to Ag+ complexation with natural colloids.

The results from both 3 kDa filtration techniques are consistent with low concentrations of dAg. It is probable that any $Ag^+$ released by dissolution from the AgNPs bound to higher molecular weight DOC compounds and were retained on the 3 kDa filters, as has been demonstrated in other studies (107). Recovery tests verified that the $Ag^+$ recovery through filters is reduced in L239 water compared to recovery from DI water (SI Table 3.13 and SI Table 3.14). Ag+ concentrations less than 100 µg $L^-$ also reduced recovery. Detailed results and discussion comparing the recovery between DI and L239 water, as well as stirred ultrafiltration and centrifugal ultrafiltration methods are included in SI (p.127). Due to the presence of ligands in natural waters, other analytical techniques should be employed to validate AgNP dissolution and Ag+ complexation.

**Table 3.5.** Ag concentration in 3 kDa filtrate (μg $L^{-1}$) of water collected from the mesocosms using both stirred ultrafiltration and centrifugal filtration methods

| | Stirred Ultrafiltration | | Centrifugal Filtration | |
|---|---|---|---|---|
| **Day** | **Rep 1** | **Rep 2** | **Rep 1** | **Rep 2** |
| **0** | - | - | 0.12 | 0.14 |
| **0.42** | - | - | 0.18 | 0.13 |
| **0.125** | - | - | 0.13 | 0.13 |
| **0.25** | - | - | 0.14 | 0.14 |
| **0.5** | - | - | 0.16 | * |
| **1** | <LOD | 0.06 | * | <LOD |
| **2** | 0.64 | 0.16 | <LOQ | <LOQ |
| **4** | 0.78 | 0.73 | 0.06 | 0.13 |
| **7** | 0.06 | <LOD | <LOD | <LOQ |
| **14** | 0.09 | 0.33 | <LOD | <LOD |
| **21** | 0.14 | n.a. | <LOD | - |
| **28** | 0.40 | 0.07 | - | - |
| **33** | 0.26 | 1.6 | - | - |

n.a.=sample not analyzed due to membrane leaking during filtration
(-) denotes that no sample was taken for the analysis
*samples removed due to outliers.

### *3.3.5. Cloud Point Extraction*

For mesocosm samples (i.e. 0.2 μm filtrate) extracted by CPE, there was a decrease over time in the concentrations of AgNPs in the extracts (Figure 3.4). This was accompanied by a decrease in the percentage of AgNPs extracted, calculated as the Ag concentration after CPE relative to the TAg concentration in the 0.2 μm filtrate before CPE (Figure 3.4). The decrease in the proportion of AgNPs extracted over time does not appear to be the result of a decrease in particle concentration, which we found had little effect on extraction efficiency (SI Table 3.4). It is likely that the temporal decrease in the percent of AgNPs extracted was due to AgNP dissolution, resulting in an increase proportion of $Ag^{+}$ (either free or complexed), as only nanoparticles are extracted by CPE. Subsequent laboratory experiments revealed a decrease in extraction efficiency with decreased particle size (SI Table 3.5). Therefore, a decrease in particle size as a result of

AgNP dissolution may have also contributed to a decline in the recovery of AgNPs by CPE over time.

It has been shown that the size and shape of AgNPs are preserved during CPE and storage in the surfactant-rich phase, offering the potential for characterization with TEM (95). TEM analysis of the surfactant rich phase of a 24 hr sample from the mesocosms revealed colloids in the nanometer size range, but no Ag signal was detected by X-ray diffraction analysis and therefore this material could not be confirmed as AgNPs (SI Figure 3.6). The concentration of Ag may have been below the LOD of the X-ray diffraction method.

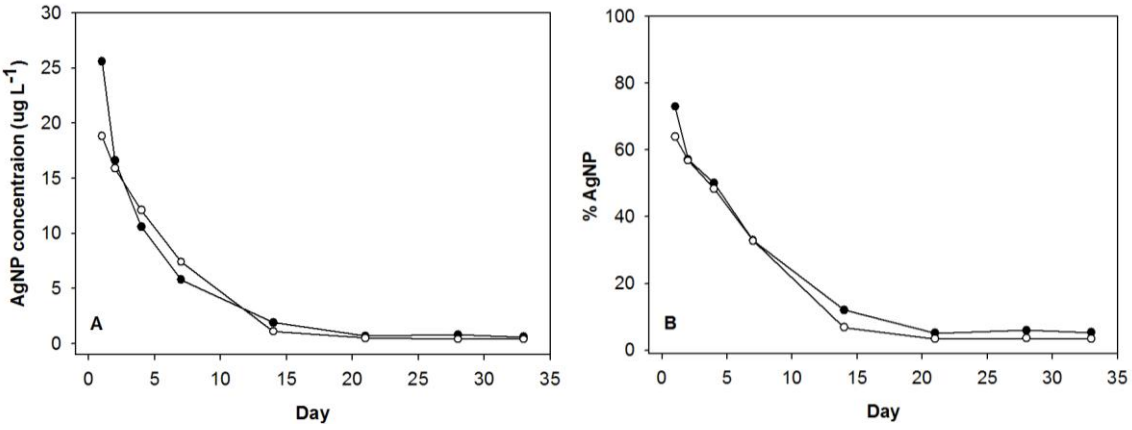


**Figure 3.4** AgNP concentration determined by CPE over time (A) and the % AgNPs extracted over time (i.e. Ag concentration after CPE relative to Ag concentration before CPE) (B).

### *3.3.6. spICP-MS*

Analysis by spICP-MS confirmed the initial 50 nm size of the metal core of the PVP-AgNPs after addition to mesocosms. The measured particle size then decreased over time (Figure 3.5). By 14 d post-addition, a high proportion of the particle sizes reached the 30 nm size limit for the spICP-MS method. The decrease in AgNP size over

time is likely a result of AgNP dissolution, and the loss of Ag mass from the AgNP core. In a recent study, spICP-MS analysis showed that dissolution caused a reduction in AgNP particle size over time, but this effect was mitigated by high concentrations of DOC and inorganic ligands (139). Our studies of AgNP stability under varying physico-chemical conditions also showed a significant decrease in AgNP size in DI water, presumably due to AgNP dissolution.(140)

Particle size distributions also showed very little evidence of homoagglomeration in the mesocosms, since after 7 days there were few Ag particles detected at sizes greater than 60 nm (Figure 3.6). Given the relatively low concentration of AgNPs in the mesocosms compared to other natural particles, it is expected that AgNPs would form hetero-agglomerates rather than homo-agglomerates (7). The concentration of bacteria alone in Lake 239 water (~$1.0 \times 10^9$ bacteria $L^{-1}$; unpublished data) was within the range of the concentration of AgNPs measured by spICP-MS in the mesocosms over the course of the experiment (i.e. $4.6 \times 10^9$ to $2.6 \times 10^8$ AgNP $L^{-1}$; Figure 3.7). Bacteria have been reported to disagglomerate and stabilize $TiO_2$ in marsh water due to preferential adsorption of nanoparticles with bacterial cell surfaces (141). Stabilization of AgNPs by biotic particles may have also occurred in these lake mesocosms, as AgNPs were shown to associate with bacterioplankton in the mesocosms (unpublished data) and in previous studies with bacterial communities in natural waters (33). It is likely that the low ionic strength and high DOC in the lake also stabilized the AgNPs against homoagglomeration, as discussed previously.

There was a decrease in the particle concentration over time (Figure 3.6), which corresponded to a decrease in the mass concentration. The AgNP concentration determined by spICP-MS decreased in the two mesocosms from 70 and 43 µg Ag $L^{-1}$ 1 hr

post-addition to 1.8 and 1.6 µg $L^{-1}$ after 21 days (Figure 3.8). The majority of Ag was initially in nanoform at sizes >30 nm, as the AgNP concentration determined by spICP-MS represented >60% of the TAg concentration. However, over time the AgNP concentrations deviated from the TAg concentration (Figure 3.8). This discrepancy is possibly a consequence of AgNP dissolution, resulting in smaller AgNPs that blend with the instrumental background below the 30 nm size detection limit. Theoretically, the decrease in AgNP size should correspond with an increase in dAg concentrations as a result of $Ag^+$ ions being released from the AgNP core. Similar to observations with the ultrafiltrate samples, no dAg was detected by the spICP-MS method. The released $Ag^+$ was either lost to environmental sinks like biotic particles or bottom sediments, complexed to DOC, or diluted below the instrumental LOD as a result of the 1:5000 dilution required for the method.

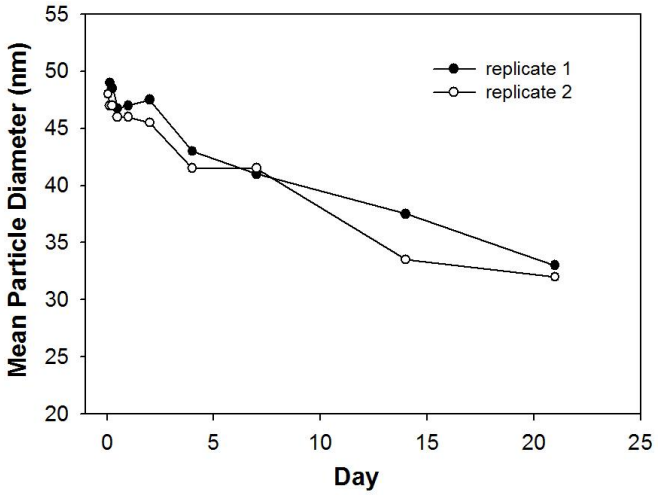


**Figure 3.5.** Average AgNP diameter in mesocosm unfiltered water over time as determined by spICP-MS.

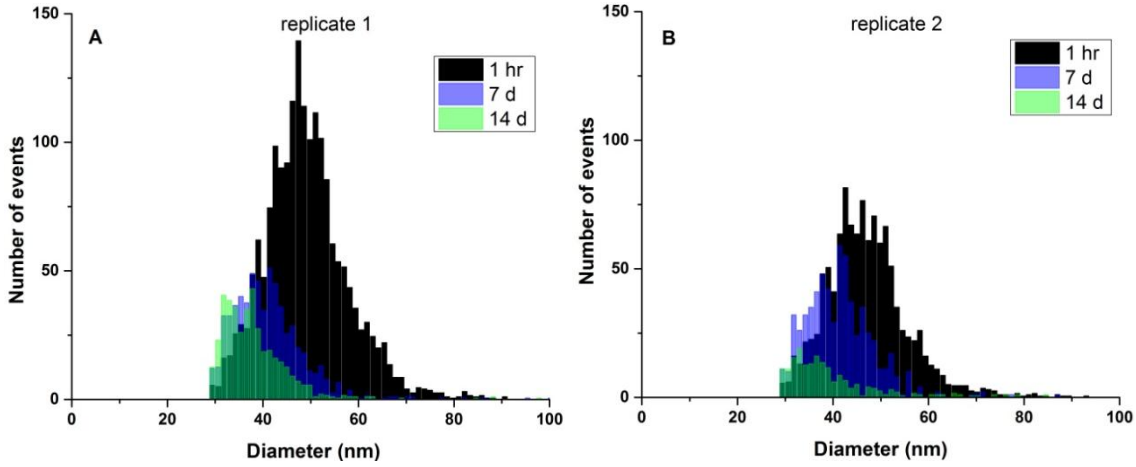


**Figure 3.6.** spICP-MS particle size distributions of representative mesocosm samples over time. The particle size limit of the analysis was 30 nm. After 14 days, particle size distributions close to the detection limit.

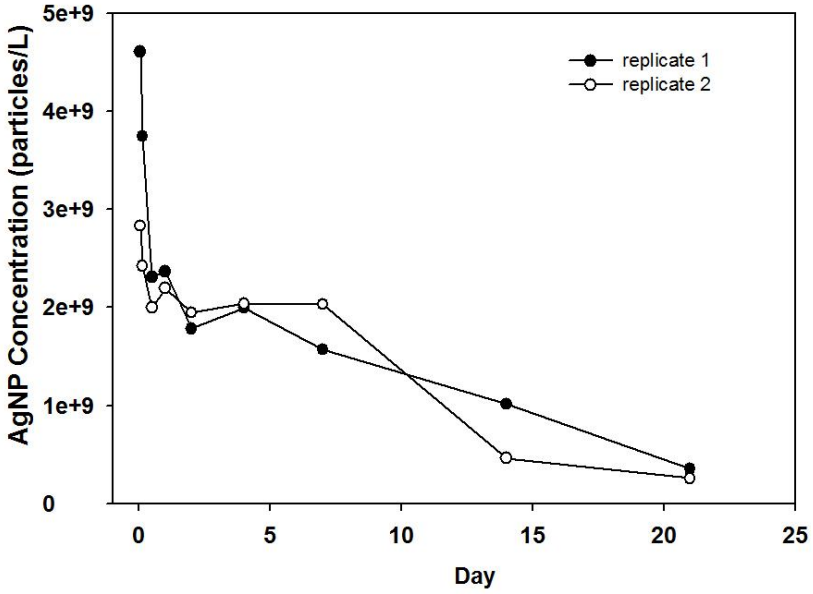


**Figure 3.7.** AgNP concentration as expressed as particles per L in mesocosms over time

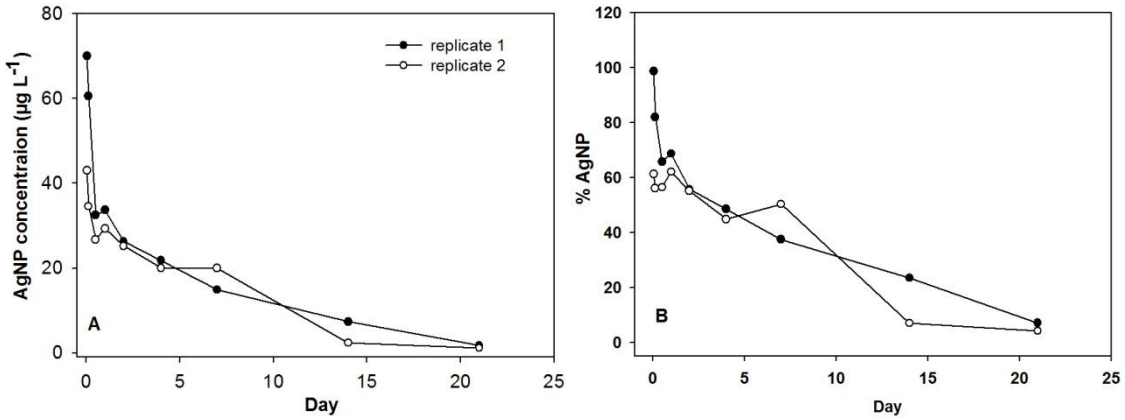


**Figure 3.8.** AgNP concentration (µg $L^{-1}$) determined by spICP-MS (A) and % AgNP (B) expressed as the AgNP concentration relative to the total Ag concentration. After 14 days, the AgNP peaks had particle size distributions close to the LOD. dAg was below the LOD at all time points.

### *3.3.7. AF4-ICP-MS*

Optimization of AF4-ICP-MS showed good analytical results in terms of size quantification. Daily size calibration of mesocosm samples with injections of a mix of 40 and 80 nm PVP-AgNPs extended through the origin (i.e., 3-point calibration) showed a strong linear relationship, with an $r^2$ greater than 0.97 and a negligible change in retention time (SI Figure 3.7). The average hydrodynamic diameter of freshly prepared 50 nm PVP-AgNP standard over multiple days of analysis was 60 ± 2 nm, which was close to the 56 nm hydrodynamic diameter determined by DLS. For mesocosm samples collected after 1 hr, the measured hydrodynamic diameter was similar to the freshly prepared 50 nm PVP standard, with sizes of 65 and 66 nm for both mesocosms, respectively (Figure 3.9). Changes in mean hydrodynamic diameters varied between 56-92 nm over the first seven days with no evidence of a decline in size over time (Table 3.6), which contradicts the trends observed in spICP-MS. After 7 days, the AgNP peaks in the fractograms were below the LOD. This apparent discrepancy between the results from spICP-MS and AF4-

ICP-MS is likely due to the accumulation of surface coatings that increased the hydrodynamic size determined by AF4-ICP-MS. The spICP-MS analytical technique uses Ag mass to determine the primary particle size, while the AF4-ICP-MS method separates particles based on their hydrodynamic diameter. Therefore, AF4-ICP-MS could have detected Ag associated with other particles or coated with molecules such as sulfides (89), organic matter (100), or biological molecules (105), that have been shown to increase the hydrodynamic radius of AgNPs.

The Ag detected in the early eluting peak of the AF4-ICP-MS fractograms increased over time (Figure 3.9). After 7 d, the early eluting peak was also accompanied by a tailing of an additional peak. This first peak may have consisted of $Ag^+$ associated with ligands in the form of small sized particles (104, 142). Any uncomplexed $Ag^+$ would have been removed in the cross flow through the membrane (142). These AF4-ICP-MS results are consistent with AgNP dissolution over time, and may indicate that the released $Ag^+$ forms complexes with organic ligands. Humic material ranges from 2 to 7 nm (143), which is within the size range of the first peak. Other studies have that demonstrated that metals detected in early eluting peaks near the void volume of AF4-ICP-MS are representative of DOC complexes. For example, Unrine et al.(107) detected large peaks near the void volume when $AgNO_3$ was added to microcosms containing plant-derived DOC, but no peak was observed in the absence of plants. Also, Dubascoux et al.(142) observed two peaks when analyzing trace metals association with natural colloids; a first narrow peak that could be metals associated with organic colloids (i.e. humic substances) and a second broad peak that could correspond to metals associated with particles.

Ag was also consistently detected in the rinse (data not shown), which could represent large agglomerated AgNPs not resolved by the method. For example,

Cumberland and Lead (101) attributed an absence of AgNPs in fractograms due to aggregation and longer elution times. The exact proportion of Ag detected in the rinse could not be determined because the purge valve was on during analysis. Future studies should optimize a gradient cross-flow method that can increase the size resolution of the void peak and reduce the amount of large AgNP agglomerates entering the rinse peak. Gradually decreasing the cross flow during sample elution can increase the size range that can be separated (144).

AgNP concentrations decreased over time, as determined from the intensity of the nanoparticle peak in AF4-ICP-MS. The initial concentrations of AgNPs determined by AF4-ICP-MS in the two mesocosms were 47 and 58 Ag μg $L^{-1}$, respectively. After 7 d, the concentrations in the two mesocoms decreased to 29 and 21 Ag μg $L^{-1}$ (Figure 3.10), respectively which is generally consistent with the concentrations determined by spICP-MS. When comparing the AgNP concentration determined by AF4-ICP-MS to the TAg concentration, there was great variability in the proportion of the TAg represented by the AgNP peak, both over time and between replicates (Figure 3.10). Hagendorfer et al.(103) suggested that variability in AF4 channel recovery is a major limitation for using this method for direct quantification of nanoparticle concentrations. Surface alterations to AgNPs may also change the recovery during AF4 separation. For example, Delay et al.(100) demonstrated that coating of AgNPs with natural organic matter (NOM) improved the recovery as a result of the steric hinderance that prevents membrane interactions. In our trials comparing PVP-AgNPs and CT-AgNPs we also observed improved peak height of PVP-AgNPs versus CT-AgNPs of smilar hydrodynamic diameter, illustrating the effect surface coating may have on AgNP quantification (SI Figure 3.9). It would appear that AF4-ICP-MS provides valuable information on the size

distribution of AgNPs in natural waters, but quantitative data on AgNP concentrations must be interpreted with caution.

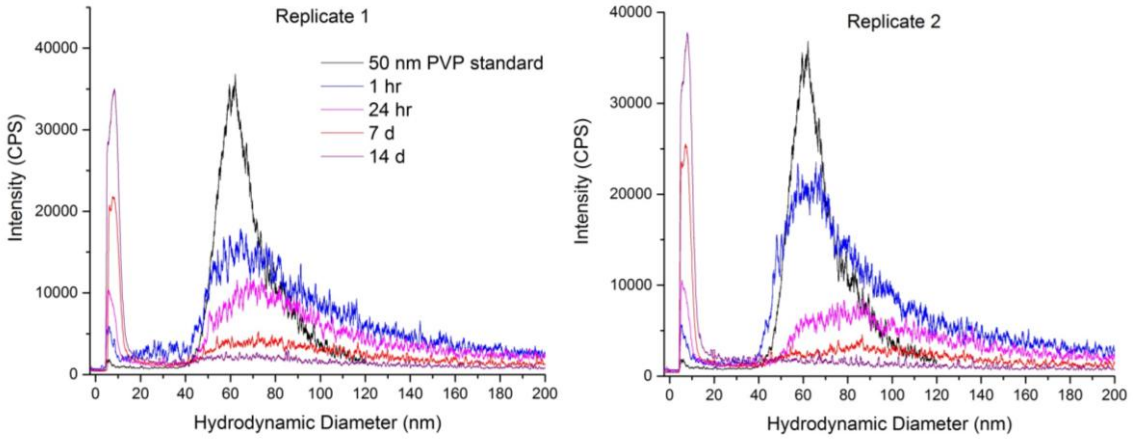


**Figure 3.9.** AF4-ICP-MS fractograms for representative mesocosm samples over time. The mesocosm samples are compared to a fresh 50 nm PVP standard. The y=axis displays the normalized $Ag^{107}$ intensity. The x-axis displays calibrated hydrodynamic diameters. Fractograms for all time points are found in the (SI Figure 3.8).

**Table 3.6.** Mean hydrodynamic diameter of AgNPs (nm) determined by AF4-ICP-MS particle size distributions. After 7 days, the AgNP peaks were below the LOD.

| Time | Mesocosm 1 | Mesocosm 2 |
|---|---|---|
| 0 hr | 56 | 81 |
| 1 hr | 65 | 66 |
| 3 hr | 63 | 56 |
| 12 hr | 67 | 61 |
| 24 hr | 64 | 82 |
| 48 hr | 92 | 67 |
| 96 hr | 80 | 68 |
| 7 d | 71 | 85 |

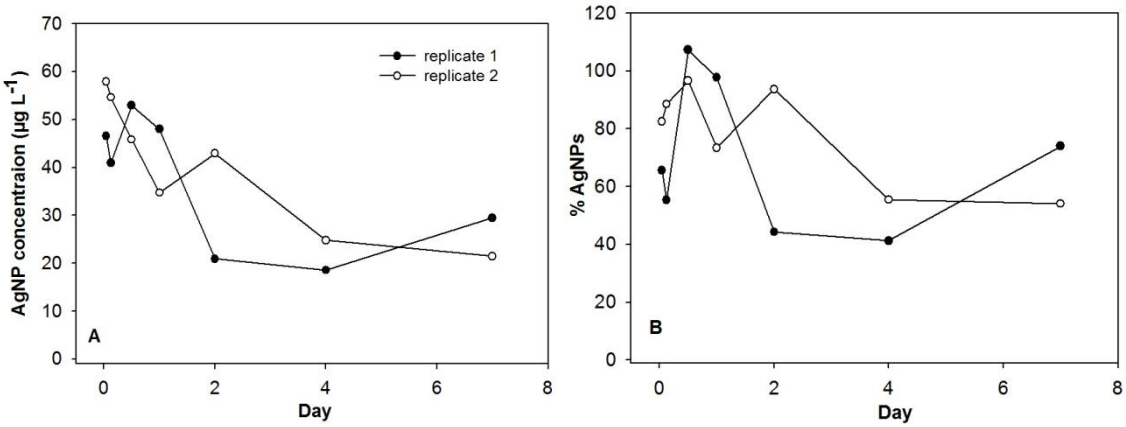


**Figure 3.10.** AgNP concentration determined by AF4-ICP-MS (A) and % AgNP (B) expressed as the AgNP concentration relative to the total Ag concentration. After 7days, the AgNP peaks were below the LOD.

### *3.3.8. Speciation Modelling*

CPE, spICP-MS, and AF4-ICP-MS results all provided evidence that AgNP dissolution was occurring over time. AgNP dissolution in the mesocosms is expected given the oxic conditions, neutral pH of the water, and the relatively high water temperatures during the study (68, 70, 121). However, centrifugal ultrafiltration results showed that there was very little dAg present in the two mesocosms. Therefore, MINEQL$^+$ modelling was used to predict the speciation of $Ag^+$ after release from AgNPs due to dissolution in the mesocosms. We tested $Ag^+$ speciation over a hypothetical range of $Ag^+$ concentrations to validate our hypothesis that the majority of released $Ag^+$ would be complexed with ligands under the water quality conditions found in Lake 239. The range of $Ag^+$ concentrations selected was 0-70 µg $L^{-1}$, in which an $Ag^+$ concentration of 70 µg $L^{-1}$ represented 100% AgNP dissolution. The model predicted that $Ag^+$ would preferentially complex with DOC and there would be no complexation with $Cl^-$ in the mesocosms (Figure 3.11). At $Ag^+$ concentrations less than 30 µg $L^{-1}$, over 95% of the $Ag^+$ was predicted to bind to DOC, after which there was an increasing proportion of free

$Ag^+$. It may be unlikely that $Ag^+$ concentrations would have been greater than 30 µg $L^{-1}$ as this concentration would represent >40% of TAg added to the mesocosms. Kittler et al. (70) monitored the long-term dissolution of AgNPs and found that a limiting value of the released Ag was observed. They reported that 50 nm PVP-AgNPs in ultrapure water at 25°C released between 40-50% of their initial weight. In pure water, particle dissolution can be impeded by the accumulation of $Ag^+$ at the particle surface (53). In natural waters, there are many factors that may prevent particle dissolution including: i) the presence of electrolytes (i.e., $S^{2-}$, $Cl^-$) causing precipitated Ag species to accumulate at the surface (53, 58) ii) the presence of organic ligands that may reduce $Ag^+$ to $Ag^{(0)}$ or absorb to the surface and block oxidation sites (68) and iii) the influence of agglomeration preventing access to reactive sites (57). Li and Lenhart (59) suggested that the aforementioned processes might have explained the low concentration of dAg measured in natural waters after the addition of AgNPs (i.e. 3% of the TAg present after 15 days). However, they also stated that the sorption of $Ag^+$ to particles found in natural waters might contribute to the low concentrations of dAg.

The strong association of $Ag^+$ for DOC is attributed to the presence of organic thiol groups. Based on thermodynamic constraints, Levard et al. (8) predicted that the majority of $Ag^+$ binds to cysteine (logK=11.9) in oxic fresh waters. Also, Bone et al.(145) found that the majority of oxidized Ag was associated with a cysteine-like complex in microcosms containing DOC. It is important to note that the Ag-DOC binding constant needs further validation with studies on organic matter from a variety of different sources,[48] as different sources of DOC may have different binding capacities. There are also many other environmental compartments that have a strong association for $Ag^+$ that are not included in the speciation modelling, including bacteria (146)(147), algae (126),

sediment (148), as well as reduced sulphur, which is an important inorganic ligand even in fully oxygenated aquatic systems (78). Therefore, the absence of $Ag^+$ observed in the present study is likely a characteristic of natural waters, where the presence of multiple, high affinity ligands prevents the accumulation of free ions in solution. This has significance if the mechanism of toxicity of AgNPs is almost entirely due to $Ag^+$ released by dissolution of the particles (45, 47). The complexation of Ag+ with ligands will thus reduce its' bioavailability and mitigate AgNP toxicity. (62, 74, 121)

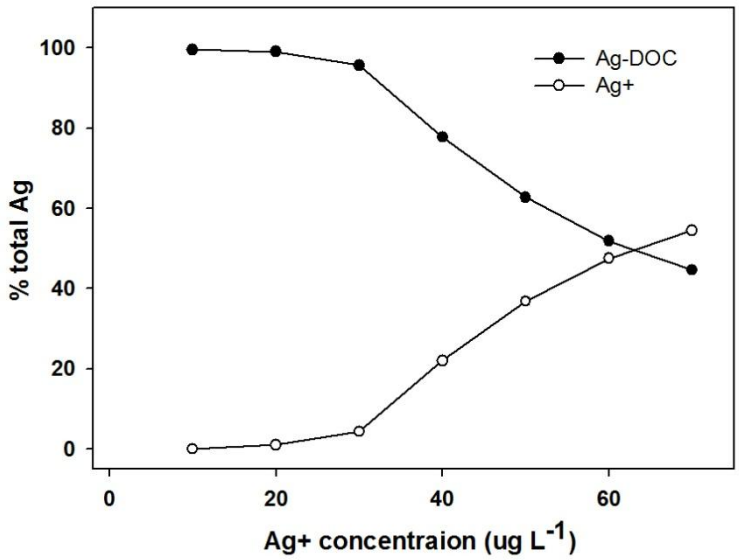


**Figure 3.11.** Silver speciation in mesocosms as a function of Ag+ concentration (µg L-) modelled using MINEQL+. The Ag species are expressed as a % TAg. No AgCl or $AgSO_4$ species were formed at any Ag+ concentration.

### *3.3.10. Mass Balance*

The concentration and relative distribution of total Ag among various compartments in the mesocosms at the end of the study is presented in Table 3.7. The Ag majority was found in water column (colloidal and particulate Ag) > sediment > periphyton. The large proportion of Ag found in the sediment (>25%) suggests that agglomeration and sedimentation was responsible for the majority of Ag dissipation from

the water column, which was also seen in wetland mesocosms dosed with AgNP (118). The periphyton on mesocosm walls also collected a portion of Ag (3-10%). The accumulation of AgNPs in biofilms has been observed in other studies (119)(127). Other important sinks not accounted for the mass balance include macrophytes and zooplankton.

**Table 3.7.** Ag concentration measured in various mesocosm compartments at the end of the study. The estimated mass of Ag in each mesocosms compartment is also presented. Data for each sediment core (average ± sd of replicate Ag analysis; n=3) and each periphyton strip (average ± sd of replicate Ag analysis; n=2) is presented. The range of recovery values for periphtyon account for uncertainty in volume of periphyton slurry as explained in text. Total Ag mass added to each mesocosm was 240 000 µg. n.a.=not analyzed due to errors in sample collection/processing.

| | **Replicate 1** | | **Replicate 2** | |
|---|---|---|---|---|
| **Compartment** | **Ag concentration** | **% Ag mass added** | **Ag concentration** | **% Ag mass added** |
| **Water Column** | | | | |
| Particles (particulate Ag) | 10.7 µg $L^{-}$ | 14 | 11.2 µg $L^{-}$ | 14 |
| Water (colloidal Ag) | 4.9 µg $L^{-}$ | 6 | 7.6 µg $L^{-}$ | 9 |
| **Sediment: Core 1** | | | | |
| 0-2 cm | 3.7 ± 1.2 µg $g^{-1}$ | 28 ± 10 | 5.6 ± 0.2 µg $g^{-1}$ | 25 ± 1 |
| 2-4 cm | 0.4 ± 0.0 µg $g^{-1}$ | 2 ± 1 | 0.9 ± 0.2 µg $g^{-}$ | 9 ± 3 |
| 4-6 cm | 0.2 ± 0 µg $g^{-1}$ | 0 | 0.2 ± 0.1 µg $g^{-1}$ | 0 |
| **Sediment: Core 2** | | | | |
| 0-2 cm | n.a. | - | 5.6 ± 0.4 µg $g^{-1}$ | 26 ± 2 |
| 2-4 cm | n.a. | - | 0.5 ± 0.1 µg $g^{-1}$ | 3 ± 1 |
| 4-6 cm | n.a. | - | 0.1 ± 0.0 µg $g^{-1}$ | 0 |
| **Periphtyon Strip 1** | 2115 ± 169 µg $g^{-1}$ | 3 ± 0 – 6 ± 0 | 2045 ± 67 µg $g^{-1}$ | 4 ± 0 – 8 ± 0 |
| **Periphyton Strip 2** | 1770 ± 77 µg $g^{-1}$ | 4 ± 0 – 8 ± 1 | 1986 ± 78 µg $g^{-1}$ | 5 ± 0 - 10 ± 0 |
| **Total Ag Recovered** | | **53-58** | | **56-68** |

### *3.3.11. Advantages and Limitations of Analytical Techniques*

The analytical techniques used to analyze AgNPs and their associated transformations each have advantages and limitations. Monitoring AgNP dissolution in natural waters using ultrafiltration techniques is challenging because it may exclude $Ag^+$ complexed with high molecular weight ligands (i.e. DOC, POM). However, ultrafiltration does provide information on the amount of "free" and/or biologically available $Ag^+$, which is the most toxic form (45, 47). Accurate analytical determination of AgNPs by CPE may not be possible in complex aqueous matrices, as demonstrated by the greatly reduced recovery in L239 water and the variation in extraction efficiency with AgNP size. Nevertheless, our CPE results do distinguish AgNPs from $Ag^+$ and thus, monitor trends in AgNP dissolution. AF4-ICP-MS and spICP-MS were the most sensitive and versatile analytical tools for understanding AgNPs transformations at environmentally relevant levels. Both methods provide data on particle size distributions that can contribute to an understanding of AgNP dissolution and agglomeration. However, spICP-MS is currently limited to analysis of nanoparticles >30 nm and AF4-ICP-MS often requires a compromise between the resolution of size separations and recovery, due to particle-membrane interactions. AF4-ICP-MS is also less sensitive and subject to longer analysis times relative to spICP-MS.

In the present study, particle size distributions determined using AF4-ICP-MS indicated no decrease in AgNP size observed in the first 7 days. Conversely, spICP-MS particle size distributions showed a decrease in AgNP size over time. The spICP-MS analytical technique uses Ag mass to determine the primary particle size, while the AF4-ICP-MS method separates particles based on their hydrodynamic diameter. It is possible that the AF4-ICP-MS detected Ag associated with other particles like DOC that increased

the hydrodynamic radius of AgNPs. Thus, the results highlight a potential advantage of AF4-ICP-MS over spICP-MS for the study of AgNP heteroagglomeration and AgNP surface modifications. In addition, AF4-ICP-MS may be a useful technique for monitoring the formation of $Ag^+$ complexes through the analysis of small sized particles in the early eluting peak. Alternatively, the measurement of the primary size of AgNPs by spICP-MS is a useful indicator of dissolution when studying AgNPs at dilute concentrations (i.e., ng Ag $L^{-1}$) and when direct measurement of $Ag^+$ is not possible due to partitioning to other environmental sinks (139). Sample preparation is another important consideration when analyzing AgNPs. The extensive dilution required for spICP-MS analysis may not have maintained agglomerates, although the dilution was performed immediately before analysis to minimize alterations to particle behaviour. Also, before samples were analyzed by spICP-MS and AF4-ICP-MS, the suspensions were sonicated and it is unclear whether this would have altered agglomeration state. These results illustrate that in order to gain a full understanding of AgNP transformations in the environment, multiple analytical methods should be used to quantify different Ag forms and to overcome the limitations of each method.

### 3.4. Conclusion

In the lake mesocosms, total Ag levels declined relatively slowly, with a $t_{1/2}$ of ~20 days. The stability of AgNPs was likely due to the low ionic strength and moderate concentrations of DOC in the lake water. All analytical techniques indicated that there was dissolution of AgNPs over time, but the concentrations of dAg, which includes $Ag^+$, were generally below detection limits. Modelling of $Ag^+$ speciation predicted that the majority of $Ag^+$ would complex with DOC, which was supported by AF4-ICP-MS

results. This observation has significance for toxicity to aquatic organisms, as the toxic free ion would not be bioavailable when associated with DOC. There was no evidence of extensive homoagglomeration of AgNPs. Given the low concentration of AgNPs in the mesocosms relative to the high amounts of other natural particles (i.e. bacteria, algae, viruses), it is probable that AgNPs became associated with suspended particulates as suggested by the particulate Ag results. This is an important fate and transformation process that requires further investigation. For example, it is uncertain weather heteroagglomeration between AgNPs and bacteriaplankton will impact AgNP stability and sedimentation out of the water column. Nonetheless, sedimentation was an important dissipation process for AgNPs representing >25% of the mass balance. Overall, the present study emphasizes that mesocosm or ecosystem level studies are needed to fully understand the transformations and fate of AgNPs in natural waters.

## Chapter 4: Summary and Conclusion

In this research, the fate of AgNPs in lake mesocosms was studied using both a continuous (i.e. drip) and one-time (i.e. plug) dosing regime. Chapter 2 presents the results from the drip mesocosms, which focused on evaluating the effect of loading rate and surface coating on AgNP fate upon continuous addition of AgNPs over time. AgNP transformations were assessed using size fractionation analysis and an end-of-study mass balance was preformed to assess the distribution of Ag among various environmental compartments. In Chapter 3, results from the plug mesocosms was presented, which focused on applying and comparing various analytical techniques, other than filtration, in understanding AgNP transformations. The following presents a summary of each section, followed by suggested areas of future work, and a conclusion from the entire study.

### 4.1. Drip Mesocosm Summary

The objective of the "drip" loading type was to determine the fate of AgNPs in lake mesocosms dosed with a continuous addition of AgNPs to surface waters. Fate of AgNPs was assessed in terms of AgNPs persistence, transformation (i.e. agglomeration and dissolution), and distribution within the environment. It was hypothesized that AgNPs would not accumulate in the water column over time due to quick dissipation. However, in the tested lake environment, the AgNPs were relatively persistence and accumulated in the water column to concentrations that were 30-40% of the targeted levels. The physiochemical conditions contributed to AgNP stability. The tested lake environment had high DOC concentraions and low ionic strength, which reduced AgNP agglomeration and subsequent sedimentation from the water column.

A secondary objective of the drip mesocosm study was to evaluate the effect of loading (i.e. amount) and type of surface coating (i.e. PVP, CT) on the fate of AgNPs. PVP-AgNPs were hypothesized to have reduced agglomeration rates and increased particle persistence as compared to CT-AgNPs. This hypothesis was based off laboratory studies in the literature which found that the steric stabilization imparted by PVP-AgNPs had greater stability than the electrostatic stabilization of CT-AgNPs. However, the agglomeration, in terms of the amount of particulate Ag maintained on a 0.2 µm membrane, did not differ between PVP-AgNPs and CT-AgNPs. Consequently, we could not conclude that the persistence of the AgNPs differed between the two surface coatings as only one CT-AgNP mesocosm replicate had significantly lower TAg concentrations. It was also hypothesized that increased AgNP loading would have higher rates of agglomeration as a result of increased particle-particle interactions; however, this was not observed in this mesocosm study. In fact, the agglomeration among all mesocosms did not appear to differ because the % of TAg found in the particulate phase generally followed the same trends. There are a few hypotheses for not observing differences in agglomeration among the treatments, which include: 1) the method of filtration not being sensitive enough to detect differences in particle size in terms of homoagglomeration 2) the high DOC and low ionic strength preventing homoagglomeration 3) the higher concentrations of biological particles (i.e. algae) compared to AgNPs resulting in heteroagglomeration and/or bioaccumulation of $Ag^+$ rather than homo-agglomeration.

PVP-AgNPs were hypothesised to have greater dissolution than CT-AgNPs as a result of suspected decreased agglomeration for PVP-AgNPs and or/ $Ag^+$ complexation

by the citrate molecules on CT-AgNPs, as reported in the literature. Furthermore, decreased AgNP loading was hypothesized to have increased dissolution based on the proportion of dAg to TAg. However, differences in dissolution among the treatments could not be assessed as the majority of dAg measured in a 3 kDa filtrate was below the LOD. As a result, it was hypothesized that the majority of $Ag^{+}$ released from AgNPs was complexing with larger molecular weight ligands such as DOC or POM, which were retained on the filter.

The accumulation of Ag among the water, particles, periphyton, and sediment was measured at the end of the study. Ag accumulated among the various environment compartments in a dose-dependent manner. A mass balance at the end of the study was estimated to assess the distribution of AgNPs among the mesocosms compartments. Overall, the proportion of total Ag sequestered in each compartment, in decreasing order, was the water column (water and particles) > sediment > periphyton. The final mass balance for Ag in the mesocosms ranged from 42-73%. A 100% mass balance was not achieved and this may be due to the fact that not all of the environmental sinks were included, such as macroplankton, detritus, macrophytes, and biofilms on the macrophyte surfaces. Also, the volumes (i.e. sediment) and surface areas (i.e. periphtyon) used in the calculations were estimated. Finally, there was variation in the concentrations of Ag measured among periphyton and sediment sampling replicates that would reflect variation in the mass balance.

### 4.2. Plug Mesocosm Summary

The objective of the "plug" loading type was to determine the fate of AgNPs in lake mesocosms dosed with a one-time addition of AgNPs to surface waters. As compared to the drip mesocosms, more sophisticated analytical techniques, beside size fractionation by filtration, were applied to characterize transformations of AgNPs. These techniques included CPE, sp-ICP-MS, AF4-ICP-MS.

AgNPs were hypothesized to quickly dissipate from the water column, however total Ag dissipated from the water column at a slower rate than expected with a half life of ~20 days. The high DOC and low ionic strength contributed to the stability of AgNPs reducing the extent of homoagglomeration between particles.

AgNP agglomeration in natural waters was hypothesized to include both hetero- and homo-agglomeration, leading to larger particle sizes. The 0.2 µm filtration, spICP-MS, and AF4-ICP-MS techniques were used to assess agglomeration. The particulate Ag on the 0.2 µm retentate varied between 21-56% and it was hypothesized that the majority of the particulate Ag consisted of AgNP hetero-agglomerates or Ag+ accumulation with POM. The particle size distributions determined by spICP-MS results also suggested very little homoagglomeration between particles occurred. AF4-ICP-MS particle size distributions had no distinct temporal trends with mean hydrodynamic diameters varying between 56 and 92 nm over 7 days. However, it was hypothesized that the presence of Ag in the rinse phase represented AgNP agglomerates unresolved by the method. Heteroagglomeration with POM was suspected to result in sedimentation and dissipation of Ag from the water column and this was confirmed by the large proportion >25 % of Ag found in the sediments of plug mesocosms.

AgNPs were hypothesized to dissolve over time and release Ag+, resulting in smaller particle sizes. The results of analysis by CPE, spICP-MS, and AF4-ICP-MS all indicated that dissolution of AgNPs occurred over time. CPE showed a temporal decrease in the % of AgNPs extracted relative to total Ag, as a result of both an increased proportion of dAg and decreased particle sizes lowering the extraction efficiency of the method. spICP-MS confirmed that AgNPs decreased in size (i.e. 50 nm to 30 nm over 21 days), as a result of AgNP dissolution. The released $Ag^{+}$ was hypothesized to complex with other ligands (i.e. DOC) found in natural waters. The low concentration of dAg (<1 μg $L^{-}$) detected by ultrafiltration was the result of the released Ag+ complexing with larger molecular weight ligands such as DOC or adsorbing to POM such as algae. The increase in Ag detected in the AF4-ICP-MS void peak over time also demonstrated the temporal dissolution and subsequent Ag+ complexation with molecules 1-10 nm in size, such as DOC. MINEQL+ analysis confirmed that given the DOC concentration present in the mesocosms, the majority of released Ag+ formed Ag-DOC complexes. However, speciation with algae, sediment, and reduced sulfur are other important sinks for Ag+ that was not included in the model.

There were limitations with each method used to quantify AgNP and/or $Ag^{+}$, and assess AgNP transformations. For each method the limitations this study observed in both laboratory validation studies and mesocosm sample analysis, included:

1) 0.2 μm filtration: Using the method to assess AgNP agglomeration cannot differentiate between heteroagglomeration, homoagglomeration, or $Ag^{+}$ associated with POM.

2) 3 kDa ultra-filtration: Low recoveries at low $Ag^+$ concentrations (i.e. 44% at 1 µg $L^{-1}$ $Ag^+$). Also, the method can only measure free or low molecular weight complexes of $Ag^+$. From a biological standpoint this is useful for determining the bioavailable forms of Ag+; however, it is difficult to assess the extent of AgNP dissolution in natural waters with this method as the majority of Ag+ will readily complex with other ligands.

3) CPE: The method had sub-optimal AgNP recovery in DI water (i.e. 75%), which decreased in L239 water (i.e. 45%). Also, AgNP extraction efficiency was found to change with AgNP size, which limits the accuracy of AgNP quantification. However, for the purpose of this study, the temporal trends in the % of AgNP extracted were useful for evaluating dissolution.

4) spICP-MS: The method is limited to analysis of larger sized AgNPs (>30 nm) and may require extensive dilution than makes Ag+ undetectable.

5) AF4-ICP-MS: The method often requires a compromise between the resolution of size separations and recovery, due to particle-membrane interactions. Varying recovery between different AgNP surface coatings or over the duration of using a membrane might also affect quantification. AF4-ICP-MS is also limited to high mass detection limits for AgNP quantification and much longer analysis times as compared to spICP-MS.

### 4.3 Future Work

The mesocosm experiment was a preliminary study for the Lake Ecosystem NanoSilver (LENS) project. Future work includes a whole-lake addition study, in which the objective is to examine the fate of AgNPs upon their continuous addition from a point source and simulate AgNP release from WWTP effluent. Several suggestions are proposed in terms of the sampling and analysis of AgNPs based on the results and limitations from the mesocosms study.

In order to fully assess and understand the fate of AgNPs, sampling should include:

1) Implementation of sedimentation traps in the hypolimnion, along with temporal sampling, to determine sedimentation rates for particulate Ag.

2) Analysis of macrophytes and macroplankton for Ag to account for all environmental sinks.

3) Careful sectioning of sediment layers, which can be improved by freezing the cores then extruding them from the core tubes.

4) Measuring concentrations of sulfides so it can be included in speciation modelling.

In order to improve the quantification of AgNPs and $Ag^{+}$, the techniques in the mesocosm study should be optimized. Particular areas that need optimization are:

1) Improved detection of $Ag^{+}$. Centrifugal ultrafiltration units should be used over stirred ultra centrifugation due to ease of use, cost, higher sample throughput, and better recovery. However, the membranes should be pre-equilibrated with Ag+ to

reduce adsorptive losses of Ag+ (85). Ion exchange technique (IET) can also be used to pre-concentrate Ag+ from solution (85). spICP-MS should also be preformed with undiluted samples to ensure Ag+ concentraions are not below the detection limit.

2) Improved quantification using AF4-ICP-MS: In this study, we quantified AgNP concentration using a one-point external calibration with injection of PVP-AgNP standards analyzed under the same conditions of the mesocosm samples. However, variability in AF4 channel recovery between differently charged surfaces (i.e. fresh PVP AgNP standards vs. aged AgNP samples) and over multiple analysis of samples may affect quantification. A gradient cross-flow program should also be developed to increase the size range of separation for polydisperse natural water samples. Decreasing the cross-flow over the duration of sample elution can improve the resolution of smaller sized Ag particles and minimize the loss of large AgNP agglomerates to the rinse phase. Also, flow injection with dissolved Ag standards (20) should be used to quantify the Ag concentration in the void peak that may represent Ag+ complexes.

3) Improved size detection limits with spICP-MS: spICP-MS is the most promising technique for quantifying AgNPs due to its superior detection limits (i.e. ng $L^{-1}$). However, the technique needs to be optimized to measure smaller sized AgNPs (i.e. < 30 nm).

## 4.4 Conclusion

AgNPs are increasingly being produced and applied to consumer products, yet the implications of the environmental release of AgNPs on ecosystem health are unknown. AgNPs risk to the aquatic environment are a function of both the inherent toxicity to organisms and the exposure levels of free $Ag^{+}$, isolated AgNPs, and agglomerated AgNPs. Knowledge of the fate of AgNPs in terms of its persistence, transformations, and distribution within a lake environment is imperative to risk assessment. This was the first study to investigate the fate of AgNPs within a natural lake environment using mesocosms. Overall, this study demonstrates that AgNPs may persist in aquatic environments with low ionic strength and high DOC; and, this could result in either the accumulation of AgNPs upon continuous addition to surface waters, or the slow dissipation after a single addition to surface waters. Agglomeration is expected to remove AgNPs from surface waters through sedimentation. In natural freshwaters, with low concentrations of AgNPs, heteroagglomeration with biological particles will likely govern the extent of agglomeration. Dissolution of AgNPs to release Ag+ is also expected to occur in surface waters; but, the speciation of $Ag^{+}$ with ligands, such as DOC, controls the levels of the toxic free ion. Furthermore, to gain a full understanding of AgNP transformations in the environment, multiple analyses should be performed to quantify different Ag forms and overcome the limitations of each method.

## REFERENCES


1. Schluesener, J.K. and Schluesener, H.J. Nanosilver: application and novel aspects of toxicology. *Arch. Toxicol.* 2013, *87* (4), 569-576

2. The Project on Emerging Nanotechnologies (PEN) *October 21, 2013*

3. Maurer-Jones, M.A.; Gunsolus, I.L.; Murphy, C.J.; Haynes, C.L. Toxicity of engineered nanoparticles in the environment. *Anal. Chem.* 2013, *85* (6), 3036-3049

4. Gottschalk, F.; Sun, T.; Nowack, B. Environmental concentrations of engineered nanomaterials: Review of modeling and analytical studies. *Environ. Pollut.* 2013, *181*, 287-300

5. Nowack, B.; Ranville, J.F.; Diamond, S.; Gallego-Urrea, J.A.; Metcalfe, C.; Rose, J.; Horne, N.; Koelmans, A.A.; Klaine, S.J. Potential scenarios for nanomaterial release and subsequent alteration in the environment. *Environ. Toxicol. Chem.* 2012, *31* (1), 50-59

6. Blaser, S.A.; Scheringer, M.; MacLeod, M.; Hungerbuehler, K. Estimation of cumulative aquatic exposure and risk due to silver: Contribution of nano-functionalized plastics and textiles. *Sci. Total Environ.* 2008, *390* (2-3), 396-409

7. Lowry, G.V.; Gregory, K.B.; Apte, S.C.; Lead, J.R. Transformations of nanomaterials in the environment. *Environ. Sci. Technol.* 2012, *46* (13), 6893-6899

8. Levard, C.; Hotze, E.M.; Lowry, G.V.; Brown, G.E.,Jr. Environmental transformations of silver nanoparticles: impact on stability and toxicity. *Environ. Sci. Technol.* 2012, *46* (13), 6900-6914

9. Benn, T.M. and Westerhoff, P. Nanoparticle silver released into water from commercially available sock fabrics. *Environ. Sci. Technol.* 2008, *42* (11), 4133-4139

10. Geranio, L.; Heuberger, M.; Nowack, B. The behavior of silver nanotextiles during washing. *Environ. Sci. Technol.* 2009, *43* (21), 8113-8118

11. Pasricha, A.; Jangra, S.L.; Singh, N.; Dilbaghi, N.; Sood, K.N.; Arora, K.; Pasricha, R. Comparative study of leaching of silver nanoparticles from fabric and effective effluent treatment. *J. Environ. Sci.-China* 2012, *24* (5), 852-859

12. Kaegi, R.; Sinnet, B.; Zuleeg, S.; Hagendorfer, H.; Mueller, E.; Vonbank, R.; Boller, M.; Burkhardt, M. Release of silver nanoparticles from outdoor facades. *Environ. Pollut.* 2010, *158* (9), 2900-2905

13. Kaegi, R.; Voegelin, A.; Sinnet, B.; Zuleeg, S.; Hagendorfer, H.; Burkhardt, M.; Siegrist, H. Behavior of metallic silver nanoparticles in a pilot wastewater treatment plant. *Environ. Sci. Technol.* 2011, *45* (9), 3902-3908

14. Kaegi, R.; Voegelin, A.; Ort, C.; Sinnet, B.; Thalmann, B.; Krismer, J.; Hagendorfer, H.; Elumelu, M.; Mueller, E. Fate and transformation of silver nanoparticles in urban wastewater systems. *Water Res.* 2013, *47* (12), 3866-3877

15. Li, L.; Hartmann, G.; Doeblinger, M.; Schuster, M. Quantification of nanoscale silver particles removal and release from municipal wastewater treatment plants in germany. *Environ. Sci. Technol.* 2013, *47* (13), 7317-7323

16. Gottschalk, F.; Sonderer, T.; Scholz, R.W.; Nowack, B. Modeled environmental concentrations of engineered nanomaterials (TiO(2), ZnO, Ag, CNT, Fullerenes) for different regions. *Environ. Sci. Technol.* 2009, *43* (24), 9216-9222

17. Mueller, N.C. and Nowack, B. Exposure modeling of engineered nanoparticles in the environment. *Environ. Sci. Technol.* 2008, *42* (12), 4447-4453

18. Musee, N. Simulated environmental risk estimation of engineered nanomaterials: A case of cosmetics in Johannesburg City. *Hum. Exp. Toxicol.* 2011, *30* (9), 1181-1195

19. O'Brien, N. and Cummins, E. Nano-Scale Pollutants: Fate in irish surface and drinking water regulatory systems. *Hum. Ecol. Risk Assess.* 2010, *16* (4), 847-872

20. Hoque, M.E.; Khosravi, K.; Newman, K.; Metcalfe, C.D. Detection and characterization of silver nanoparticles in aqueous matrices using asymmetric-flow field flow fractionation with inductively coupled plasma mass spectrometry. *J. Chromatogr. A* 2012, *1233*, 109-115

21. Sondi, I. and Salopek-Sondi, B. Silver nanoparticles as antimicrobial agent: a case study on E-coli as a model for Gram-negative bacteria. *J. Colloid Interface Sci.* 2004, *275* (1), 177-182

22. Choi, O.; Deng, K.K.; Kim, N.; Ross, L.,Jr.; Surampalli, R.Y.; Hu, Z. The inhibitory effects of silver nanoparticles, silver ions, and silver chloride colloids on microbial growth. *Water Res.* 2008, *42* (12), 3066-3074

23. Dror-Ehre, A.; Mamane, H.; Belenkova, T.; Markovich, G.; Adin, A. Silver nanoparticle-E. coli colloidal interaction in water and effect on E-coli survival. *J. Colloid Interface Sci.* 2009, *339* (2), 521-526

24. Allen, H.J.; Impellitteri, C.A.; Macke, D.A.; Heckman, J.L.; Poynton, H.C.; Lazorchak, J.M.; Govindaswamy, S.; Roose, D.L.; Nadagouda, M.N. Effects from filtration, capping agents, and presence/absence of food on the toxicity of silver nanoparticles to Daphnia Magna. *Environ. Toxicol. Chem.* 2010, *29* (12), 2742-2750

25. Asghari, S.; Johari, S.A.; Lee, J.H.; Kim, Y.S.; Jeon, Y.B.; Choi, H.J.; Moon, M.C.; Yu, I.J. Toxicity of various silver nanoparticles compared to silver ions in Daphnia magna. *J. Nanobiotech.* 2012, *10*, (14) 1477-3155

26. Zhao, C. and Wang, W. Comparison of acute and chronic toxicity of silver nanoparticles and silver nitrate to Daphnia Magna. *Environ. Toxicol. Chem.* 2011, *30* (4), 885-892

27. Navarro, E.; Piccapietra, F.; Wagner, B.; Marconi, F.; Kaegi, R.; Odzak, N.; Sigg, L.; Behra, R. Toxicity of silver nanoparticles to chlamydomonas reinhardtii. 2009. *Environ. Sci. Technol.* 2008, *42* (23), 8959-8964.

28. Oukarroum, A.; Bras, S.; Perreault, F.; Popovic, R. Inhibitory effects of silver nanoparticles in two green algae, Chlorella vulgaris and Dunaliella tertiolecta. *Ecotoxicol. Environ. Saf.* 2012, *78*, 80-85

29. Arnaout, C.L. and Gunsch, C.K. Impacts of silver nanoparticle coating on the nitrification potential of nitrosomonas europaea. *Environ. Sci. Technol.* 2012, *46* (10), 5387-5395

30. Yang, Y.; Wang, J.; Xiu, Z.; Alvarez, P.J.J. Impacts of silver nanoparticles on cellular and transcriptional activity of nitrogen-cycling bacteria. *Environ. Toxicol. Chem.* 2013, *32* (7), 1488-1494.

31. Pradhan, A.; Seena, S.; Pascoal, C.; Cassio, F. Can metal nanoparticles be a threat to microbial decomposers of plant litter in streams? *Microb. Ecol.* 2011, *62* (1), 58-68.

32. Das, P.; Xenopoulos, M.A.; Williams, C.J.; Hoque, M.E.; Metcalfe, C.D. Effects of silver nanoparticles on bacterial activity in natural waters. *Environ. Toxicol. Chem.* 2012, *31* (1), 122-130.

33. Das, P.; Williams, C.J.; Fulthorpe, R.R.; Hoque, M.E.; Metcalfe, C.D.; Xenopoulos, M.A. Changes in bacterial community structure after exposure to silver nanoparticles in natural waters. *Environ. Sci. Technol.* 2012, *46* (16), 9120-9128.

34. Farmen, E.; Mikkelsen, H.N.; Evensen, O.; Einset, J.; Heier, L.S.; Rosseland, B.O.; Salbu, B.; Tollefsen, K.E.; Oughton, D.H. Acute and sub-lethal effects in juvenile Atlantic salmon exposed to low mu g/L concentrations of Ag nanoparticles. *Aquat. Toxicol.* 2012, *108*, 78-84

35. Cunningham, S.; Brennan-Fournet, M.E.; Ledwith, D.; Byrnes, L.; Joshi, L. Effect of nanoparticle stabilization and physicochemical properties on exposure outcome: acute toxicity of silver nanoparticle preparations in zebrafish (Danio rerio). *Environ. Sci. Technol.* 2013, *47* (8), 3883-3892

36. Kim, J.Y.; Kim, K.; Lee, B.G.; Lim, B.J.; Kim, S.D. Developmental toxicity of Japanese medaka embryos by silver nanoparticles and released ions in the presence of humic acid. *Ecotoxicol. Environ. Saf.* 2013, *92*, 57-63.

37. Hwang, E.T.; Lee, J.H.; Chae, Y.J.; Kim, Y.S.; Kim, B.C.; Sang, B.; Gu, M.B. Analysis of the toxic mode of action of silver nanoparticles using stress-specific bioluminescent bacteria. *Small* 2008, *4* (6), 746-750

38. Kim, T.; Kim, M.; Park, H.; Shin, U.S.; Gong, M.; Kim, H. Size-dependent cellular toxicity of silver nanoparticles. *J. Biomed. Mater. Res. Part A* 2012, *100A* (4), 1033-1043

39. Lim, D.; Roh, J.; Eom, H.; Choi, J.; Hyun, J.; Choi, J. Oxidative stress-related PMK-1 P38 MAPK activation as a mechanism for toxicity of silver nanoparticles to reproduction in the nematode Caenorhabditis elegans. *Environ. Toxicol. Chem.* 2012, *31* (3), 585-592

40. Choi, O. and Hu, Z. Size dependent and reactive oxygen species related nanosilver toxicity to nitrifying bacteria. *Environ. Sci. Technol.* 2008, *42* (12), 4583-4588

41. Zhao, C. and Wang, W. Regulation of sodium and calcium in Daphnia magna exposed to silver nanoparticles. *Environ. Toxicol. Chem.* 2013, *32* (4), 913-919

42. Lok, C.N.; Ho, C.M.; Chen, R.; He, Q.Y.; Yu, W.Y.; Sun, H.Z.; Tam, P.K.H.; Chiu, J.F.; Che, C.M. Proteomic analysis of the mode of antibacterial action of silver nanoparticles. *J. Prot. Res.* 2006, *5* (4), 916-924

43. Lubick, N. Nanosilver toxicity: ions, nanoparticles-or both? *Environ. Sci. Technol.* 2008, *42* (23), 8617-8617

44. Kennedy, A.J.; Hull, M.S.; Bednar, A.J.; Goss, J.D.; Gunter, J.C.; Bouldin, J.L.; Vikesland, P.J.; Steevens, J.A. Fractionating nanosilver: importance for determining toxicity to aquatic test organisms. *Environ. Sci. Technol.* 2010, *44* (24), 9571-9577

45. Yang, X.; Gondikas, A.P.; Marinakos, S.M.; Auffan, M.; Liu, J.; Hsu-Kim, H.; Meyer, J.N. Mechanism of silver nanoparticle toxicity is dependent on dissolved silver and surface coating in Caenorhabditis elegans. *Environ. Sci. Technol.* 2012, *46* (2), 1119-1127

46. Zhao, C. and Wang, W. Importance of surface coatings and soluble silver in silver nanoparticles toxicity to Daphnia magna. *Nanotoxicology* 2012, *6* (4), 361-370

47. Newton, K.M.; Puppala, H.L.; Kitchens, C.L.; Colvin, V.L.; Klaine, S.J. Silver nanoparticle toxicity to Daphnia magna is a function of dissolved silver concentration. *Environ. Toxicol. Chem.* 2013, *32* (10), 2356-2364

48. Zhao, C. and Wang, W. Regulation of sodium and calcium in Daphnia magna exposed to silver nanoparticles. *Environ. Toxicol. Chem.* 2013, *32* (4), 913-919

49. Xiu, Z.; Zhang, Q.; Puppala, H.L.; Colvin, V.L.; Alvarez, P.J.J. Negligible Particle-Specific Antibacterial Activity of Silver Nanoparticles. *Nano Lett.* 2012, *12* (8), 4271-4275

50. Morones, J.; Elechiguerra, J.; Camacho, A.; Holt, K.; Kouri, J.; Ramirez, J.; Yacaman, M. The bactericidal effect of silver nanoparticles. *Nanotechnol.* 2005, *16* (10), 2346-2353

51. Hotze, E.M.; Phenrat, T.; Lowry, G.V. Nanoparticle aggregation: challenges to understanding transport and reactivity in the environment. *J. Environ. Qual.* 2010, *39* (6), 1909-1924

52. Petosa, A.R.; Jaisi, D.P.; Quevedo, I.R.; Elimelech, M.; Tufenkji, N. Aggregation and deposition of engineered nanomaterials in aquatic environments: role of physicochemical interactions. *Environ. Sci. Technol.* 2010, 6532-6549

53. Li, X.; Lenhart, J.J.; Walker, H.W. Dissolution-accompanied aggregation kinetics of silver nanoparticles. *Langmuir* 2010, *26* (22), 16690-16698

54. Li, X.; Lenhari, J.J.; Walker, H.W. Aggregation kinetics and dissolution of coated silver nanoparticles. *Langmuir* 2012, *28* (2), 1095-1104

55. Huynh, K.A. and Chen, K.L. Aggregation kinetics of citrate and polyvinylpyrrolidone coated silver nanoparticles in monovalent and divalent electrolyte solutions 2010. *Environ. Sci. Technol.* 2011, *45* (13), 5564-5571

56. Gebauer, J.S. and Treuel, L. Influence of individual ionic components on the agglomeration kinetics of silver nanoparticles. *J. Colloid Interface Sci.* 2011, *354* (2), 546-554

57. He, D.; Bligh, M.W.; Waite, T.D. Effects of aggregate structure on the dissolution kinetics of citrate-stabilized silver nanoparticles. *Environ. Sci. Technol.* 2013, *47* (16), 9148-9156

58. Levard, C.; Reinsch, B.C.; Michel, F.M.; Oumahi, C.; Lowry, G.V.; Brown, G.E., Jr. Sulfidation processes of PVP-coated silver nanoparticles in aqueous solution: impact on dissolution rate. *Environ. Sci. Technol.* 2011, *45* (12), 5260-5266

59. Li, X. and Lenhart, J.J. Aggregation and dissolution of silver nanoparticles in natural surface water. *Environ. Sci. Technol.* 2012, *46* (10), 5378-5386

60. Gao, J.; Youn, S.; Hovsepyan, A.; Llaneza, V.L.; Wang, Y.; Bitton, G.; Bonzongo, J.J. Dispersion and toxicity of selected manufactured nanomaterials in natural river water samples: effects of water chemical composition *Environ. Sci. Technol.* 2009, *43* (9), 3322-3328

61. Chinnapongse, S.L.; MacCuspie, R.I.; Hackley, V.A. Persistence of singly dispersed silver nanoparticles in natural freshwaters, synthetic seawater, and simulated estuarine waters. *Sci. Total Environ.* 2011, *409* (12), 2443-2450

62. Kennedy, A.J.; Chappell, M.A.; Bednar, A.J.; Ryan, A.C.; Laird, J.G.; Stanley, J.K.; Steevens, J.A. Impact of organic carbon on the stability and toxicity of fresh and stored silver nanoparticles. *Environ. Sci. Technol.* 2012, *46* (19), 10772-10780

63. Turner, A.; Brice, D.; Brown, M.T. Interactions of silver nanoparticles with the marine macroalga, Ulva lactuca. *Ecotoxicol.* 2012, *21* (1), 148-154

64. Velzeboer, I.; Hendriks, A.J.; Ragas, A.M.J.; Van de Meent, D. Aquatic ecotoxicity tests of some nanomaterials. *Environ. Toxicol. Chem.* 2008, *27* (9), 1942-1947

65. Bae, E.; Park, H.; Lee, J.; Kim, Y.; Yoon, J.; Park, K.; Choi, K.; Yi, J. Bacterial cytotoxicity of the silver nanoparticle related to physicochemical metrics and agglomeration properties. *Environ. Toxicol. Chem.* 2010, *29* (10), 2154-2160

66. Kvitek, L.; Panacek, A.; Soukupova, J.; Kolar, M.; Vecerova, R.; Prucek, R.; Holecova, M.; Zboril, R. Effect of surfactants and polymers on stability and antibacterial activity of silver nanoparticles (NPs). *J. Phys. Chem. C* 2008, *112* (15), 5825-5834

67. McLaughlin, J. and Bonzongo, J.J. Effects of natural water chemistry on nanosilver behavior and toxicity to Ceriodaphnia dubia and Pseudokirchneriella subcapitata. *Environ. Toxicol. Chem.* 2012, *31* (1), 168-175

68. Liu, J. and Hurt, R.H. Ion release kinetics and particle persistence in aqueous nano-silver colloids. *Environ. Sci. Technol.* 2010, *44* (6), 2169-2175

69. Elzey, S. and Grassian, V.H. Agglomeration, isolation and dissolution of commercially manufactured silver nanoparticles in aqueous environments. *J. Nano. Res.* 2010, *12* (5), 1945-1958

70. Kittler, S.; Greulich, C.; Diendorf, J.; Koeller, M.; Epple, M. Toxicity of silver nanoparticles increases during storage because of slow dissolution under release of silver ions. *Chem. Mater.* 2010, *22* (16), 4548-4554

71. Angel, B.M.; Batley, G.E.; Jarolimek, C.V.; Rogers, N.J. The impact of size on the fate and toxicity of nanoparticulate silver in aquatic systems. *Chemosphere* 2013, *93* (2), 359-365

72. Levard, C.; Mitra, S.; Yang, T.; Jew, A.D.; Badireddy, A.R.; Lowry, G.V.; Brown, G.E., Jr. Effect of chloride on the dissolution rate of silver nanoparticles and toxicity to E. coli. *Environ. Sci. Technol.* 2013, *47* (11), 5738-5745

73. Gondikas, A.P.; Morris, A.; Reinsch, B.C.; Marinakos, S.M.; Lowry, G.V.; Hsu-Kim, H. Cysteine-induced modifications of zero-valent silver nanomaterials: implications for particle surface chemistry, aggregation, dissolution, and silver speciation. *Environ. Sci. Technol.* 2012, *46* (13), 7037-7045

74. Gao, J.; Powers, K.; Wang, Y.; Zhou, H.; Roberts, S.M.; Moudgil, B.M.; Koopman, B.; Barber, D.S. Influence of suwannee river humic acid on particle properties and toxicity of silver nanoparticles. *Chemosphere* 2012, *89* (1), 96-101

75. Lee, D.; Fortin, C.; Campbell, P. Contrasting effects of chloride on the toxicity of silver to two green algae, Pseudokirchneriella subcapitata and Chlamydomonas reinhardtii. *Aquat. Toxicol.* 2005, *75* (2), 127-135

76. Ratte, H. Bioaccumulation and toxicity of silver compounds: A review. *Environ. Toxicol. Chem.* 1999, *18* (1), 89-108

77. Reidy, B.; Haase, A.; Luch, A.; Dawson, K.A.; Lynch, I. Mechanisms of silver nanoparticle release, transformation and toxicity: a critical review of current knowledge and recommendations for future studies and applications. *Materials* 2013, *6* (6), 2295-2350

78. Bianchini, A. and Bowles, K.C. Metal sulfides in oxygenated aquatic systems: implications for the biotic ligand model. *Comp. Biochem. Phys. C-Toxicol. & Pharmacol.* 2002, *133* (1-2), 51-64

79. Choi, O.; Cleuenger, T.E.; Deng, B.; Surampalli, R.Y.; Ross, L., Jr.; Hu, Z. Role of sulfide and ligand strength in controlling nanosilver toxicity. *Water Res.* 2009, *43* (7), 1879-1886

80. Ma, R.; Levard, C.; Marinakos, S.M.; Cheng, Y.; Liu, J.; Michel, F.M.; Brown, G.E., Jr.; Lowry, G.V. Size-controlled dissolution of organic-coated silver nanoparticles. *Environ. Sci. Technol.* 2012, *46* (2), 752-759

81. Zhang, W.; Yao, Y.; Sullivan, N.; Chen, Y. Modeling the primary size effects of citrate-coated silver nanoparticles on their ion release kinetics. *Environ. Sci. Technol.* 2011, *45* (10), 4422-4428

82. Tolaymat, T.M.; El Badawy, A.M.; Genaidy, A.; Scheckel, K.G.; Luxton, T.P.; Suidan, M. An evidence-based environmental perspective of manufactured silver nanoparticle in syntheses and applications: A systematic review and critical appraisal of peer-reviewed scientific papers. *Sci. Total Environ.* 2010, *408* (5), 999-1006

83. El Badawy, A.M.; Luxton, T.P.; Silva, R.G.; Scheckel, K.G.; Suidan, M.T.; Tolaymat, T.M. Impact of environmental conditions (pH, Ionic Strength, and Electrolyte Type) on the surface charge and aggregation of silver nanoparticles suspensions. *Environ. Sci. Technol.* 2010, *44* (4), 1260-1266

84. Dobias, J. and Bernier-Latmani, R. Silver release from silver nanoparticles in natural waters. *Environ. Sci. Technol.* 2013, *47* (9), 4140-4146

85. Hadioui, M.; Leclerc, S.; Wilkinson, K.J. Multimethod quantification of Ag+ release from nanosilver. *Talanta* 2013, *105*, 15-19

86. Hasselloev, M.; Readman, J.W.; Ranville, J.F.; Tiede, K. Nanoparticle analysis and characterization methodologies in environmental risk assessment of engineered nanoparticles. *Ecotoxicol.* 2008, *17* (5), 344-361

87. von der Kammer, F.; Ferguson, P.L.; Holden, P.A.; Masion, A.; Rogers, K.R.; Klaine, S.J.; Koelmans, A.A.; Horne, N.; Unrine, J.M. Analysis of engineered nanomaterials in complex matrices (environment and biota): General considerations and conceptual case studies. *Environ. Toxicol. Chem.* 2012, *31* (1), 32-49

88. Delay, M. and Frimmel, F.H. Nanoparticles in aquatic systems. *Anal. Bioanal. Chem.* 2012, *402* (2), 583-592

89. Bednar, A.J.; Poda, A.R.; Mitrano, D.M.; Kennedy, A.J.; Gray, E.P.; Ranville, J.F.; Hayes, C.A.; Crocker, F.H.; Steevens, J.A. Comparison of on-line detectors for field flow fractionation analysis of nanomaterials. *Talanta* 2013, *104*, 140-148

90. Kowalczyk, B.; Lagzi, I.; Grzybowski, B.A. Nanoseparations: strategies for size and/or shape-selective purification of nanoparticles. *Current Opinion in Colloid & Interface Sci.* 2011, *16* (2), 135-148

91. Gimbert, L.; Haygarth, P.; Beckett, R.; Worsfold, P. Comparison of centrifugation and filtration techniques for the size fractionation of colloidal material in soil suspensions using sedimentation field-flow fractionation. *Environ. Sci. Technol.* 2005, *39* (6), 1731-1735

92. Mitrano, D.M.; Lesher, E.K.; Bednar, A.; Monserud, J.; Higgins, C.P.; Ranville, J.F. Detecting nanoparticulate silver using single-particle inductively coupled plasma-mass spectrometry. *Environ. Toxicol. Chem.* 2012, *31* (1), 115-121

93. Misra, S.K.; Dybowska, A.; Berhanu, D.; Luoma, S.N.; Valsami-Jones, E. The complexity of nanoparticle dissolution and its importance in nanotoxicological studies. *Sci. Total Environ.* 2012, *438*, 225-232

94. Kennedy, A.J.; Hull, M.S.; Bednar, A.J.; Goss, J.D.; Gunter, J.C.; Bouldin, J.L.; Vikesland, P.J.; Steevens, J.A. Fractionating nanosilver: Importance for determining toxicity to aquatic test organisms. *Environ. Sci. Technol.* 2010, 9571-9577

95. Liu, J.; Chao, J.; Liu, R.; Tan, Z.; Yin, Y.; Wu, Y.; Jiang, G. Cloud point extraction as an advantageous preconcentration approach for analysis of trace silver nanoparticles in environmental waters. *Anal. Chem.* 2009, *81* (15), 6496-6502

96. Hartmann, G.; Hutterer, C.; Schuster, M. Ultra-trace determination of silver nanoparticles in water samples using cloud point extraction and ETAAS. *J. Anal. At. Spectrom.* 2013, *28* (4), 567-572

97. Chao, J.; Liu, J.; Yu, S.; Feng, Y.; Tan, Z.; Liu, R.; Yin, Y. Speciation analysis of silver nanoparticles and silver ions in antibacterial products and environmental waters via cloud point extraction-based separation. *Anal. Chem.* 2011, *83* (17), 6875-6882

98. Baalousha, M.; Stolpe, B.; Lead, J.R. Flow field-flow fractionation for the analysis and characterization of natural colloids and manufactured nanoparticles in environmental systems: A critical review. *J. Chromat. A* 2011, *1218* (27), 4078-4103

99. Gigault, J. and Hackley, V.A. Differentiation and characterization of isotopically modified silver nanoparticles in aqueous media using asymmetric-flow field flow fractionation coupled to optical detection and mass spectrometry. *Anal. Chim. Acta* 2013, *763*, 57-66

100. Delay, M.; Dolt, T.; Woellhaf, A.; Sembritzki, R.; Frimmel, F.H. Interactions and stability of silver nanoparticles in the aqueous phase: Influence of natural organic matter (NOM) and ionic strength. *J. Chromat. A.* 2011, *1218* (27), 4206-4212

101. Cumberland, S.A. and Lead, J.R. Particle size distributions of silver nanoparticles at environmentally relevant conditions. *J. Chromat. A.* 2009, *1216* (52), 9099-9105

102. Bolea, E.; Jimenez-Lamana, J.; Laborda, F.; Castillo, J.R. Size characterization and quantification of silver nanoparticles by asymmetric flow field-flow fractionation coupled with inductively coupled plasma mass spectrometry. *Anal. Bioanal. Chem.* 2011, *401* (9), 2723-2732

103. Hagendorfer, H.; Kaegi, R.; Parlinska, M.; Sinnet, B.; Ludwig, C.; Ulrich, A. Characterization of silver nanoparticle products using asymmetric flow field flow fractionation with a multidetector approach - a comparison to transmission electron microscopy and batch dynamic light scattering. *Anal. Chem.* 2012, *84* (6), 2678-2685

104. Mitrano, D.M.; Barber, A.; Bednar, A.; Westerhoff, P.; Higgins, C.P.; Ranville, J.F. Silver nanoparticle characterization using single particle ICP-MS (SP-ICP-MS) and asymmetrical flow field flow fractionation ICP-MS (AF4-ICP-MS). *J. Anal. At. Spectrom.* 2012, *27* (7), 1131-1142

105. Poda, A.R.; Bednar, A.J.; Kennedy, A.J.; Harmon, A.; Hull, M.; Mitrano, D.M.; Ranville, J.F.; Steevens, J. Characterization of silver nanoparticles using flow-field flow fractionation interfaced to inductively coupled plasma mass spectrometry. 2011. *J. Chromat. A.* 2011, *1218* (27), 4219-4225

106. Baalousha, M.; Stolpe, B.; Lead, J.R. Flow field-flow fractionation for the analysis and characterization of natural colloids and manufactured nanoparticles in environmental systems: A critical review. *J. Chromat. A.* 2011, *1218* (27), 4078-4103

107. Unrine, J.M.; Colman, B.P.; Bone, A.J.; Gondikas, A.P.; Matson, C.W. Biotic and abiotic interactions in aquatic microcosms determine fate and toxicity of Ag nanoparticles. Part 1. aggregation and dissolution. *Environ. Sci. Technol.* 2012, *46* (13), 6915-6924

108. Gigault, J. and Hackley, V.A. Observation of size-independent effects in nanoparticle retention behavior during asymmetric-flow field-flow fractionation. *Anal. Bioanal. Chem.* 2013, *405* (19), 6251-6258

109. Ulrich, A.; Losert, S.; Bendixen, N.; Al-Kattan, A.; Hagendorfer, H.; Nowack, B.; Adlhart, C.; Ebert, J.; Lattuada, M.; Hungerbuehler, K. Critical aspects of sample handling for direct nanoparticle analysis and analytical challenges using asymmetric field flow fractionation in a multi-detector approach. *J. Anal. At. Spectrom.* 2012, *27* (7), 1120-1130

110. Dubascoux, S.; Le Hecho, I.; Hassellöv, M.; Von Der Kammer, F.; Gautier, M.P.; Lespes, G. Field-flow fractionation and inductively coupled plasma mass spectrometer

coupling: History, development and applications. *J. Anal. At. Spectrom.* 2010, *25* (5), 613-623.

111. Loeschner, K.; Navratilova, J.; Legros, S.; Wagner, S.; Grombe, R.; Snell, J.; von der Kammer, F.; Larsen, E.H. Optimization and evaluation of asymmetric flow field-flow fractionation of silver nanoparticles. *J. Chromato. A.* 2013, *1272*, 116-125

112. Neubauer, E.; v.d. Kammer, F.; Hofmann, T. Influence of carrier solution ionic strength and injected sample load on retention and recovery of natural nanoparticles using Flow Field-Flow Fractionation. *J. Chromato. A.* 2011, *1218* (38), 6763-6773

113. Pace, H.E.; Rogers, N.J.; Jarolimek, C.; Coleman, V.A.; Higgins, C.P.; Ranville, J.F. Determining transport efficiency for the purpose of counting and sizing nanoparticles via single particle inductively coupled plasma mass spectrometry *Anal. Chem.* 2012, *84* (10), 4633-4633

114. Laborda, F.; Jimenez-Lamana, J.; Bolea, E.; Castillo, J.R. Selective identification, characterization and determination of dissolved silver(I) and silver nanoparticles based on single particle detection by inductively coupled plasma mass spectrometry. *J. Anal. At. Spectrom.* 2011, *26* (7), 1362-1371

115. Laborda, F.; Jimenez-Lamana, J.; Bolea, E.; Castillo, J.R. Critical considerations for the determination of nanoparticle number concentrations, size and number size distributions by single particle ICP-MS. *J. Anal. At. Spectrom.* 2013, *28* (8), 1220-1232

116. Tuoriniemi, J.; Cornelis, G.; Hassellov, M. Size discrimination and detection capabilities of single-particle ICP-MS for environmental analysis of silver nanoparticles. *Anal. Chem.* 2012, *84* (9), 3965-3972

117. Odum, E. The Mesocosm. *Bioscience* 1984, *34* (9), 558-562

118. Lowry, G.V.; Espinasse, B.P.; Badireddy, A.R.; Richardson, C.J.; Reinsch, B.C.; Bryant, L.D.; Bone, A.J.; Deonarine, A.; Chae, S.; Therezien, M.; Colman, B.P.; Hsu-Kim, H.; Bernhardt, E.S.; Matson, C.W.; Wiesner, M.R. Long-term transformation and fate of manufactured Ag nanoparticles in a simulated large scale freshwater emergent wetland. *Environ. Sci. Technol.* 2012, *46* (13), 7027-7036

119. Cleveland, D.; Long, S.E.; Pennington, P.L.; Cooper, E.; Fulton, M.H.; Scott, G.I.; Brewer, T.; Davis, J.; Petersen, E.J.; Wood, L. Pilot estuarine mesocosm study on the environmental fate of Silver nanomaterials leached from consumer products. *Sci. Total Environ.* 2012, *421-422*, 267-72.

120. Domingos, R.F.; Baalousha, M.A.; Ju-Nam, Y.; Reid, M.M.; Tufenkji, N.; Lead, J.R.; Leppard, G.G.; Wilkinson, K.J. Characterizing manufactured nanoparticles in the environment: multimethod determination of particle sizes. *Environ. Sci. Technol.* 2009, *43* (19), 7277-7284

121. Xiu, Z.; Ma, J.; Alvarez, P.J.J. Differential effect of common ligands and molecular oxygen on antimicrobial activity of silver nanoparticles versus silver ions. *Environ. Sci. Technol.* 2011, *45* (20), 9003-9008

122. Blanchfield, P.J.; Paterson, M.J.; Shearer, J.A.; Schindler, D.W. Johnson and Vallentyne's legacy: 40 years of aquatic research at the Experimental Lakes Area. *Can. J. Fish. Aquat. Sci.* 2009, *66* (11), 1831-1836

123. Hintelmann, H. and Ogrinc, N. Determination of stable mercury isotopes by ICP/MS and their application in environmental studies. *Biogeochemistry of Environmentally Important Trace Elements* 2003, *835*, 321-338.

124. Olejnik, S.F. and Algina, J. Parametric ANCOVA vs. rank transform ANCOVA when assumptions of conditional normality and homoscedasticity are violated. *J. Educat. Stat.* 1984, *9*, 129.

125. Janes, N. and Playle, R.C. Modeling Silver-Binding to Gills of Rainbow-Trout (Oncorhynchus-Mykiss). *Environ. Toxicol. Chem.* 1995, *14* (11), 1847-1858

126. Cordery, J.; Wills, A.; Atkinson, K.; Wills, B. Extraction and recovery of silver from low-grade liquors using microalgae. *Minerals Eng.* 1994, *7* (8), 1003-1015

127. Fabrega, J.; Zhang, R.; Renshaw, J.C.; Liu, W.; Lead, J.R. Impact of silver nanoparticles on natural marine biofilm bacteria. *Chemosphere* 2011, *85* (6), 961-966

128. El Badawy, A.M.; Silva, R.G.; Morris, B.; Scheckel, K.G.; Suidan, M.T.; Tolaymat, T.M. Surface charge-dependent toxicity of silver nanoparticles. *Environ. Sci. Technol.* 2011, *45* (1), 283-287

129. Zhao, C. and Wang, W. Biokinetic uptake and efflux of silver nanoparticles in Daphnia magna. *Environ. Sci. Technol.* 2010, *44* (19), 7699-7704

130. Geisler-Lee, J.; Wang, Q.; Yao, Y.; Zhang, W.; Geisler, M.; Li, K.; Huang, Y.; Chen, Y.; Kolmakov, A.; Ma, X. Phytotoxicity, accumulation and transport of silver nanoparticles by Arabidopsis thaliana. *Nanotoxicol.* 2013, *7* (3), 323-337

131. Rascio, N. The underwater life of secondarily aquatic plants: Some problems and solutions. *Crit. Rev. Plant Sci.* 2002, *21* (4), 401-427

132. Jackson, L.; Rowan, D.; Cornett, R.; Kalff, J. Myriophyllum spicatum pumps essential and nonessential trace-elements from sediments to epiphytes. *Can. J. Fish. Aquat. Sci.* 1994, *51* (8), 1769-1773

133. Bloesch, J.; Bossard, P.; Buhrer, H.; Burgi, H.R.; Uehlinger, U. Can results from limnocorral experiments be transferred to in situ conditions?. *Hydrobiologia* 1988, *159*, 297.

134. Wilson, H.F. and Xenopoulos, M.A. Ecosystem and seasonal control of stream dissolved organic carbon along a gradient of land use. *Ecosystems* 2008, *11* (4), 555-568

135. Chao, J.; Liu, J.; Yu, S.; Feng, Y.; Tan, Z.; Liu, R.; Yin, Y. Speciation analysis of silver nanoparticles and silver ions in antibacterial products and environmental waters via cloud point extraction-based separation. *Anal. Chem.* 2011, *83* (17), 6875-6882

136. Bolea, E.; Laborda, F.; Castillo, J.R. Metal associations to microparticles, nanocolloids and macromolecules in compost leachates: Size characterization by asymmetrical flow field-flow fractionation coupled to ICP-MS. *Anal. Chim. Acta* 2010, *661* (2), 206-214

137. Moore, M.N. Do nanoparticles present ecotoxicological risks for the health of the aquatic environment? *Environ. Int.* 2006, *32* (8), 967-976

138. Navarro, E.; Baun, A.; Behra, R.; Hartmann, N.B.; Filser, J.; Miao, A.; Quigg, A.; Santschi, P.H.; Sigg, L. Environmental behavior and ecotoxicity of engineered nanoparticles to algae, plants, and fungi. *Ecotoxicol.* 2008, *17* (5), 372-386

139. Mitrano, D.M.; Ranville, J.F.; Bednar, A.; Kazor, K.; Hering, A.S.; Higgins, C.P. Tracking dissolution of silver nanoparticles at environmentally relevant concentrations in laboratory, natural and processed water using single particle ICP-MS (spICP-MS). *Environ Sci Nano* 2014, *Published Online*.

140. Telgmann, L.; Metcalfe, C.D.; Hintelmann, H. Rapid size characterization of silver nanoparticles by single particle ICP-MS and isotope dilution. 2014, *Submitted.*

141. Horst, A.M.; Neal, A.C.; Mielke, R.E.; Sislian, P.R.; Suh, W.H.; Maedler, L.; Stucky, G.D.; Holden, P.A. Dispersion of TiO2 nanoparticle agglomerates by Pseudomonas aeruginosa. *Appl. Environ. Microbiol.* 2010, *76* (21), 7292-7298

142. Dubascoux, S.; Le Hecho, I.; Gautier, M.P.; Lespes, G. On-line and off-line quantification of trace elements associated to colloids by As-Fl-FFF and ICP-MS. *Talanta* 2008, *77* (1), 60-65

143. Kawahigashi, M.; Sumida, H.; Yamamoto, K. Size and shape of soil humic acids estimated by viscosity and molecular weight. *J. Colloid Interface Sci.* 2005, *284* (2), 463-469

144. Qureshi, R.N. and Kok, W.T. Optimization of asymmetrical flow field-flow fractionation (AF4). *LC GC North America* 2010, *29*.

145. Bone, A.J.; Colman, B.P.; Gondikas, A.P.; Newton, K.M.; Harrold, K.H.; Cory, R.M.; Unrine, J.M.; Klaine, S.J.; Matson, C.W.; Di Giulio, R.T. Biotic and abiotic interactions in aquatic microcosms determine fate and toxicity of Ag nanoparticles: Part 2-toxicity and Ag speciation. *Environ. Sci. Technol.* 2012, *46* (13), 6925-6933

146. Mullen, M.; Wolf, D.; Ferris, F.; Beveridge, T.; Flemming, C.; Bailey, G. Bacterial sorption of heavy-metals. *Appl. Environ. Microbiol.* 1989, *55* (12), 3143-3149.

147. Yamanaka, M.; Hara, K.; Kudo, J. Bactericidal actions of a silver ion solution on Escherichia coli, studied by energy-filtering transmission electron microscopy and proteomic analysis. *Appl. Environ. Microbiol.* 2005, *71* (11), 7589-7593

148. Jacobson, A.; McBride, M.; Baveye, P.; Steenhuis, T. Environmental factors determining the trace-level sorption of silver and thallium to soils. *Sci. Total Environ.* 2005, *345* (1-3), 191-205

149. nanoComposix Tech Note: Zeta/ pH curves and isoelectric point data for standard nanocomposix silver citrate and PVP nanoparticle dispersions. 2012.

150. Wu, Z. and Tseng, W. Combined cloud point extraction and Tween 20-stabilized gold nanoparticles for colorimetric assay of silver nanoparticles in environmental water. *Anal. Methods* 2011, *3* (12), 2915-2920.

# APPENDICIES

## Chapter 2 Supporting Information

*Sediment and Periphtyon Recovery*

**SI Table 2.1.** Recovery of Ag from standard reference material

| Sediment (NIST SRM 1994) | | Oyster tissue (NIST # 1566) | |
|---|---|---|---|
| **Sample set** | **Concentraion measured (mg kg$^{-1}$)** | **Sample set** | **Concentration measured (mg kg$^{-1}$)** |
| Pre-sample | 6.3 | Periphtyon sub-sample 1 | 0.526, 0.521 |
| Sediment 0-2 cm | 6.5, 6.5, 6.8 | Periphyton sub-sample 2 | 0.518 |
| Sediment 2-4 cm | 6.3, 6.3, 6.8 | | |
| Sediment 4-6 cm | 6.7, 6.4, 6.7 | | |

**SI Table 2.2.** Percent of Ag recovered after different amounts were spiked onto L239 sediment and GF/F filters (used for periphyton analysis)

| | Amount of Ag spiked (ng) | | | |
|---|---|---|---|---|
| | **400** | **500** | **1000** | **2000** |
| **Sediment** | 115 ± 14 | 123 ± 7 | 108 ± 7 | 100 ± 4 |
| **GF/F filters** | - | 95 ± 1 | 101 ± 3 | 101 ± 1 |

*Calculations for End of Study Mass Balance*

***Water and Particles***

The Ag mass found in the water and particles was determined by multiplying the concentration by the volume of water measured in the mesocosms at the end of the study.

***Sediment***

The average background Ag concentrations measured in pre-sample sediment (0-3 cm) was subtracted from the average Ag concentraion of post-experimental cores (ng g$^{-1}$ dry weight). Background Ag concentraions were 0.265 ± 0.047 µg g$^{-1}$. The average Ag concentraion in each 2 cm section was then multiplied by the bulk density of the

corresponding 2 cm core section (g dry weight per $cm^3$). The Ag mass in the mesocosm sediment was determined by multiplying the Ag concentration ($ng/cm^3$) in each core section by the total volume of sediment in a 2 cm layer. The volume of sediment assuming a diameter of 2 m and a height of 2 cm was 62,832 $cm^3$.

***Periphyton***

To calculate the Ag mass on the periphyton of mesocosm walls, the following calculations were preformed:

$$\text{Ag mass on strip} = \text{Ag mass on filter} \times \frac{\text{volume of whole sample}}{\text{volume of sample filtered}*}$$

**The total volume of sample filtered was not recorded for all of the samples, so a range of values was determined based on the known minimum amount of sample filtered and an estimation of the maximum volume of sample present.*

$$\text{Ag concentration on strip (mass/ cm}^2) = \frac{Ag\ mass\ on\ strip}{Surface\ area\ of\ strip}$$

Where, the surface area of strip sampled = 100 cm*5 cm*2 (given that both sides were exposed)
`= 1000 $cm^2$

Ag mass on mesocosm walls = Ag on strip ($mass/cm^2$)* Surface area of mesocosm walls

Where, the surface area on mesocosm walls = 2* π*r*h, where diameter = 2 m and height=1.7 m

= 106 760 $cm^2$

***Total Ag recovered***

The total Ag recovered (%) was determined by the sum of Ag in each compartment divided by the total Ag added to the respective mesocosms. The total Ag added to each mesocosm was 20 470 µg to low drips, 81 880 µg to medium drips, 327 520 µg to high drips.

*Water Chemistry Results*

**SI Table 2.3.** Dissolved oxygen concentration (mg $L^{-}$) at various depths in the mesocosm measured during the duration of the study.

| Day | Date | Depth | Mesocosm (Treatment/Replicate) | | | | | | | | | |
|---|---|---|---|---|---|---|---|---|---|---|---|---|
| | | | Cont 1 | Cont 2 | Low PVP 1 | Low PVP 2 | Med PVP 1 | Med PVP 2 | High PVP 1 | High PVP 2 | High CT 1 | High CT 2 |
| 4 | 27-Jun- | Surfac | 8.06 | 7.38 | 7.50 | 7.06 | 7.31 | 7.16 | 7.35 | 7.73 | 7.36 | 7.29 |
| | | 1m | 7.44 | 7.13 | 7.30 | 7.37 | 7.08 | 7.55 | 7.15 | 7.37 | 7.24 | 7.35 |
| | | Botto | 7.83 | 7.20 | 7.42 | 7.20 | 7.42 | 7.61 | 7.20 | 7.24 | 7.28 | 7.10 |
| 11 | 04-Jul-12 | Surfac | 8.24 | 7.94 | 7.47 | 7.73 | 7.76 | 8.08 | 8.15 | 8.38 | 8.23 | 8.07 |
| | | 1m | 8.37 | 8.01 | 7.34 | 7.30 | 7.36 | 8.07 | 8.22 | 8.45 | 8.25 | 8.30 |
| | | Botto | 8.28 | 7.85 | 7.46 | 8.01 | 7.98 | 8.27 | 8.15 | 8.38 | 8.07 | 8.20 |
| 18 | 11-Jul-12 | Surfac | 7.99 | 7.03 | 7.57 | 7.78 | 7.43 | 7.65 | 7.72 | 7.57 | 7.56 | 7.51 |
| | | 1m | 7.72 | 7.11 | 7.64 | 7.82 | 7.42 | 7.46 | 7.69 | 7.57 | 7.47 | 7.33 |
| | | Botto | 7.80 | 7.25 | 7.52 | 7.42 | 7.41 | 7.29 | 7.84 | 7.43 | 7.68 | 7.44 |
| 25 | 17-Jul-12 | Surfac | 8.01 | 7.52 | 7.38 | 7.52 | 7.11 | 7.26 | 7.49 | 7.52 | 7.27 | 7.72 |
| | | 1m | 7.87 | 7.49 | 8.02 | 7.24 | 6.92 | 7.36 | 7.66 | 7.61 | 7.37 | 7.65 |
| | | Botto | 7.82 | 7.34 | 8.28 | 8.01 | 7.41 | 7.01 | 7.40 | 7.71 | 7.20 | 7.58 |
| 32 | 24-Jul-12 | Surfac | 8.32 | 7.92 | 8.00 | 7.50 | 7.69 | 7.50 | 7.80 | 7.78 | 7.55 | 7.93 |
| | | 1m | 8.42 | 8.02 | 8.25 | 7.56 | 7.78 | 7.61 | 8.04 | 8.04 | 7.80 | 8.03 |
| | | Botto | 8.26 | 8.07 | 8.34 | 7.61 | 8.09 | 7.68 | 8.39 | 8.10 | 7.94 | 8.02 |
| 39 | 31-Jul-12 | Surfac | 8.47 | 7.62 | 7.55 | 7.39 | 7.62 | 7.68 | 7.60 | 7.50 | 7.45 | 7.56 |
| | | 1m | 8.08 | 7.70 | 7.70 | 7.47 | 7.67 | 7.86 | 7.77 | 7.62 | 7.70 | 7.68 |
| | | Botto | 7.62 | 7.73 | 7.73 | 7.52 | 7.80 | 7.88 | 7.94 | 7.81 | 7.83 | 7.77 |

**SI Table 2.4.** Temperature (°C) at various depths in the mesocosm measured during the duration of the study

| Day | Date | Depth | Mesocosm (Treatment/Replicate) | | | | | | | | | |
|---|---|---|---|---|---|---|---|---|---|---|---|---|
| | | | Cont 1 | Cont 2 | Low PVP 1 | Low PVP 2 | Med PVP 1 | Med PVP 2 | High PVP 1 | High PVP 2 | High CT 1 | High CT 2 |
| 4 | 27-Jun-12 | Surface | 21.4 | 21.5 | 21.4 | 21.5 | 21.5 | 21.6 | 21.6 | 21.5 | 21.6 | 21.7 |
| | | 1m | - | 21.3 | 21.4 | 21.4 | 21.4 | 21.4 | 21.4 | 21.4 | 21.4 | 21.4 |
| | | Bottom | 21.3 | 21.3 | 21.3 | 21.3 | 21.3 | 21.4 | 21.3 | 21.3 | 21.3 | 21.4 |
| 11 | 04-Jul-12 | Surface | 24.8 | 24.8 | 24.5 | 24.9 | 24.9 | 24.9 | 24.8 | 24.8 | 24.9 | 24.9 |
| | | 1m | 24.8 | 24.8 | 24.7 | 24.8 | 24.8 | 24.8 | 24.8 | 24.8 | 24.8 | 24.8 |
| | | Bottom | 24.6 | 24.6 | 24.6 | 24.4 | 24.6 | 24.8 | 24.5 | 24.6 | 24.5 | 24.7 |
| 18 | 11-Jul-12 | Surface | 24.4 | 24.4 | 24.5 | 24.6 | 24.6 | 24.7 | 24.6 | 24.6 | 24.6 | 24.6 |
| | | 1m | 24.5 | 24.5 | 24.5 | 24.5 | 24.5 | 24.5 | 24.5 | 24.5 | 24.5 | 24.5 |
| | | Bottom | 24.4 | 24.4 | 24.5 | 24.4 | 24.3 | 24.4 | 24.4 | 24.3 | 24.3 | 24.4 |
| 25 | 17-Jul-12 | Surface | 24.1 | 24.2 | 24.1 | 24.1 | 24.2 | 24.4 | 24.5 | 24.4 | 24.4 | 24.4 |
| | | 1m | 23.0 | 23.2 | 23.1 | 23.2 | 23.2 | 23.2 | 23.1 | 23.2 | 23.3 | 23.5 |
| | | Bottom | 22.8 | 23.0 | 22.8 | 23.0 | 23.0 | 23.1 | 23.0 | 23.0 | 23.1 | 23.3 |
| 32 | 24-Jul-12 | Surface | 26.0 | 26.0 | 26.1 | 26.2 | 26.3 | 26.4 | 26.4 | 26.2 | 26.4 | 26.0 |
| | | 1m | 25.0 | 25.0 | 25.0 | 25.1 | 25.0 | 25.0 | 24.9 | 25.0 | 25.0 | 25.3 |
| | | Bottom | 24.9 | 24.9 | 24.9 | 24.9 | 24.9 | 24.9 | 24.7 | 24.9 | 24.7 | 25.3 |
| 39 | 31-Jul-12 | Surface | 25.4 | 25.7 | 25.5 | 25.9 | 25.9 | 25.9 | 25.9 | 25.7 | 25.9 | 25.5 |
| | | 1m | 24.3 | 24.3 | 24.2 | 24.3 | 24.3 | 24.3 | 24.2 | 24.3 | 24.3 | 24.5 |
| | | Bottom | 24.3 | 24.1 | 24.1 | 24.2 | 24.1 | 24.2 | 24.1 | 24.1 | 24.1 | 24.5 |

**SI Table 2.5.** Conductivity (μS $cm^{-1}$) at various depths in the mesocosm measured during the duration of the study

| Day | Date | Mesocosm (Treatment/Replicate) | | | | | | | | | |
|---|---|---|---|---|---|---|---|---|---|---|---|
| | | Cont 1 | Cont 2 | Low PVP 1 | Low PVP 2 | Med PVP 1 | Med PVP 2 | High PVP 1 | High PVP 2 | High CT 1 | High CT 2 |
| 4 | 27-Jun-12 | 32.1 | 32.7 | 31.1 | 31.5 | 31.2 | 31.4 | 31.3 | 30.9 | 31.0 | 32.5 |
| 11 | 04-Jul-12 | 33.0 | 34.5 | 31.6 | 32.5 | 32.1 | 32.7 | 32.1 | 31.6 | 31.8 | 32.4 |
| 18 | 11-Jul-12 | 34.9 | 36.2 | 32.5 | 33.5 | 33.3 | 34 | 33.2 | 33.1 | 33.0 | 36.5 |
| 25 | 17-Jul-12 | 34.9 | 36.4 | 32.1 | 33.3 | 33.2 | 33.9 | 33 | 31.1 | 31.1 | 34.8 |
| 32 | 24-Jul-12 | 35.8 | 37.1 | 32.9 | 34.3 | 33.8 | 35 | 34 | 33.5 | 33.4 | 38.0 |
| 39 | 31-Jul-12 | 36.0 | 37.3 | 33.0 | 34.2 | 33.7 | 35 | 34 | 33.3 | 33.8 | 38.1 |

**SI Table 2.6.** pH level measured in mesocosm during the duration of the study.

| Day | Date | Mesocosm (Treatment/Replicate) | | | | | | | | | |
|---|---|---|---|---|---|---|---|---|---|---|---|
| | | Cont 1 | Cont 2 | Low PVP 1 | Low PVP 2 | Med PVP 1 | Med PVP 2 | High PVP 1 | High PVP 2 | High CT 1 | High CT 2 |
| 4 | 27-Jun-12 | 7.16 | 7.31 | 7.30 | 7.31 | 7.31 | 7.30 | 7.30 | 7.31 | 7.31 | 7.25 |
| 11 | 04-Jul-12 | 7.14 | 7.14 | 7.12 | 7.15 | 7.20 | 7.22 | 7.25 | 7.20 | 7.24 | 7.25 |
| 18 | 11-Jul-12 | 7.18 | 7.22 | 7.22 | 7.32 | 7.15 | 7.20 | 7.20 | 7.16 | 6.40 | 7.23 |
| 25 | 17-Jul-12 | 7.12 | 7.22 | 7.21 | 7.20 | 6.91 | 7.14 | 7.21 | 7.13 | 7.20 | 7.19 |
| 32 | 24-Jul-12 | 6.97 | 7.02 | 7.07 | 7.06 | 7.16 | 7.13 | 7.09 | 7.00 | 6.95 | 7.09 |
| 39 | 31-Jul-12 | 6.79 | 6.97 | 7.05 | 7.23 | 7.24 | 7.17 | 7.21 | 7.08 | 7.21 | 7.23 |
| 46 | 08-Aug-12 | 6.59 | 6.92 | 6.89 | 7.04 | 6.99 | 6.91 | 7.09 | 6.89 | 6.94 | 7.01 |
| 51 | 13-Aug-12 | 7.05 | 6.98 | 7.06 | 7.05 | 7.04 | 7.08 | 7.04 | 7.15 | 7.17 | 7.32 |

**SI Table 2.7**. Concentration of major anions and cations present in each mesocosm. Samples collected July 2nd, 2012.

| Treatment | Replicate | Major Anions and Cations (mg $L^{-1}$) | | | | | |
|---|---|---|---|---|---|---|---|
| | | $Ca^{2+}$ | $K^{+}$ | $Mg^{2+}$ | $Na^{+}$ | $Cl^{-}$ | $SO_4^{2-}$ |
| Control | 1 | 3.94 | 0.45 | 0.93 | 1.13 | 0.27 | 2.20 |
| | 2 | 3.98 | 0.45 | 0.91 | 1.16 | 0.25 | 2.21 |
| Low Drip PVP | 1 | 3.72 | 0.43 | 0.86 | 1.13 | 0.24 | 2.24 |
| | 2 | 3.66 | 0.42 | 0.87 | 1.13 | 0.24 | 2.24 |
| Med Drip PVP | 1 | 3.71 | 0.47 | 0.88 | 1.13 | 0.25 | 2.24 |
| | 2 | 3.72 | 0.47 | 0.90 | 1.15 | 0.26 | 2.24 |
| High Drip PVP | 1 | 3.51 | 0.45 | 0.85 | 1.13 | 0.25 | 2.22 |
| | 2 | 3.66 | 0.44 | 0.86 | 1.14 | 0.25 | 2.25 |
| High Drip CT | 1 | 3.98 | 0.46 | 0.96 | 1.16 | 0.26 | 2.19 |
| | 2 | 4.14 | 0.47 | 0.96 | 1.16 | 0.36 | 2.19 |

**SI Table 2.8.** DOC concentration in mesocosm water over time (mg $L^{-1}$).

| Day | Date | Mesocosm (Treatment/Replicate) | | | | | | | | | |
|---|---|---|---|---|---|---|---|---|---|---|---|
| | | Cont 1 | Cont 2 | Low PVP 1 | Low PVP 2 | Med PVP 1 | Med PVP 2 | High PVP 1 | High PVP 2 | High CT 1 | High CT 2 |
| 0 | 21-Jun-12 | 8.3 | 7.3 | 8.2 | 7.4 | 9.1 | 7.6 | 7.4 | 7.7 | 7.8 | 8.8 |
| 4 | 27-Jun-12 | 8.7 | 8.0 | 8.0 | 7.9 | 7.9 | 7.7 | 8.4 | 8.1 | 8.5 | 8.4 |
| 11 | 04-Jul-12 | 8.4 | 9.2 | 8.8 | 8.1 | 9.4 | 8.6 | 8.1 | 9.5 | 8.9 | 8.1 |
| 18 | 11-Jul-12 | 8.1 | 10.9 | 8.2 | 8.4 | 7.7 | 9.1 | 8.6 | 8.0 | 8.8 | 8.0 |
| 25 | 18-Jul-12 | 8.8 | 9.3 | - | 8.6 | 9.3 | 8.2 | 9.2 | 8.5 | 9.6 | 8.4 |
| 32 | 25-Jul-12 | 8.4 | 8.6 | 8.4 | 8.5 | - | 8.7 | 8.0 | 8.9 | 8.7 | 8.8 |
| 39 | 01-Aug-12 | 8.5 | 7.3 | 8.6 | 7.4 | 8.3 | - | 7.4 | 7.7 | 8.4 | 8.8 |

*ANCOVA Results*

**SI Table 2.9.** Linear regression results for Ag accumulation in various fractions over time.

| Fraction | Treatment/Replicate | Linear Regression Model | r2 |
|---|---|---|---|
| **TAg** | Low Drip PVP 1 | LogDay=1.2 + 1.3Log[Ag] | 0.95 |
| | Low Drip PVP 2 | LogDay=1.2 + 1.4Log[Ag] | 0.97 |
| | Medium Drip PVP 1 | LogDay=0.4 + 1.3Log[Ag] | 0.97 |
| | Medium Drip PVP 2 | LogDay= 0.3 + 1.5Log[Ag] | 0.98 |
| | High Drip PVP 1 | LogDay=-0.5 + 1.3Log[Ag] | 0.98 |
| | High Drip PVP 2 | LogDay=-0.6 + 1.4Log[Ag] | 0.98 |
| | High Drip CT 1 | LogDay=-0.6 + 1.6Log[Ag] | 0.97 |
| | High Drip CT 2 | LogDay=-0.6 + 1.4Log[Ag] | 0.99 |
| **Colloidal Ag** | Low Drip PVP 1 | LogDay=-0.92 + 0.54Log[Ag] | 0.92 |
| | Low Drip PVP 2 | LogDay=-0.91 + 0.48Log[Ag] | 0.87 |
| | Medium Drip PVP 1 | LogDay=-0.42 + 0.67Log[Ag] | 0.94 |
| | Medium Drip PVP 2 | LogDay=-0.33 + 0.54Log[Ag] | 0.92 |
| | High Drip PVP 1 | LogDay= 0.26 + 0.55Log[Ag] | 0.79 |
| | High Drip PVP 2 | LogDay=0.234 + 0.61Log[Ag] | 0.80 |
| | High Drip CT 1 | LogDay=0.23 + 0.58Log[Ag] | 0.91 |
| | High Drip CT 2 | LogDay=0.32 + 0.54Log[Ag] | 0.72 |
| **Particulate Ag** | Low Drip PVP 1 | LogDay=-1.65 + 1.0Log[Ag] | 0.94 |
| | Low Drip PVP 2 | LogDay=-1.49 + 0.95Log[Ag] | 0.93 |
| | Medium Drip PVP 1 | LogDay=-0.84 + 0.79Log[Ag] | 0.84 |
| | Medium Drip PVP 2 | LogDay=-0.78 + 0.84Log[Ag] | 0.93 |
| | High Drip PVP 1 | LogDay=-0.32 + 1.0Log[Ag] | 0.88 |
| | High Drip PVP 2 | LogDay=-0.27 + 0.87Log[Ag] | 0.81 |
| | High Drip CT 1 | LogDay=-0.13 + 0.71Log[Ag] | 0.85 |
| | High Drip CT 2 | LogDay=-0.23 + 0.95Log[Ag] | 0.90 |

**SI Table 2.10.** ANCOVA results comparing the effect of loading rate and surface coating on Ag accumulation in various fractions over time.

| Fraction | Experiment | Intercept Significant | Slope Significant | LSmeans Differences |
|---|---|---|---|---|
| **TAg** | Loading Rate | yes; $p<0.01$ | no; $p=0.6761$ | Differences between loading rates. No difference between replicates |
| | Surface Coating | yes; $p<0.01$ | no; $p=0.098$ | CT 1 significantly lower than PVP 1 and CT 2 |
| **Colloidal Ag** | Loading Rate | yes; $p<0.01$ | no; $p=0.6551$ | Differences between loading rates. No difference between replicates |
| | Surface Coating | no; $p=0.9187$ | no; $p=0.9684$ | no |
| **Particulate Ag** | Loading Rate | yes; $p<0.01$ | no; $p=0.6425$ | Differences between loading rates. No difference between replicates |
| | Surface Coating | no; $p=0.1750$ | no; $p=0.4038$ | no |

*Sediment Results*

**SI Table 2.11.** Characterization of mesocosm sediment (0-2 cm layer) for bulk density, loss on ignition, and particle size. .

| Treatment | Replicate | bulk density ($g/cm^3$) | loss on ignition (%) | particle size | | |
|---|---|---|---|---|---|---|
| | | | | % silt | % sand | % clay |
| CONTROL 1 | Core 1 | 0.29 | 3.7 | 62 | 38 | 0 |
| | Core 2 | 0.23 | 4.7 | 53 | 47 | 0 |
| CONTROL 2 | Core 1 | 0.45 | 2.5 | 65 | 35 | 0 |
| | Core 2 | 0.38 | 2.6 | 64 | 36 | 0 |
| LOW DRIP PVP 1 | Core 1 | 0.39 | 3.3 | 57 | 43 | 0 |
| | Core 2 | 0.21 | 5.0 | 50 | 50 | 0 |
| LOW DRIP PVP 2 | Core 1 | 0.42 | 2.9 | 60 | 40 | 0 |
| | Core 2 | 0.28 | 3.8 | 55 | 45 | 0 |
| MED DRIP PVP 1 | Core 1 | 0.63 | 3.2 | 63 | 37 | 0 |
| | Core 2 | 0.40 | 3.1 | 61 | 39 | 0 |
| MED DRIP PVP 2 | Core 1 | 0.18 | 3.4 | 58 | 42 | 0 |
| | Core 2 | 0.37 | 3.3 | 64 | 36 | 0 |
| HIGH DRIP PVP 1 | Core 1 | 0.45 | 3.1 | 64 | 36 | 0 |
| | Core 2 | 0.27 | 3.3 | 59 | 41 | 0 |
| HIGH DRIP PVP 2 | Core 1 | 0.30 | 3.5 | 57 | 43 | 0 |
| | Core 2 | 0.24 | 3.9 | 55 | 45 | 0 |
| HIGH DRIP CT 1 | Core 1 | 0.43 | 3.7 | 52 | 48 | 0 |
| | Core 2 | 0.27 | 4.2 | 57 | 43 | 0 |
| HIGH DRIP CT 2 | Core 1 | 0.22 | 4.6 | 64 | 36 | 0 |
| | Core 2 | 0.28 | 4.5 | 59 | 41 | 0 |
| | **MEAN** | 0.33 | 3.8 | 58 | 42 | 0 |
| | **SD** | 0.12 | 0.7 | 5 | 5 | 0 |

*Mass Balance Results*

**SI Table 2.12.** Results of Ag analysis in mesocosm sediment. Highlighted are outliers that were removed from the data set. Plug results are presented in Chapter 3.

| Treatment | Core | ng Ag/g | | Bulk Density ($g/cm^3$) | ng Ag/cm3 | | Ag mass in mesocosm sediment (ng) | % Ag mass in sediment |
|---|---|---|---|---|---|---|---|---|
| | | mean | sd | | mean | sd | | |
| CONTROL 1 | Core 1 | 399 | 45 | 0.29 | 115 | 13 | - | - |
| | Core 2 | 439 | 42 | 0.23 | 101 | 10 | - | - |
| CONTROL 2 | Core 1 | 253 | 9 | 0.38 | 114 | 4 | - | - |
| | Core 2 | 248 | 16 | 0.45 | 91 | 3 | - | - |
| LOW DRIP PVP 1 | Core 1 | 369 | 29 | 0.39 | 142 | 11 | 2548 | 11 |
| | Core 2 | 682 | 27 | 0.21 | 145 | 6 | 5502 | 24 |
| LOW DRIP PVP 2 | Core 1 | 433 | 56 | 0.42 | 181 | 23 | 4433 | 19 |
| | Core 2 | 758 | 59 | 0.28 | 214 | 17 | 8673 | 37 |
| MED DRIP PVP 1 | Core 1 | 2702 | 482 | 0.39 | 1054 | 188 | 59716 | 65 |
| | Core 2 | 1622 | 53 | 0.62 | 1001 | 33 | 52862 | 57 |
| MED DRIP PVP 2 | Core 1 | 1259 | 235 | 0.18 | 230 | 43 | 11242 | 12 |
| | Core 2 | 943 | 106 | 0.37 | 351 | 40 | 15762 | 17 |
| HIGH DRIP PVP 1 | Core 1 | 2066 | 60 | 0.45 | 932 | 27 | 50921 | 14 |
| | Core 2 | 3539 | 1187 | 0.27 | 938 | 315 | 55541 | 15 |
| HIGH DRIP PVP 2 | Core 1 | 2578 | 244 | 0.3 | 778 | 74 | 43598 | 12 |
| | Core 2 | 3702 | 908 | 0.24 | 896 | 220 | 51828 | 14 |
| HIGH DRIP CT 1 | Core 1 | 759 | 90 | 0.53 | 420 | 47 | 16450 | 4 |
| | Core 2 | 5304 | 158 | 0.27 | 1453 | 43 | 85483 | 23 |
| HIGH DRIP CT 2 | Core 1 | 5868 | 215 | 0.22 | 1303 | 48 | 77449 | 21 |
| | Core 2 | 4559 | 503 | 0.28 | 1267 | 140 | 75543 | 20 |
| PLUG 1 | Core 1 | 3745 | 1245 | 0.31 | 1176 | 391 | 67782 | 28 |
| | Core 2 | 750 | 22 | 0.42 | 311 | 9 | 60416 | 25 |
| PLUG 2 | Core 1 | 5607 | 190 | 0.18 | 1026 | 35 | 12799 | 5 |
| | Core 2 | 5555 | 431 | 0.19 | 1072 | 83 | 63151 | 26 |

**SI Table 2.13.** Measured water volumes for each mesocosm at the end of the study.

| Treatment | Replicate | Volume (L) |
|---|---|---|
| Control | 1 | 2709 |
| | 2 | 2392 |
| Low Drip PVP | 1 | 2599 |
| | 2 | 2599 |
| Med Drip PVP | 1 | 2709 |
| | 2 | 2709 |
| High Drip PVP | 1 | 3475 |
| | 2 | 2709 |
| High Drip CT | 1 | 3198 |
| | 2 | 2709 |

## Chapter 3 Supporting Information

*Sediment Characterization*

**SI Table 3.1.** Characterization of mesocosm sediment (0-2 cm layer) for bulk density, loss on ignition, and particle size. For bulk density, each core was dried to a constant mass at 60$^{O}$C. For loss on ignition, one sub-sample of each dried core was heated at 400$^{o}$C for 10 hours. Particle sizing was preformed on two subsamples per core using the Horiba LA-950.

| mesocosm | core | loss on ignition (%) | particle size | | | bulk density (g cm$^{3-1}$) |
|---|---|---|---|---|---|---|
| | | | % silt | % sand | % clay | |
| Replicate 1 | 1 | 4.6 | 54 | 46 | 0 | 0.31 |
| | 2 | 3.6 | 59 | 41 | 0 | 0.42 |
| Replicate 2 | 1 | 5.0 | 50 | 50 | 0 | 0.18 |
| | 2 | 4.6 | 56 | 44 | 0 | 0.19 |
| **MEAN** | | 4 | 55 | 45 | 0 | - |
| **SD** | | 1 | 4 | 4 | 0 | - |

*CPE Materials and Methods*

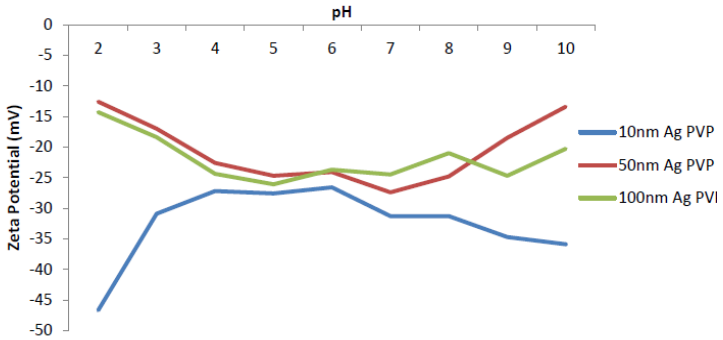


**SI Figure 3.1.** Zeta Potentials of PVP capped silver nanoparticles over a pH range of 2-10. Experiment was preformed by nanoComposix (149)

**SI Table 3.2.** TEM Operating Conditions

| | |
|---|---|
| Working Mode | HR-TEM, low dose TEM, nanoprobe, free lens control |
| Gun | LaB6-cathode thermionic gun |
| Point-to-point resolution | 0.24 nm |
| Line Resolution | 0.17 nm |
| Operation Voltage | 200kV |

*Cloud-Point Extraction Method Validation*

The extraction efficiency of the CPE method was tested in both DI and L239 water. The recovery of AgNPs was 75% in DI and decreased to 41% in L239 water, indicating matrix effects on method performance (SI Table 3.3). This contradicts previous studies that have shown WWTP influent, effluent, and lake water to have minimal effect on the extraction efficiency of AgNPs (96)(97). It has also been demonstrated that humic acids (0-30 mg $L^{-1}$) have no effect on the method (95). Nevertheless, our laboratory results still show the method to be effective at distinguishing AgNP from Ag+. In both DI and L239, less than 2% of Ag was extracted in the sole presence of Ag+; and same amounts of Ag were extracted from a mixture of AgNPs and Ag+ and from a solution with only AgNPs. Many studies have reported the selectivity of CPE for AgNPs (95, 135, 150). It is important to note that CPE is incapable of extracting metal-ion humic acid colloids due to the stronger affinity of Ag+ for thiosulfate ($S_2O_3$) added during the CPE procedure (150). Therefore, despite the lower recoveries observed in L239 laboratory trials, the application of CPE for observing trends in AgNP concentration is valuable for the mesocosm study. Particle concentration had no effect on CPE recovery (SI Table 3.4), but recovery decreased with AgNP size (SI Table 3.5).

**SI Table 3.3.** Extraction efficiencies by CPE of $Ag^+$ (36 µg Ag $L^-$), 50 nm PVP-AgNPs (27 µg Ag $L^-$), and a mixture of $Ag^+$ (36 µg Ag $L^-$) with 50 nm PVP-AgNPs (27 µg Ag $L^{-1}$) in DI and 0.2 µm pre-filtered Lake 239 water

| | **Extraction efficiencies (%, mean ± sd, n=3)** | | |
|---|---|---|---|
| | **$Ag^+$** | **AgNPs** | **Ag+AgNPs[A]** |
| **DI** | 2 ± 0 | 75 ± 2 | 74 ± 4 |
| **L239** | 2 ± 1 | 41 ± 9 | 40 ± 8 |

[A] Apparent extraction efficiency with respect to concentration of AgNPs and assuming Ag+ was not extracted

**SI Table 3.4.** Extraction efficiencies by CPE of 50 nm PVP-AgNPs at various AgNP concentrations

| AgNP concentration[A] (µg Ag $L^{-1}$) | Extraction efficiency (%, mean ± SD, n=3) |
|---|---|
| 7 | 86 ± 1 |
| 17 | 77 ± 3 |
| 30 | 75 ± 2 |
| 53 | 83 ± 5 |
| 65 | 83 ± 1 |

[A] Determined by measured Ag concentration before extraction adjusted for the amount of dAg present in the stock solution

**SI Table 3.5.** Extraction efficiencies by CPE of various sizes of PVP-AgNPs spiked at a nominal concentraion of 40 µg $L^{-}$

| Size (nm) | Extraction efficiency[A] (%, mean ± sd, n=3) |
|---|---|
| 10 | 52 ± 2 |
| 20 | 54 ± 4 |
| 40 | 73 ± 1 |
| 50 | 74 ± 1 |
| 60 | 72 ± 2 |
| 80 | 83 ± 1 |

[A] Extraction efficiency with respect to measured Ag concentration before extraction adjusted for the amount of dAg present in each stock solution

*AF4-ICP-MS Materials and Methods*

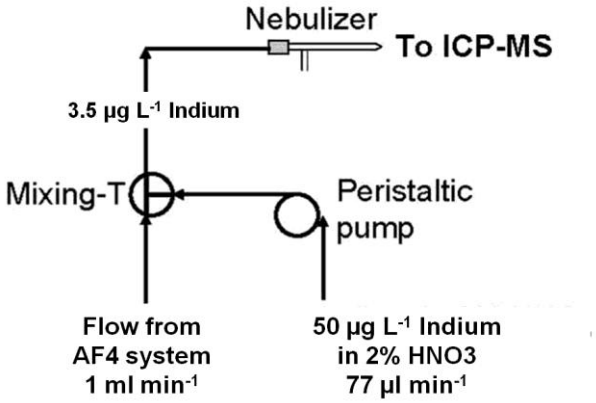


**SI Figure 3.2.** Schematic of AF4-ICP-MS analytical method.

**SI Table 3.6.** Instrumentation and data acquisition parameters for AF4-ICP-MS analysis.

| | |
|---|---|
| ICP-MS model | XSeries 2 (Thermo Scientific) |
| Nebulizer | Conikal U-series (isoSPEC;1mL $min^{-1}$) |
| Spray chamber | Conical with impact bed |
| Cones | Ni |
| Analysis mode | Time resolved analysis |
| Isotopes monitored | $^{107}Ag$, $^{115}In$ |
| Dwell time | 20 000 µs |

**SI Table 3.7.** Size information for AgNP standards by TEM and DLS analysis provided by the manufacturer (NanoComposix).

| AgNP | TEM diameter (nm) | DLS hydrodynamic diameter (nm) |
|---|---|---|
| 20 nm PVP | 20.0 ± 1.8 | 25.8 |
| 40 nm PVP | 40.7 ± 4.1 | 49.3 |
| 50 nm PVP | 48.3 ± 3.7 | 56.3 |
| 60 nm PVP | 59.9 ± 3.9 | 77.1 |
| 80 nm PVP | 82.1 ± 4.4 | 93.3 |

*AF4-ICP-MS Method Optimization and Validation*

The carrier fluid and cross-flow were optimized to obtain maximum recovery of 50 nm PVP material (SI Table 3.8). 0.05% SDS provided both the greatest recovery and reproducibility and thus, was selected as the carrier fluid. When comparing the cross-flows of 1.0 mL $min^{-1}$ to 0.7 mL $min^{-1}$ similar recoveries of fresh 50 nm PVP-AgNPs were obtained (SI Table 3.8). However, at a cross-flow of 0.7 mL $min^{-1}$ there was less beak broadening and greater peak height (SI Figure 3.3). Given the low concentrations of AgNPs added to the mesocosms, a cross-flow of 0.7 mL/min was selected for the analysis to obtain the best detection limit as possible at the expense of lost size resolution (SI Figure 3.4). For size determination, a three point calibration curve was used using 40 and 80 nm PVP AgNP standards and extending the regression line through the orgin (hydrodynamic diameter vs. retention time). The three point calibration curve determined with PVP AgNP standards was compared to CT AgNP standards to evaluate the effect of surface coating on separation. The PVP AgNP curve quantified the hydrodynamic diameter of the 50 nm PVP-AgNPs as 61 nm and the CT AgNP curve quantified the hydrodynamic diameter as 63 nm. Therefore, surface coating had minimal effect on retention time.

For the quantification of silver, external calibration using 50 nm PVP AgNP standards injected into the AF4-ICP-MS system was preformed to generate a calibration curve (response vs. concentration) with an $R^2$ of 0.99 (SI Figure 3.5). Given the excellent linear relationship, subsequent analysis of mesocosm samples used a one-point calibration curve to save time on the analysis.

**SI Table 3.8.** Recovery and retention time of 50 nm PVP-AgNPs analyzed in various mobile phases and cross-flow rates.

| Carrier Fluid | Cross-Flow (mL/min) | Recovery (%) mean ± sd (n=3) | Retention Time (min) mean ± sd (n=3) |
|---|---|---|---|
| 0.025% FL-70 | 1.0 | 60 ± 9 | 13.7 ± 0.9 |
| 0.05% FL-70 | 1.0 | 37 ± 5 | 14.5 ± 0.7 |
| 0.05% SDS | 1.0 | 95 ± 2 | 14.7 ± 0.4 |
| 0.05% SDS | 0.7 | 109 ± 9 | 10.7 ± 0.0 |

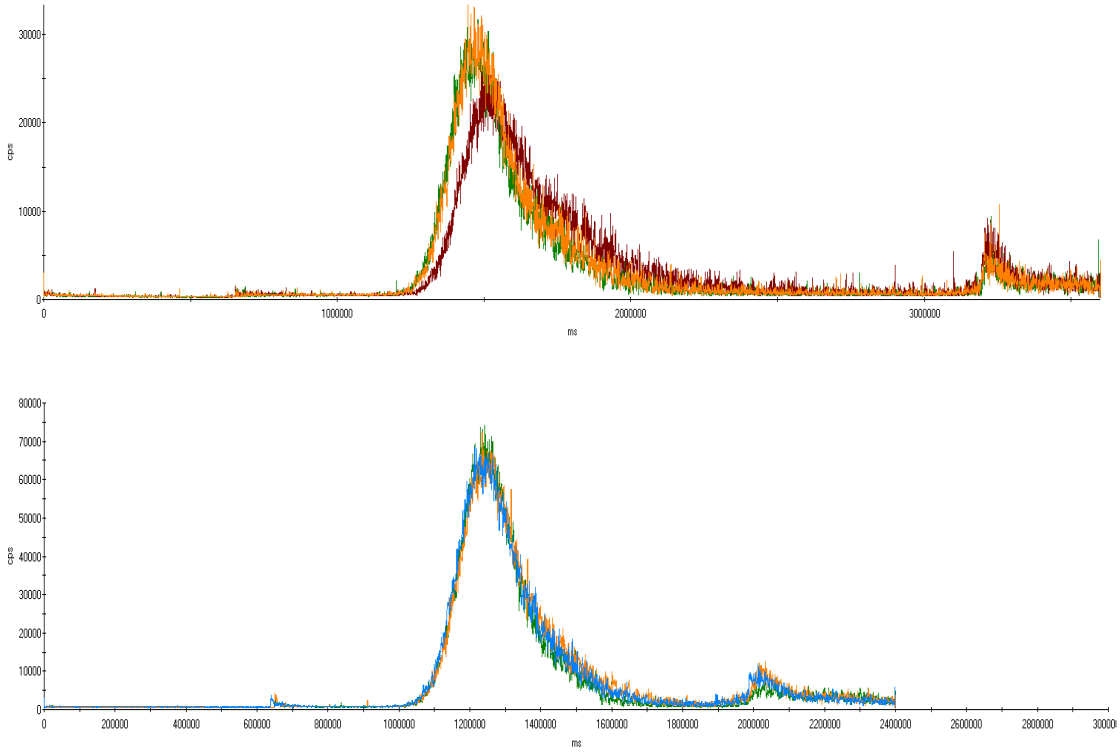


**SI Figure 3.3.** Compairison of replicate injections of 50 nm PVP-AgNPs (100 µg $L^{-}$) at a cross-flow of 1.0 mL $min^{-1}$ (top) and 0.7 mL $min^{-1}$ (bottom) in 0.05% SDS carrier fluid.Raw fractograms are presented.

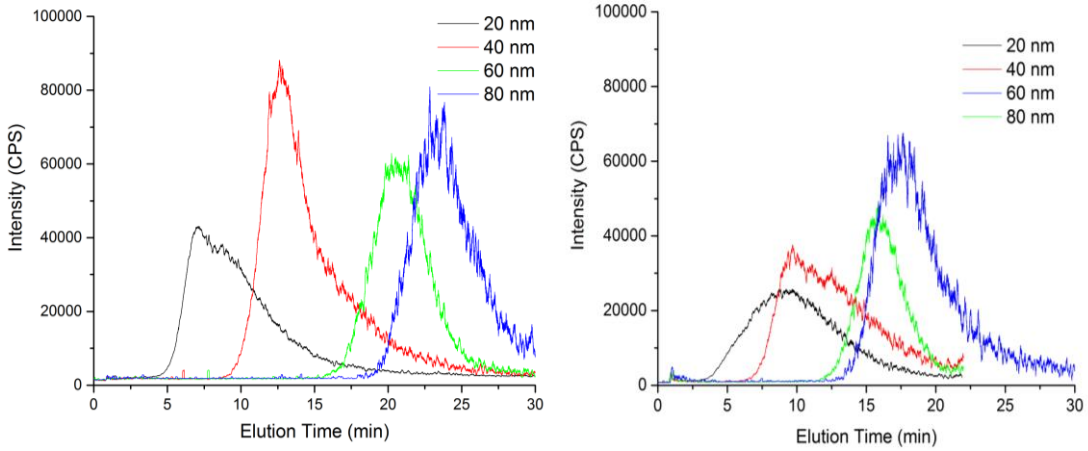


**SI Figure 3.4** AF4-ICP-MS fractograms for various sizes of PVP-AgNPs (100 µg $L^{-1}$) analyzed at a cross-flow of 1.0 mL/min (left) and 0.7 mL/ min (right)

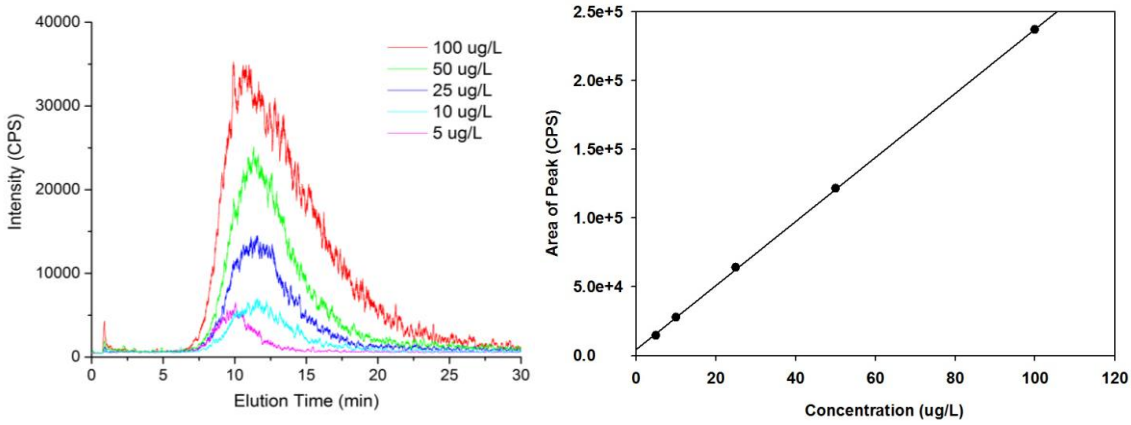


**SI Figure 3.5.** AF4-ICP-MS fractograms for various concentrations of 50 nm PVP AgNP and the resulting standard curve. Measured at a cross-flow of 0.7 mL/min.

*Water Chemistry Results*

**SI Table 3.9.** Dissolved oxygen concentration (mg $L^{-1}$), temperature ($^{o}C$), and conductivity (µS $cm^{-1}$) in plug mesocosms at various water depths over time

| Sample Day | Sample Date | Depth | DO (mg $L^{-1}$) | | Temperature ($^{o}C$) | | Conductivity (µS $cm^{-1}$) | |
|---|---|---|---|---|---|---|---|---|
| | | | Rep 1 | Rep 2 | Rep 1 | Rep 2 | Rep 1 | Rep 2 |
| 1 | 11-Jul-12 | Surface | 7.81 | 7.56 | 24.5 | 24.6 | 32.8 | 32.9 |
| | 11-Jul-12 | 1m | 7.52 | 7.47 | 24.5 | 24.5 | | |
| | 11-Jul-12 | Bottom | 7.69 | 7.68 | 24.4 | 24.3 | | |
| 7 | 17-Jul-12 | Surface | 6.86 | 6.75 | 24.7 | 24.2 | 31.2 | 34.8 |
| | 17-Jul-12 | 1m | 7.31 | 6.76 | 23.3 | 23.3 | | |
| | 17-Jul-12 | Bottom | 7.55 | 6.33 | 23.3 | 23.0 | | |
| 14 | 24-Jul-12 | Surface | 7.73 | 7.44 | 26.4 | 26.5 | 33.5 | 33.9 |
| | 24-Jul-12 | 1m | 8.17 | 7.54 | 25.0 | 24.9 | | |
| | 24-Jul-12 | Bottom | 8.35 | 7.66 | 24.9 | 24.9 | | |
| 21 | 31-Jul-12 | Surface | 7.57 | 7.54 | 25.9 | 25.9 | 33.3 | 33.8 |
| | 31-Jul-12 | 1m | 8.00 | 7.69 | 24.3 | 24.3 | | |
| | 31-Jul-12 | Bottom | 8.15 | 7.76 | 24.1 | 24.1 | | |

**SI Table 3.10.** pH level in plug mesocosm water over time

| Sample Day | Sample Date | pH level | |
|---|---|---|---|
| | | Rep 1 | Rep 2 |
| 1 | 11-Jul-12 | 7.18 | 7.20 |
| 7 | 18-Jul-12 | 7.20 | 7.21 |
| 14 | 25-Jul-12 | 7.10 | 7.12 |
| 21 | 01-Aug-12 | 7.17 | 7.22 |
| 33 | 08-Aug-12 | 7.08 | 7.19 |

**SI Table 3.11.** DOC concentration (mg $L^{-1}$) in plug mesocosms over time

| Sample Day | Sample Date | DOC (mg/L) | |
|---|---|---|---|
| | | Rep 1 | Rep 2 |
| pre-sample | 21-Jun-12 | 8.186 | 7.357 |
| 1 | 11-Jul-12 | 8.165 | 8.636 |
| 7 | 18-Jul-12 | 8.815 | 8.795 |
| 14 | 25-Jul-12 | 8.368 | 8.573 |
| 21 | 01-Aug-12 | 8.524 | 7.357 |

**SI Table 3.12.** Concentration of major anions and cations present in L239 (sampled Aug, 2012). Mean ± sd of sub-samples is presented (n=3).

| Major Anions and Cations (mg $L^{-1}$) | | | | | |
|---|---|---|---|---|---|
| $Ca^{2+}$ | $K^{+}$ | $Mg^{2+}$ | $Na^{+}$ | $Cl^{-}$ | $SO_4^{2-}$ |
| 3.45±0.04 | 0.43±0.00 | 0.85±0.01 | 1.10±0.01 | 0.27±0.01 | 2.23±0.01 |

*Ultrafiltration Recovery Tests*

The low concentrations of dAg measured by ultrafiltration may be a reflection of dAg complexes being retained on the filters. To test this, the recovery of Ag+ through filters was compared in L239 and DI water with concentrations ranging from 1 to 100 µg $L^{-1}$ (SI Table 3.13 and SI Table 3.14). The Ag+ recovery through the pre-filters (0.2 µm and 0.45 µm) was greater than 90% in DI water across all Ag+ concentrations. In L239 water the recovery decreased at Ag concentrations <100 µg $L^{-1}$. Conversely, the Ag+ recovery through 3 kDa membranes was lower in L239 than DI water across all Ag+ concentrations. Overall, the filtration recovery tests show that Ag+ recovery decreases in complex water matrices, likely due to complexation with ligands. Also, in both sample matrices and across filters, recovery decreased with Ag+ concentration because of a greater proportional loss of Ag+ to the filtering apparatus or membrane. Future studies should equilibrate membranes with Ag by passing sample solution through before analysis to reduce adsorptive losses of Ag+ in samples with low Ag concentrations (85).

The 3 kDa filtration results with mesocosm water showed that greater dAg concentrations are measured using stirred ultrafiltration as compared to centrifugal filtration. It was hypothesized that this could be due to the method of filtration, in which samples in the stirred ultrafiltration apparatus are "stirred" in the reservoir above the membrane preventing deposition of larger molecules that could block membrane pores (86). However, recovery tests comparing the two filtration apparatus showed similar recovery for both DI and L239 water. Consequently, the greater dAg concentrations in mesocosm samples measured using stirred ultrafiltration as compared to centrifugal filtration may be result from the dissimilar sample handling (i.e. non flash frozen samples versus flash frozen samples) or the different times of analysis. The prolonged stirring in the stirred

ultrafiltration method may also promote AgNP dissolution and/or release of chemisorbed dAg, but this requires further investigation. Overall, the better recovery, ease of use, lower cost, and higher sample throughput of centrifugal filtration make it a better option for dAg analysis for future studies.

**SI Table 3.13.** Recovery of Ag+ through pre-filter membranes in both DI and L239 whole water. The 0.2 µm polycarbonate membrane was used before stirred ultrafiltration and the 0.45 µm membrane was used before centrifugal filtration. Ag+ was spiked in water 24 hrs before analysis.

| | **0.2 µm polycarbonate filtration % Ag recovery (mean ± sd, n=3)** | | | **0.45 µm polycarbonate filtration % Ag recovery (mean ± sd, n=3)** | | |
|---|---|---|---|---|---|---|
| | **100 µg $L^{-1}$** | **10 µg $L^{-1}$** | **1 µg $L^{-1}$** | **100 µg $L^{-1}$** | **10 µg $L^{-1}$** | **1 µg $L^{-1}$** |
| **DI** | 99 ± 1 | 99 ± 1 | 93 ± 2 | 101 ± 1 | 97 ± 2 | 96 ± 0 |
| **L239** | 95 ± 2 | 78 ± 1 | 58 ± 1 | 94 ± 1 | 79 ± 1 | 83 ± 5 |

**SI Table 3.14.** Recovery of Ag+ using stirred ultrafiltrtaion and centrifugal filtration (3 kDa regenerated cellulose membranes) in both DI and pre-filtered (0.2 µm) L239 water. Ag+ was spiked in water 24 hrs before analysis.

| | **Stirred Ultrafiltration % Ag recovery (mean ± sd, n=3)** | | | **Centrifugal Filtration % Ag recovery (mean ± sd, n=3)** | | |
|---|---|---|---|---|---|---|
| | **100 µg $L^{-1}$** | **10 µg $L^{-1}$** | **1 µg $L^{-1}$** | **100 µg $L^{-1}$** | **10 µg $L^{-1}$** | **1 µg $L^{-1}$** |
| **DI** | 93 ± 4 | 64 ± 1* | 44 ± 10* | 93 ± 1 | 78 ± 2 | 58 ± 2 |
| **L239** | 73 ± 7 | 40 ± 7 | 2 ± 3 | 75 ± 1 | 49 ± 1 | 6 ± 1 |

*n=2; sample removed due to membrane leaking.

*CPE Results*

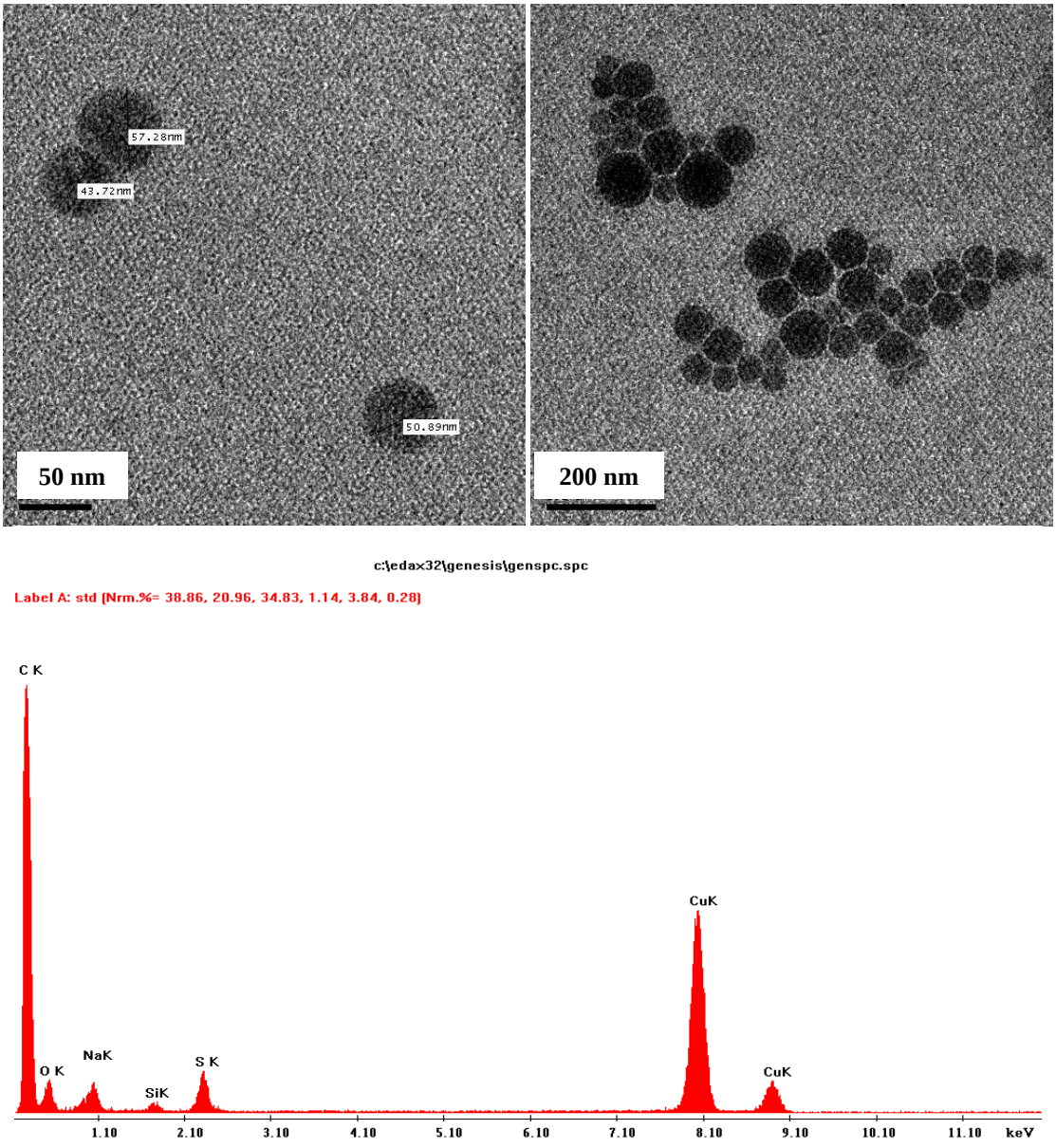


**SI Figure 3.6.** TEM image of nanoparticles in the TX-114 rich phase after CPE of mesocosm sample (24 hr, replicate 1; top). The nanoparticles could not be confirmed as AgNPs because no Ag was detected in EDS (bottom).

*AF4-ICP-MS Results*

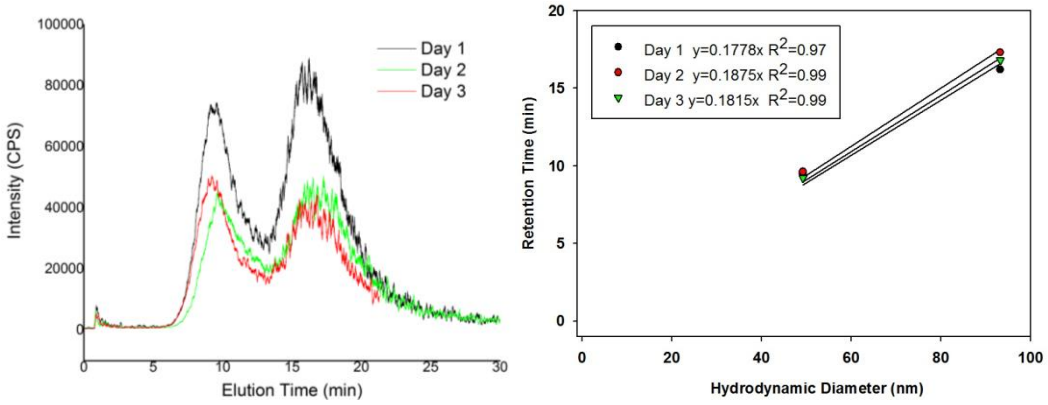


**SI Figure 3.7.** AF4-ICP-MS fractograms and standard curve for injection of 40 +80 nm PVP AgNP standards (100 µg $L^{-1}$ in milliQ) for daily size calibration of mesocosm samples

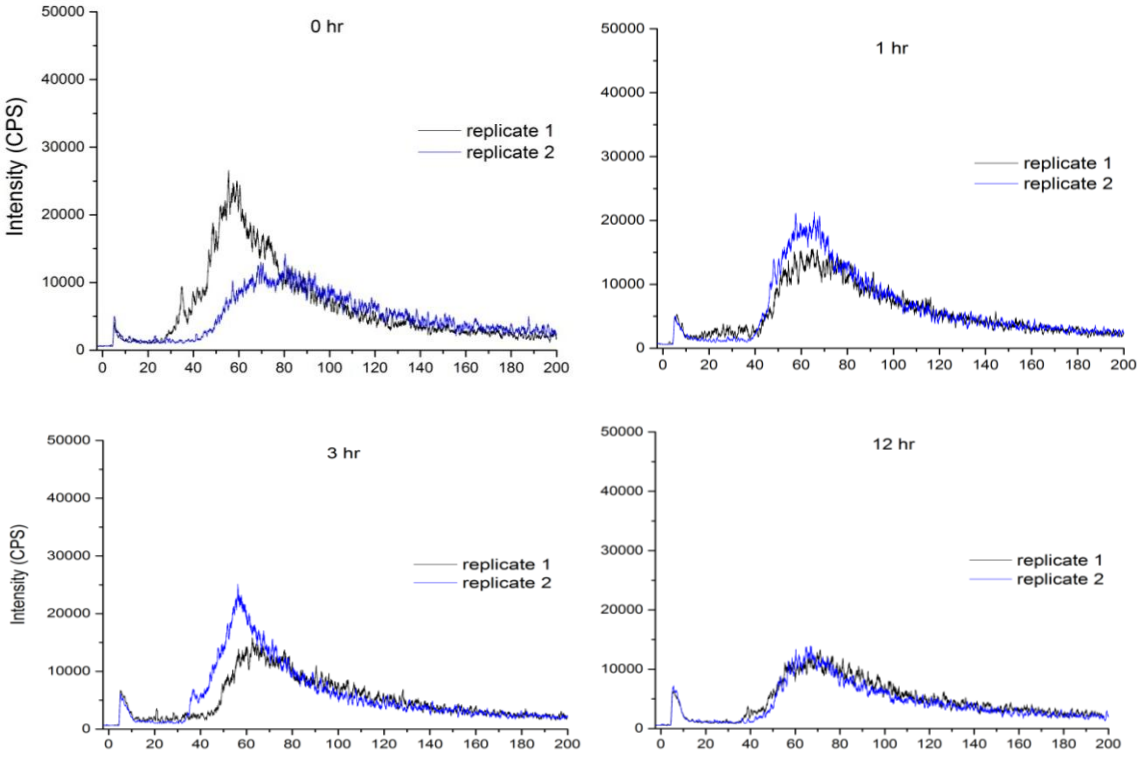


**SI Figure 3.8.** AF4-ICP-MS fractograms for mesocosm samples. The y axis displays normalized $Ag^{107}$ intensity. The x-axis displays calibrated hydrodynamic diameters. Figure continued on next page.

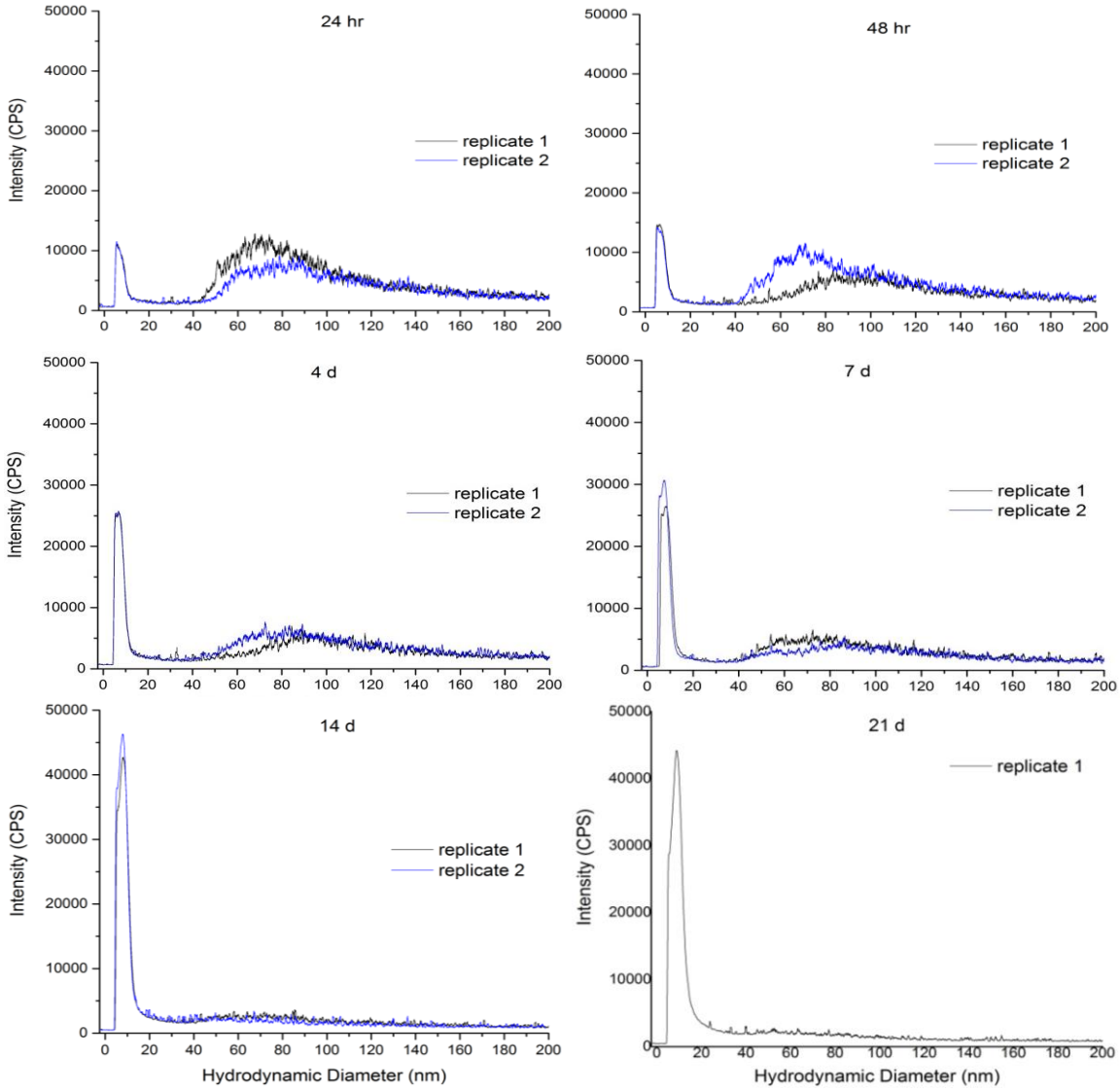


**SI Figure 3.8.** AF4-ICP-MS fractograms for mesocosm samples. No sample for replicate 2-21 d was available.

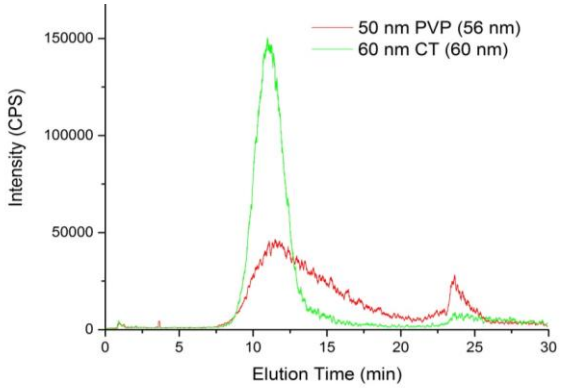


**SI Figure 3.9.** AF4-ICP-MS fractograms comparing the signal intensity of CT-AgNPs versus PVP-AgNPs of similar hydrodynamic diameter (value shown in brackets).